Experimental investigations on the dynamic behavior and fracture of composite materials

DISSERTATION

zur Erlangung des Grades eines Doktors

der Ingenieurwissenschaften

vorgelegt von

M.Sc. Mohammad Reza Khosravani

eingereicht bei der Naturwissenschaftlich-Technischen Fakultät

der Universität Siegen

Siegen 2018

Acknowledgement

Abstract

Various types of composites are known to have excellent and superior mechanical properties. The extremely high strength to weight ratio and the high resistance to corrosion as favorable mechanical properties, converts the composites to multifunctional structures in various applications. This thesis focuses on details of experimental investigations of fracture mechanics on two different composite materials: a *sandwich composite T-joint* and an *ultra-high performance concrete (UHPC)*.

The utilization of sandwich composites in aviation industry is significantly increased. In this respect, the aim of the current research is to identify the damage mechanism of sandwich composite T-joints and to obtain accurate material behavior under various loading and environmental conditions. For investigation of the sandwich composite T-joints, series of experimental tests have been carried out in quasi-static and dynamic loading conditions and failure mechanisms are investigated. Moreover, effects of working conditions during the flight on the behavior of the sandwich composite are studied. To this end, the natural environment is simulated experimentally which influences the strength of the T-joints. This effect is determined by accelerated ageing of the honeycomb sandwich T-joints.

Developments of material science as one pillar of modern technology, leads to substitute metallic materials with cementitious composites which can be counted a milestone in human living standards. Although a huge potential in application of UHPC material is given, technical information about the dynamic behavior of this material is still limited. In this dissertation, in order to study the UHPC response to the dynamic loading, series of spalling tests and dynamic Brazilian experiments have been conducted. In this regard, a linear elastic fracture mechanics-based approach is used to study the dynamic fracture and determine material properties under a high rate of loading. Parallel to the experiments, the performed tests on both mentioned composites, are numerically simulated in commercial finite element software.

By the obtained results from experiments on the sandwich composite T-joints, reliable technical information about the fracture behavior of this type of joint is provided. The achieved results prepare not only new data for the designers, but can also be used for future computational models of adhesively bonded composite T-joints. The outcomes of the experiments at high rate of loading on UHPC material, presents data regarding to response of this material to dynamic loading regime. The data extracted from the experiments can speed up the robust design and it is beneficial for future material developments and load carrying capabilities of this cementitious composite materials.

Zusammenfassung

Viele Arten von Kompositen zeichnen sich durch hervorragende mechanische Eigenschaften aus. Das extrem hohe Verhältnis von Härte zu Gewicht und die Resistenz gegenüber Korrosion sind bevorzugte mechanische Eigenschaften, welche im Werkstoffverbund zu multifunktionalem Verhalten beitrangen und zu einer Vielzahl an Anwendungsmöglichkeiten führen. In der vorliegenden Arbeit wurde der Schwerpunkt auf experimentelle Untersuchungen und die Anwendung der Theorie der Bruchmechanik auf zwei verschiedene Werkstoffverbunde gelegt: *zusammengesetzte Sandwich T-Stücke* und *ultrahochfester Beton (UHFB)*.

In der Luftfahrtindustrie hat die Verarbeitung von Sandwich-Werkstoffen erheblich zugenommen. Zielsetzungen dieser Forschungsarbeit sind die Identifikation des Schädigungsmechanismus von Sandwich T-Stücken und das Spezifizieren des präzisen Materialverhaltens unter verschiedenen Belastungen und Umgebungseinflüssen. Eine Serie von Untersuchungen der T-Stücke ist im quasistatischen und dynamischen Belastungsfall erfolgt- gekoppelt an verschiedene Modelle der Bruchmechanik. Zusätzlich wird der natürliche Umgebungseinfluss, wie er während des Fluges auf das Werkstück wirkt, untersucht. Hierzu wird der Werkstoffverbund künstlich und somit beschleunigt gealtert, um die Auswirkungen auf die Festigkeit beurteilen zu können.

Die Entwicklung der Materialwissenschaften als ein Träger moderner Technologie führt zum Austausch der Metalle mit Zement-basierten Verbundwerkstoffen, welche als Meilenstein zur Verbesserung des Lebensstandards beitragen. Obwohl ein hohes Potential in der Anwendung von UHFB gesehen wird, sind die technischen Informationen über das dynamische Verhalten limitiert. Hier werden eine Reihe von Spaltungsversuchen und sogenannte Brazilian-Tests durchgeführt, sodass eine Aussage über das Verhalten von UHFB im dynamischen Fall getroffen werden kann. Die Untersuchung des dynamischen Bruchs und die Bestimmung der Materialeigenschaften unter hohen Belastungen basieren auf dem Ansatz eines linear-elastischen Materialverhaltens. Die durchgeführten Experimente, angewandt auf die beiden oben genannten Werkstoffe, werden mit einer kommerziellen Finiten-Elemente Software simuliert.

Die resultierenden experimentellen Werte für das T-Stück und technische Informationen ermöglichen eine Bewertung des Bruchverhaltens für diese Klasse von Verbindungen. Die in dieser Arbeit erzielten Ergebnisse liefern nicht nur neue Informationen für die Entewicklung der Werkstoffverbunde, sondern Bilden ebenfalls eine Grundlage für zukünftige Rechenmodelle hinsichtlich der genannten T-Stücke. Es wurde festgestellt, dass das Experiment bei hohen Belastungsraten zuverlässige Werte liefert. Die Errungenschaften sind von großer Bedeutung für die lasttragenden Möglichkeiten des auf Zement basierten Materials.

Contents

List of Figures

List of Tables

1. Introduction

1.1. Research background

Materials play an essential role in improving human production, development of science and also living standards. With developments on the science and technology, various materials invented, and now material became a symbol of human progress in the science. However, materials are basis of the new technology, and materials science, energy and information science are the pillar of the modern technology. Materials science is the integrated discipline, with relationship with mechanical engineering. This thesis, in two phases focuses on details of experimental investigations and application of fracture mechanics on two different composite materials: a *sandwich composite T-joint* and *ultra-high performance concrete.*

High-tech demands of the aviation industry require a detailed knowledge of the mechanical and structural response of composite structures. The utilization of various composites has become increasingly attractive alternative to metals for numerous aircraft components. Many of the high-performance components in aviation industry are made of honeycomb sandwich materials. Their superior mechanical properties, in particular the unique stiffness to weight ratio, make them a favorable material in aviation applications. High durability, high corrosion resistance and damage tolerance are other properties of this family of material. In sandwich structures, the combination of face sheets and a core with different mechanical properties provides a coupled mechanical response which is difficult to predict. This holds particularly for connections and joints of such composites. Since the application of sandwich structures is rising in numbers and complexity, a detailed knowledge about the response and behavior of these materials under a variety of loading regimes, and also under different environmental conditions is necessary. In this respect, adhesively-bonded honeycomb sandwich T-joints are studied in this thesis. All the T-joint specimens are provided in cooperation with Diehl Service Modules GmbH [1] which is a certified company specializing in the design, production and maintenance of aircraft interiors. These specimens are produced by the material and manufacturing process which is used in many aircraft galley systems, see Fig. 1.1.

In applications for aircraft interior, the employed composites should meet mechanical properties and processability requirements. Composite parts in aircraft interior such as

Figure 1.1.: Narrow body of a galley under construction by sandwich composite (left) and final product for both Airbus and Boeing narrow body platform (right), photos from [1].

stowage bins, galley and sidewall panels are fabricated mainly by reinforced epoxy or phenolic resin, because of unique mechanical properties and excellent fire resistance. In practical use, damage on overhead stowage bins has been observed due to daily wear and to the changes in environmental conditions [5]. Moreover, the space behind the sandwich parts inside the aircraft cabin is usually used for fixing electrical wires or hoses which can lead to a permanent static loading. Although a large variety of aircraft interior components are designed and fabricated, experimental investigations on such adhesively-bonded honeycomb sandwich T-joint have not been performed so far. Therefore, the current research is an attempt to provide precise data for optimizing future engineering structural design. Moreover, since these sandwiches experienced various environmental condition and also a high rate of loading during their service life, accelerated ageing conditions are conducted and series of dynamic tensile tests have been performed to determine the behavior of the studied specimens. Based on the data of aged specimens, the remaining service life can be expected.

As the second composite material in this thesis, ultra-high performance concrete (UHPC), an innovative cementitious-based composite is investigated. This material and its variant are counted as new generation of concrete which have infiltrated to the various engineering applications. Despite of the huge potential in application, technical information about the dynamic behavior of this material is still limited. In the present day scenario, use of UHPC has been extended to a large number of applications, for instance, highway bridge, urban elements, nuclear facilities and penetration resistant structures. All shows that the number of completed UHPC projects has increased dramatically. In Fig. 1.2 application of UHPC material in Museum of European and Mediterranean Civilisations (MuCEM) is shown. UHPC material and its variant are currently under developments and study of their mechanical properties are still a subject of ongoing researches. These properties are including elastic and tensile moduli

under dynamic loading regime, creep behavior and freeze-thaw durability. In experimental investigations on tensile behavior of concrete and cementitious composites, attention to many test details is required.

In this thesis, in order to provide reliable data for next material developments and future computational models, UHPC specimens are constructed and series of tests under high strain rate have been carried out. By the spalling tests and dynamic Brazilian experiments, dynamic elastic modulus and dynamic tensile strength are determined. Moreover, dynamic fracture energy of this class of material is calculated. Since the UHPC samples are prepared with different recipes, the relationship of composition with dynamic mechanical properties, is also studied.

Figure 1.2.: Application of UHPC material in Museum of European and Mediterranean Civilisations, Marseille, French, photo from [2].

The obtained results form the experiments on the sandwich composite T-joints, provides reliable technical information about fracture behavior of this type of joint. By series of the tests before and after accelerated ageing conditions on sandwich T-joints, evaluation of the residual strength after usage on aircraft can be performed. Based on the data of the aged specimens, the remaining service life can be expected. The results prepared not only new data for the designers, but can also be used for future computational models of sandwich structures.

The outcomes of the spalling and dynamic Brazilian tests on UHPC material, presents failure mechanism of this material. It also provides precise data regarding to response of UHPC to the high rate of loading. These achievements are beneficial for future material design and load carrying capabilities of this cementitious composites material. Moreover, since there is lack of numerical models for this class of material, the determined mechanical properties can be used for next numerical modeling.

1.2. Objectives and scope of the research

Design of the structures required the knowledge of the material's strength and resistance. Lack of engineering data about behavior of material under various loading regimes leads to inappropriate construction and engineering fabrication. In this thesis, the dynamic fracture behavior of two brittle composite materials in various types of loading conditions are investigated which have never been rigorously investigated, so far. In this regard, two classes of composite materials are studied in this PhD thesis.

In the first group of studied composites, adhesively-bonded sandwich T-joints experimentally and also by numerical simulations have been investigated. The sandwich T-joints specimens are provided in cooperation with [1]. The main scientific and technical objectives which can be addressed within the scope of this part of the current research are as follows:

- assessment of current test techniques to apply on the adhesively-bonded honeycomb sandwich T-joints,

- determine experiment conditions for both static and dynamic loading regimes and conduct series of tests,

- accomplish accelerated ageing conditions to study behavior of the specimens,

- damage identification for the sandwich T-joints,

- perform the numerical simulation of the sandwich T-joint in a commercial finite element software (Abaqus) and simulate the experiments,

- document achieved data according to the response of sandwich T-joints to various loading rate and environmental conditions.

The specimens on the second group of studied composites are made by ultra-high performance concrete. Since this new class of material can response the need of aesthetics, strength and resilience of the various demands, its application is dramatically increased. For future material developments, precise data about the behavior of this material under high rate of loading is crucial. Therefore, various UHPC specimens with different geometries and recipes are constructed in contribution with [6] and utilized for various tests. In this thesis, series of spalling and dynamic Brazilian experiments have been carried out and the project's research objectives in this part are defined as:

- provision of different groups of specimens for the experiments,

- modify SHPB to run spalling tests on the cylindrical UHPC specimens,

- determine the dynamic mechanical properties of the constructed UHPC by spalling tests,

- numerical verification of UHPC specimens on spalling tests,

- employ SHPB to perform dynamic Brazilian experiments on circular and flat end UHPC samples,

- determine the dynamic tensile strength of the UHPC samples at high strain rate,

- numerical analysis of Brazilian test in Abaqus,

- document obtained results of the experiments at high rate of loading.

1.3. Outline of the present work

A brief outline of the coming chapters and their content is listed below. This will guide the reader through the structure and the basic conceptions of each chapter of the present thesis.

Chapter 2: The second chapter of this dissertation covers the historical background, classification and applications of composite materials. In the first part of this chapter, definition of fibrous composites, first usage and classification of composite materials are presented. Then, sandwich structures and their applications on the aircraft are explained. In the second part of this chapter, historical background of UHPC material as a cementitious-based composite is presented.

Chapter 3: This chapter described details of the studied sandwich T-joints and UHPC specimens. For this purpose, all the components of the honeycomb sandwich T-joints are explained and their mechanical properties are mentioned. Then, fabrication method of the sandwich T-joins are presented which are scaled part of the aircraft galley. Since some of the T-joints are experienced accelerated ageing, the detail of this environmental condition is discussed here. Moreover, details of the utilized UHPC specimens are also explained. Since the studied UHPC are prepared by different recipes, all the compositions are described.

Chapter 4: In this part of thesis, we review applications of artificial intelligence (AI) in the field of fracture mechanics and mechanical faults. In this chapter, the state of the art of five AI methods which are used in the field of fracture mechanics, is surveyed. This review is performed from the technical point of view on particular applications of artificial neural networks, Bayesian networks, genetic algorithms, fuzzy logic and case-based reasoning. After an overview of AI methods, sub-domains of engineering fracture mechanics with respect to the fault and failure analysis are described. The existing works are analyzed and discussed in four categories as sub-domains of fracture mechanics: (a) failure mode and failure mechanism identification, (b) damage and failure detection

and diagnosis, (c) fault and error detection, diagnosis and (d) mechanical fracture and fracture parameters. Our analysis and discussion in this paper shows the advantages, limitations and research gaps in this field. Finally, perspectives and future research directions are outlined.

Chapter 5: This chapter covers the experimental setup and the obtained results from all conducted tests on both groups of composite specimens. Indeed, in the first part of this chapter the characterization of adhesively-bonded composite T-joint is presented. For this purpose, details of series of experiments under quasi-static and dynamic tensile tests on aged and unaged specimens are explained, and the obtained results are presented. Then, crack propagation and fractographic examinations which are performed on the sandwich T-joins are discussed. In the second part of this chapter, details of the experiments on the UHPC material are presented comprehensively. In this respect, specifications of spalling test are outlined. Details of conducted spalling tests are explained and the achieved results are mentioned. Moreover, basis of the Brazilian test are presented, and then the performed dynamic Brazilian experiments on circular and flat end UHPC specimens are described. In the sequel, the microscopic inspections which are carried out on the fractured UHPC specimens, is reported.

Chapter 6: In the sixth chapter, numerical simulations are comprehensively presented. In this research, the studied sandwich T-joints are simulated by the three-dimensional finite element models in commercial software Abaqus. The analyses are computed and the resulting deformed structures before and after fracture are shown. Moreover, the spalling test is numerically simulated by MATLAB program. Within this context two numerical fracture methods are compared with respect to determination of main parameter like the tensile strength and the specific fracture energy. Finally, conducted dynamic Brazilian tests on UHPC specimens are also simulated in Abaqus. In this respect, to compute crack initiation and propagation, the eXtended finite element method was chosen and a two-dimensional model is implemented. The obtained results form all of the above-mentioned simulations shows good agreement with the experiments.

Chapter 7: The last chapter, concludes this thesis. It is explained that the obtained results form tests on sandwich composite can be used for applications development of this material. Furthermore, in this chapter it is briefly described that the determined mechanical properties of studied UHPC, can be used for future material development, and improvement of load carrying capabilities of this class of materials.

1.4. Publications of this dissertation

1. Mohammad Reza Khosravani, Kerstin Weinberg. Experimental investigations of the environmental effects on stability and integrity of composite sandwich T-joints. *Materials Science and Engineering Technology*, 48:753-759 (2017)

2. Sara Nasiri, Mohammad Reza Khosravani, Kerstin Weinberg. Fracture mechanics and mechanical fault detection by artificial intelligence methods: A review. *Engineering Failure Analysis*, 81:270-293 (2017)

3. Mohammad Reza Khosravani, Mohammad Silani, Kerstin Weinberg. Fracture studies of Ultra-High Performance Concrete using dynamic Brazilian tests. *Theoretical and Applied Fracture Mechanics*, 93:302-310 (2018)

4. Mohammad Reza Khosravani, Peter Wagner, Dirk Fröhlich, Reinhard Trettin, Kerstin Weinberg. Dynamic fracture investigations of Ultra-High Performance Concrete. Under review (2018)

5. Mohammad Reza Khosravani, Kerstin Weinberg. Characterization of sandwich composite T- joints under different ageing conditions. Under review (2018)

6. Kerstin Weinberg, Mohammad Reza Khosravani. On the tensile resistance of UHPC at impact. *The European Physical Journal Special Topics*, Accepted (2018)

7. Mohammad Reza Khosravani, Denis Anders, Kerstin Weinberg. Experimental tests and numerical investigations on strain rate effects on strength of composites sandwich T-joints. To be submitted (2018)

8. Mohammad Reza Khosravani, Kerstin Weinberg. Split Hopkinson bar and its applications on dynamic characterization of concrete and UHPC. To be submitted (2018)

2. Composites: historical background, classification and applications

In this chapter, definition and historical background of composite materials are presented. After that, classification of composites is discussed. Since the studied T-joints are made by sandwich composites, detail of this material is outlined and their applications on aerospace industry and particularity in aircraft interior are described.

In the second phase of this chapter, an introduction to cementitious composite and specifically UHPC material is presented.

2.1. Definition and history of composite materials

Composite materials are not new materials as such materials are known and have been used by ancient people. By the definition, a composite is a solid material, composed by two or more different and distinct substances, keep their physical properties, while provide desirable properties on the whole. Earliest uses of composite, is related to ancient people around 3400 B.C. which they glued wood strips at different angles to make plywood. Later, papyrus dipped in plaster or layers of linen were used to mummify by Egyptians. Another earlier uses of composite materials was to reinforcing mud with straw around 1500 B.C. by ancient constructors and artists.

In the 13th century, Mongols people around 1200 A.D. combined wood, bamboo, bone, horns, cattle tendons, silk and natural pine resin. With this composition, they made first composite bows which were powerful and highly accurate. It was feared weapons on the earth until the invention of firearms one century later. On the last three decades of 19th century, a revolution on chemistry occurred and synthetic resins transformed from a liquid to solid state in a cross-linked molecular structure. Early synthetic resins comprised melamine, celluloid and Bakelite.

Plastics, polystyrene, polyester and phenolic were developed in the early 1900's. Reinforcement was needed to provide the strength and rigidity. Bakelite is an early innovative plastic which is thermosetting phenol formaldehyde resin, formed from elimination reaction of phenol. It was used for its non-conductivity and heat-resistant properties in electrical insulator, radio and telephone casing and also in jewelry, kitchen walls, and

children's toys.

The most important decade for the composite industry is the thirties. In 1935, first glass fiber introduced and launched the fiber reinforced polymer (FRP) industry. One year later, unsaturated polyester resins were patented. Their curing properties converted them to the superior choice for resin in today's manufacturing. Also, in this decade other higher performance resin system like epoxies became available.

FRP industry came from research into real production by the Second World War. High strength to weight properties of fiberglass composites led to usage of them in radar domes and other electronic equipment. Although, the war attempted to develop first commercial model of boat frame, but was not developed and the technology was quickly commercialized after the war. In 1947 fully composite automotive has been mad and tested. The result was successful and it led to first generation of Chevrolet Corvette which was introduced in the 1953. It was made by fiberglass performs impregnated with resin and molded in matched metal dies. During these years, several methods for molding also were developed. Finally, two methods namely compression molding of sheets molding compound (SMC) and bulk molding compound (BMC) appeared as preferable forms of molding for the automotive and also other industries.

Several manufacturing methods developed in the early 1950's. For instance, pultrusion, vacuum bag molding and large-scale filament winding developed on that time. Filament winding converted to the base for the large scale rocket motors that led some discoveries on space in the 1960's and later. Also, pultrusion is used currently in the manufacture of linear components such as molding.

First carbon fiber was patented in 1961 and some years later carbon fiber composite were commercially available. Stiffness to weight ratio of thermoset parts are improved by carbon fibers. Thus, more applications in automotive industry, aerospace, sporting and consumer goods have been created. The marine industry was the largest customer of the composite material on that time. Fibers made from ultra-high molecular weight polyethylene in early 1970's. Large industrial developments occurred and usage of fiber in aerospace components, structural applications, sporting equipment, medicine industry and many other applications grown. On the other hand, new and improved resins caused more expand on composite application and market, specifically in higher temperature and corrosive applications. In comparison, the automotive industry outmatched marine industry as number one market of composite material which is keeping it up to today.

In the middle of 1990s, composite passed mainstream of manufacturing and construction. Composite materials used as an adequate replacement for traditional materials like metals by industrial designers and engineers. Application of composite materials developed more and consumers came into direct contact with composites from handles on their automotive to beauty painted entry doors of their homes. Composite began to effect on electrical transmission market by special products such as pole in line hardware and insulators [7].

Generally, composites can be constructed of any composition of two or more materials, whether metallic, non-metallic, organic or inorganic. Although larger part of historical

and durability information about FRP composite is related to the aerospace, marine and automotive industries, composites also used as a construction material for some decades. Currently, development is continued and grew number of applications and composite just found their way into nanotechnology. In the following part, classification of composites is presented.

2.1.1. Classification of composite materials

Composites and metals are significantly different regarding to the physical characteristics. Most of the composite materials are made by only two materials. In this case, one is the matrix. The matrix is enclosed and attached together fibers or fragments of the second material which is named reinforcement. The composite material can be heterogeneous mixture of two or more homogeneous phases that have been bonded together. The phases can be of essentially any material class, such as metal, polymer, ceramic, carbon or even void space. By this definition most highly porous materials are defined as composites. Several classifications have been done to classify the composite materials. For example they classified by:

- basic material combination, e.g., metal-organic or metal-inorganic,

- bulk-form characteristics, e.g., matrix systems or laminates,

- distribution of constitutes, e.g., continues or discontinues,

- function. e.g., electrical or structural.

Although, structural and geometrical specification have effects on properties of composites, clearly intrinsic properties of each composed materials have critical role on obtained composite properties [8]. In another classification, all composite materials are in the following three main categories:

- particle-reinforced (large-particle and dispersion-strengthened),

- fiber-reinforced (continuous and short fiber),

- structural (laminates and sandwich panels).

Evolution of composites regard to relationship to different classes of materials is shown in Fig. 2.1. Although thermoplastics and thermosets sound similar, they indicates different properties. With usage of fiber reinforced plastics, both thermoplastic and thermosets can bused as matrix. Thermoplastic matrix composites are tougher and less brittle than thermosets, with high impact resistance and damage tolerance. The thermoplastic composites production process is more energy intensive, because of the high temperatures and pressures required to melt the plastic and impregnate fibers with the

matrix. Thermoset composites are generally cheaper and easier to produce. They are commonly used for high-heat applications, since the thermoset matrix doesn't melt like thermoplastics. In some applications, the composites based on thermoset matrices can substitute for steel and concrete because of their higher resistance to oxidation than steel and also better freeze-thaw resistance than concrete. To be sure that designed material covered the service requirements, we should predict behavior of composite material accurately as result of the modeling. In recent years, theories about elastic behavior of composites are growth and developed and also predictions of elastic behavior of this material are most of the time satisfactory [9].
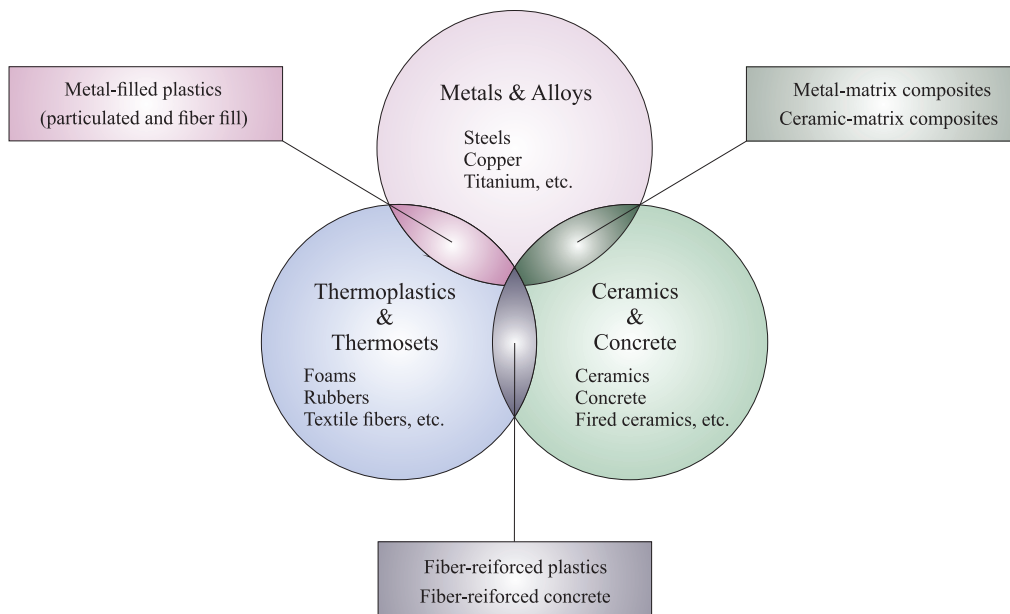
Figure 2.1.: Development of composite materials between different classes of materials.

The mechanical properties and several engineering aspects of different type of composite have been discussed in a number of books in last decades [10, 11, 12, 13, 14, 15]. Composite materials are subclass of anisotropic materials, concerning unidirectional composites they can be classified as orthotropic. Properties of the orthotropic materials are different in three mutually perpendicular directions. Compared with the metals, composites have different response to fatigue loading, corrosion and hydrothermal environment. About response to the impact, it should be mentioned here that, metals deformed but not really fractured while impacted, in contrast, composites made with thermoset matrices are extremely brittle and have low impact-toughness.

There is strong capacity in composite materials by suitable selecting the components, crystallographic characteristic and combination of the interfaces. These capabilities allow designing composite material regarding to the requests in different industries and

applications. Indeed, correct choosing an appropriated combination of matrix and rein-forcement, produced new material which exactly meet demanded of specific application.

Because of unique characteristics, composite materials can be considered versatile materials. Some of these properties are counted as high strength to weight ratio, im-proved fire resistance, longer fatigue durability, electrical properties, chemical, corrosion and weathering resistance, low thermal conductivity and design flexibility. Advances in composite science, leads using carbon fiber instead of glass which is lighter and stronger. After that, carbon nanotubes are used successfully to make new composites. These are extremely lighter and stronger than composite which are made by normal carbon fibers. Barely Visible Impact Damage (BVID) is a type of damage in composite material caused by a low velocity impact, which can be occurred during the operation or maintenance. This impact leads to minor damage on the surface of the composite and it's not readily detectable by visual inspection. The BVIDs can leads to significant internal damage within the laminate composites, for instance, delamination, fiber fracture and matrix cracking. The initial delaminations can slowly grow under alternating or fluctuating stress and leads to a loss in stiffness and finally a catastrophic failures.

The high-tech demands led to production of advance composite materials. This type of composites showed greater toughness. However, regarding to the advantages and despite to disadvantages, usage and consumption of composites is extremely increased over a wide range of applications. The following part, deals with one of the most applicable type of composite structure.

2.1.2. Sandwich-structured composites

Sandwich composite describes usually two almost thin and stiff facings which called skins (face sheets) which are separated by thicker core material. Unique properties of this composition make it desirable choice for large domain of industries. In fact, sand-wich structures exceptionally have high flexural stiffness to weight ratio compared with Monique and other architectures. Technical assessment shows the sandwich structure has high flexural stiffness to weight ratio, lower lateral deformations, higher buckling resistance and also higher natural frequencies, so it is shown important role in the struc-tures and used in wide variety of applications. The mechanical behavior of a sandwich composite depends on the material utilized for construction, geometry of the face sheets and especially the core topology design. Over the years various ordered cellular architec-tures with improved mechanical properties are applied to sandwich core configurations. The behavior of a sandwich beam under loading is different compared with a beam with a constant elastic cross section. The main concept of the sandwich panel is that exter-nal surfaces transfer loads effected by bending (compression and flexural load), while the core transfers load caused by shearing. Sandwich structure shows high fatigue resis-tance, and provide excellent mechanical properties to much lower weight than traditional monolithic materials. Different parts on the aircrafts are deal with bending loads. Ac-tually, bending of a plate by source of loading over the surface is equal to capturing the

edge and applying a moment or rotation. Bending theory assumed that the structure resist this moment by linear variation of stress through thickness. Therefore, maximum stresses occur at top and bottom surfaces. Stress at the middle of the plate thickness is zero (natural axis). The main advantage of the sandwich structure is that core separated the stiff outer skins and placing skins as far as possible from natural axis. Along to other properties, composite sandwich structures have energy absorbing properties to better withstand impact which is important issue not only for aircraft design, but also for automotive and mining industries. A composite sandwich consists of three main parts as is shown in Fig. 2.2. It is combination of different materials which are connected to each other and whole assembly employed properties of each separate component. Less material is used on manufacturing by sandwich material, so resources and weight are saved and leads to less energy consumption on manufacturing.
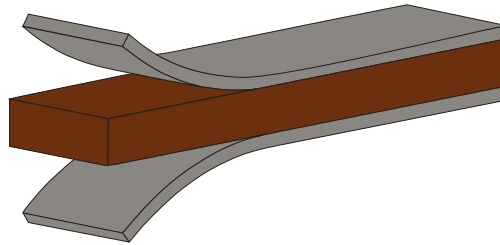
Figure 2.2.: Schematic of 3D composite sandwich part.

Advances in topology design and fabrication methods in sandwich composites, are answered lots of demands and requests. For instance, they are appropriate for thermal protection while they provided efficient load support. In fact, their superior mechanical properties, prepared them for use as multifunctional structures. Although there are several important advantages by consumption of sandwich structures, optimization in sandwich structures should be considered to determine minimum weight for structural geometry and loading conditions.

Generally, sandwich core materials are classified into two groups: (A): Homogeneous support of the skins, and (B): Non-homogeneous support of the skins. The homogeneous support of the skins can be made by open or close cells, and non-homogeneous support of the skins can be structured by punctual support, unidirection support, regional support and bi-directional support (honeycomb cores).

Most common materials which are consumed for cores, facings and adhesives are as follows, respectively:

  - cores: honeycomb, plywood, aluminum, rigid foam, balsa,

  - facing: aluminum alloy, FRP, fiberglass, plywood, stainless steel,

  - adhesives: epoxy, urethane.

It should be mentioned that, some other types of materials can also be used for the above mentioned parts [16]. In this project, honeycomb is used as core on the T-joint specimens. As it is mentioned in [17], the first honeycomb core patent, which consists manufactruring method for the fabrication of Kraft paper honeycomb, is the Budwig patent, issued in 1905, Germany. In general, honeycomb can be made from Nomex, Aluminum or thermoplastics. Usually, honeycombs are made by expansion process or corrugated process. The second production method is most common method for high density honeycomb materials. The honeycomb material which is used on the specimens for current project, is fabricated by expansion method. The honeycomb sandwich plates which are used in the T-joint specimens of this current project, are manufactured by Euro-Composite [18] a global player in the field of high-quality and sophisticated composite materials. In [19] Euro-Composite described comprehensively manufacturing process of honeycomb core material made by aramid paper and phenolic resin used in aircraft structures. It should be noted that Nomex is a synthetic aromatic polyamide polymer which provided superior properties when converted to various sheet forms.

In response to the requests in various industries, honeycomb cells are produced in different configurations. They produced in triangular, square, hexagonal and some other shapes. Most common cellular honeycomb configuration is standard hexagon. It is basic configuration and it is available for metallic and nonmetallic materials. Fig. 2.3 shows three different types of honeycomb as core on composite sandwich plates.
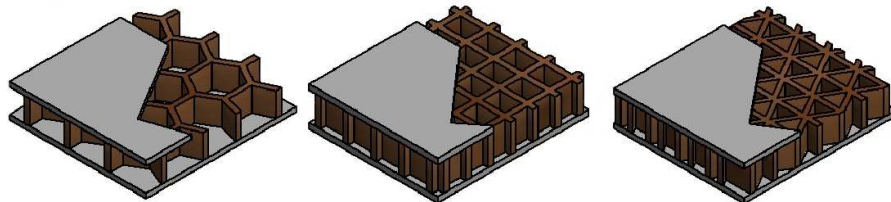
Figure 2.3.: Different forms of honeycomb as core in composite sandwich plate.

The expansion process is started with arranging large number of sheets of substrate material that adhesive node lines already printed. After that, adhesive lines are cures to form a HOneycomb Before Expansion (HOBE) block. This can be cutted and stretched perpendicular to the strip bonds to create hexagonal structures. To obtain expanded blocks, the HOBE could be expanded. Then, expanded block are cutted to desired thickness (T). Finally, the expanded sheets are adjusted and cutted in desired ribbon direction (L) and transverse to the ribbon direction (W). By expanding and overexpanding in the W direction, other configurations with different mechanical properties can be provided. In particular, for aramid fiber honeycomb which is used in the studied specimens of the current research, outstanding properties are as follows:

- high thermal and fire resistance,

- wide range of cell size and densities,

- possibility in choosing from different strengths,

- high level of formability,

- high acoustic insulation properties,

- relatively low dielectric properties.

Another part in the sandwich-structured composite is skin. Skin which is also called face sheet can be made from composition of different fiber with epoxy, for instance glass fiber or carbon fiber with epoxy. Although there is limitation on these materials, they have special properties which converted them to preferable materials for designers and manufacturers. For stiffness critical applications carbon fiber reinforced plastic is used as the skin. The skins should provide the stiffness and strength of the part while honeycomb core separated the skins and transmit shear forces.

Comparison between stiffness and weight of solid panel with sandwich panel is shown in Fig. 2.4. As it shown, by choosing sandwich part instead of single skin part, the flexural strength and rigidity can be significantly increased. The values are taken from ATM Airframe Handbook [20] which are calculated by using typical beam theory. Indeed, strength and stiffness of the structure, is dramatically increased by separating two materials with a lightweight material in between. The ratio between the core depth (t_c) and the facing thickness (t_f) is typically large, $t_c/t_f \geq 4$ which allows for a number of simplifying stress analysis assumptions. By employing the face sheets impact resistance and wear resistance would be increased.
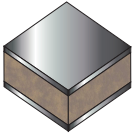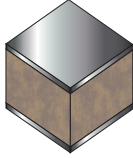
	Solid material	Core thickness t	Core thickness 3t
Stiffness	1.0	7.0	37.0
Flexural strength	1.0	3.5	9.2
Weight	1.0	1.03	1.06

Figure 2.4.: Comparison of stiffness, strength and weight of solid panel and sandwich panel.

Several aspects on different sandwich composites are studied and investigated by researchers in the last years experimentally and by numerical simulations [21, 22, 23, 24, 25, 26]. In [21] composite T-joint specimen made of multi layers of woven are investigated. The researchers conducted experimental and numerical analysis to study bending strength of transversely stitched T-joint. Experimental tests and finite element analysis (FEA) performed to determine failure modes. They found that proportional limit increased when the T-joint web thickness is increased. Also, increasing the base flange thickness had effect on increasing the proportional limit and flexural stiffens. By the omprehensive fractographic analysis it's shown damage progresses in the failed specimens while load is increased. Later, structural properties of z-pinned composite T-joints determined in [23]. The researchers extended previous study and proved that increase the volume content of z-pins causes a rapid increase to the ultimate strength and failure displacement of T-joints. In fact, their research shows z-pin increased the T-joint properties on both pull-off (pure normal tension) and mixed loading (normal tension and in-plane secondary bending). Regarding to their research, z-pinning does not significant effect on the in-plane elastic properties of the composite and so it couldn't increase fracture resistance of T-joint against the crack initiation. In work [24] sandwich structures which are used in high-speed trains are experimentally tested. The authors conducted three-point bending test on sandwich composite made by aluminum skins and Polymethacrylimide foam core. They obtained static strength which shows agreement with the prediction formula. Moreover, cyclic loading is used to investigate fatigue properties and damage evolution. More recently, ageing effects on static mechanical properties of carbon fiber reinforced composite are investigated in [26]. Here the researchers fabricated specimens by laminated panels and exposed the specimens to an ageing temperature of 200°C which represents aerodynamic heating at the surface of the aircraft. By means of low velocity impact tests, variations in failure mechanism are determined.

In fabrication of sandwich composites panels, low density materials (metallic or non-metallic) like aluminum, Kevlar and polypropylene are employed as a core. However, applications of sandwich-structured composites dramatically increased and these applications in the aviation industry, especially in civil aircrafts are discussed in the following part.

2.1.3. Aerospace applications of sandwich composites

Application of composite in aircraft interiors is concerned to the several decades ago. There is some years distance between design of sandwich structure and commercial production of them. Indeed, aerospace industry has an important role in development of composite materials. In 1971 Kevlar introduced to the world which is registered trademark for a para-aramid synthetic fiber. On that time, it was used as a replacement for steel in racing tires. At present, it has lots of applications, because of high tensile strength to weight ratio and various parts in aircraft cabin interiors such as overhead bins, side walls, ceiling and bulkheads are made by Kevlar and Nomex (contain aramid

fibers) honeycomb cores. These types of sandwich-structured composite parts can be employed in aircraft industry and also in similar applications on other transportation industries. Generally, assembly cost is about 50 percent of the costs of an airframe. Composites provides considerable reduction not only on amount of assembly labor, but also on quantity of required fasteners [16].

In the first uses of modern composite in aircraft, boron-reinforced epoxy composite was used for the skins of the empennages of fighters. Although honeycomb sandwich structures are light, stiff and a vital element of many modern aircraft interior designs, they need local reinforcement in load-bearing areas or in fixation points like inserts. Reinforcing and also edge finishing of such panels can be time consuming and costly issue, but it is necessary. Reinforcement is needed on open sandwich edges to prevent from impact damages and moisture ingress. The use of composite materials in commercial aircraft is attractive because reduced airframe weight leads fuel efficiency and therefore lowers operating costs. The formability of composite materials has been used to particular advantage in helicopter manufacture to reduce the numbers of component parts and therefore cost.

Currently, aircraft interior are made by sandwich parts which kept a core between outer skins. The separation of the skins, which carry the load, by a low density core, increases the moment of inertia of the structure with little increase in weight producing an efficient structure. The design process of sandwich structure is essentially one of optimization wherein a property such as weight or stiffness to unit weight is minimized. Four different materials are used in composite aircraft sandwich structures. They are Aramid paper honeycomb, Glass cloth honeycomb, Aramid cloth honeycomb and Aluminum alloy honeycomb. The structure in passenger aircraft and especially components inside the cabin involved different types of composite materials where requests are not only high stiffness to weight ratio but also fire safety properties is an important factor. Although lots of parts in aircraft interior made by sandwich structure (honeycomb core) and adhesively joints, lack of dependable failure criteria still exist.

Several parts of aircraft interior are made by sandwich composites. Some advantages of the usage of composites in aircraft interior are as follows:

- reduction of weight,

- excellent fire resistance properties,

- reduction of energy and material consumption,

- high corrosion resistance,

- modular design,

- quick installation,

- flexibility in color and surface design.

Utilization of the composites and sandwich-structured composites are not limited to the aircraft interior and it's expanded to use in other parts as well. For instance, landing gear doors, ailerons and doors are manufactured by Kevlar and Nomex honeycombs which are strong and light.

Aircraft fairing is a structure which is produced a smooth outline and reduces drag. In fact, aircraft and spacecraft usually experienced substantial vibrations and fatigue in wing-body fairing. To reduce vibration and fatigue, several attempts have been conducted in the past to solve the problem, but they have been heavy and expensive damper devices which also increased weight and complexity and other types of problem occurred. Another application of honeycomb in today aircraft industry is making wing-body fairing which is attached between wing and the body of the aircraft and it was made by aluminum in the past.

It should be noted that beside of civil aircraft (both private and commercial aircrafts), military aircrafts also have parts which are made by composite materials. However, there are some limitations on usage of composite materials on military aircrafts. For instance, not only cost of composite substructure preparation is too much, but also the cost of repairing damaged part is too costly as well and limited tolerance of the composite to ballistic impact are made some limitations on application of composite in military aircrafts [27].

Sandwich-structured composites provides high flexibility in design and production, since the complex shapes and complicated geometries can be easily fabricated by them. In contrast, maintenance of the parts which are fabricated by the carbon fiber is difficult. Indeed, biggest concern for composite materials on aircraft is the maintenance, repair and overhaul. Generally, the maintenance and repair of metals in aircraft are much more standardized compared with composite materials. Damage and defect can be occurred almost in any stage of production procedure or during service time. In several cases, it's possible to recognize damage by visual inspections. As a type of damage, BVID can be occurred in sandwich composite in aviation industry. In design of the composite structures three issues have been considered: (a) Strength as related to BVID, (b) Damage tolerance as related to Visible Impact Damage (VID) and (c) Environment and events related to several issues such as temperature, moisture, bird impact and tool damage. Small damages defined as BVID may not be found during heavy maintenance general visual inspection using typical lighting conditions. BVID can cause significant degradation of structural properties. Buckling failure may occur if the damaged laminate is subjected to high compressive loading. In the design stage, it is considered the airframe must support design limit loads without failure. Regarding this aspect, all structure is required to have a viable repair plan as part of the product definition data. Since composites have been used in structurally critical areas, the need for better methods of evaluating structural integrity is increased. In this respect, and in composite material quality assurance and control, nondestructive tests can be used. For instance, test can be performed based on the monitoring of the nonlinear elastic material behavior of damaged material.

Various developments have been conducted during several decades of composite uses in aerospace industry. Since 1970 utilization of composite materials in aircraft production is significantly increased. Moreover, as substitution materials for metals, the composites are extremely used on the older aircraft.

It should be noted, beside of aircrafts, other aerospace vehicles used composite materials as well. For instance, helicopters, satellites, missiles and space shuttle used honeycomb. Fig. 2.5 shows estimated usage of composite structure in aerospace [28]. As can be seen, commercial aircraft with more than 60% of the market share is the biggest consumer. In 2015 it is reported that more than 36000 commercial aircraft will be required for the demand of next 20 years [29]. In [30] it is predicted that aerospace composite market to reach US$ 24.8 Bn by 2024.
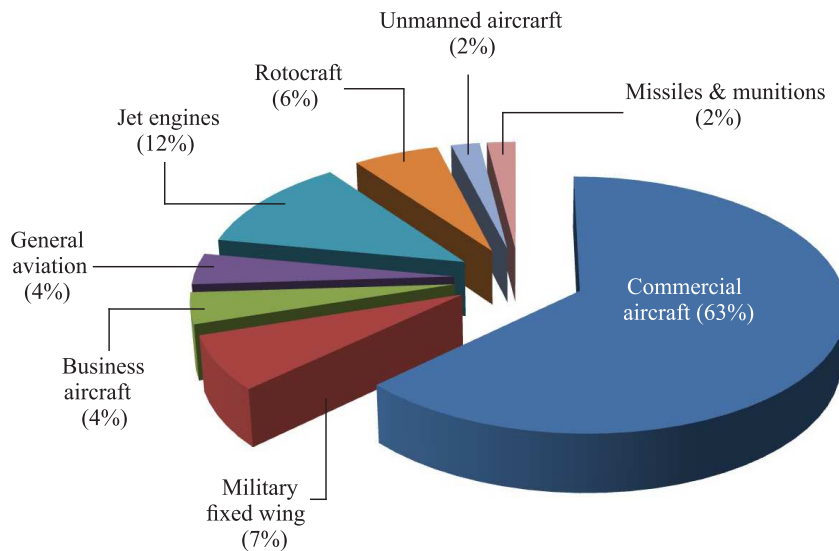
Figure 2.5.: Predicted 2013-2022 market of composite structures in aviation industry.

Fuel costs increased and on the other hand aircrafts have large effect on environment and climate changes. Thus, commercial flyers are under pressure to improve the performance, and weight reduction is a key factor in this matter. Significant increase in passenger aircraft, emerging economics, competition in low cost carries play vital role in progress on the market aerospace composites. As reported in [30] carbon fiber composites shows more than half of the total demand of aerospace composite in 2015, but since manufacturing process of aramid fiber composites is comparatively easy, this type of composite is also on the path of the progress. However, future of composite looks for expansion and exciting new innovative product is always on the horizon.

2.2. Introduction to cementitious composites

The second studied composite in this research is a concrete-like material which is a cementitious composite. In recent years, many types of cementitious composites with and without fiber have been developed by materials scientists. These developments provides new opportunities in engineering constructions. In this work, focus is placed on a non-fiber cement-based composite. Since, all these composites are concrete-like materials, in the following part history of concrete is presented. Then invention and the first applications of the studied material is explained.

2.2.1. Historical background of concrete

Various types of lime and mortars are described and characterized ancient time. On the book entitled "The Ten Books on Architecture" which is excellent historical reference into ancient construction methods, scientists and researchers indicated that the cement mentioned and described in the historical books is similar and somehow admirable compared with Portland cement used currently [31].

The word "concrete" may indicates several different versions, but all had their own unique mixture. The records of concrete usage shows at least 6500 B.C. when it used to build structures that are survive to this day, but cement is thought to be older than humanity itself, and recorded having formed naturally 12 million years ago [32, 33]. From the late Middle ages, concrete was used mainly in foundations. Until the mid-eighteen century, concrete and mortar are used in traditional buildings, what we now named concrete and lime mortar. Pure lime hardens by reaction with atmospheric carbon dioxide from calcium carbonate. It is a slow process and cannot occur under water, so such lime is named non-hydraulic. The greatest civil engineer of the 18th century, John Seamton found that the calcination of limestone containing clay led a lime that hardened under water (hydraulic lime). He used hydraulic lime to rebuild Eddystone Lighthouse in Cornwall, England which he had been commissioned to build in 1756, but had to first invent a material that would not be affected by water. Later, James Parker in 1796, patented a natural hydraulic cement by calcining nodules of impure limestone containing clay, called Parker's Cement or Roman Cement. The word 'cement' was used to signify this material until the middle century, when it came to refer to its replacement Portland cement [34]. As it is stated in [35] perhaps the first recommendation of an idea for reinforcing concrete was description by J.C. Loudon in 1830. He suggested that flat roofs can be constructed of a latticework of iron tie-rods thickly embedded in cement, and cased with flat tiles. Later, earliest patent of reinforcing concrete was by W.B. Wilkson [36]. In Canada, the first production of lime and hydraulic cement carried out in 1830, afterwards for the first time systematic experimental tests of tensile and compressive strength took place in Germany, 1836. About three decades later, importance of true clinkering documented and the first American patent for Portland cement issued. From the 1870s, almost every week in technical press published examples of houses made

basically from concrete, which show growing interest to this material. In 1936, the first major concrete dams were built, which they still exist today [37].

Concrete can be defined as cement-matrix composite. It's consists of a hard, chemically inter particulate substance known as an aggregate which is bonded together by cement and water. This aggregate can be composed by stone, crushed stone, gravel, ashes, slag. In the beginning utilization of concrete, it has been realized that various sizes of the aggregate leads to resulting concrete with different strength. Also, it is declared that the aggregate should be clean to avoid degradation of the concrete. These days, aggregate usually categorized by size. Fine aggregate refers to the size of the aggregate particulates which are small and when they used it leads to smooth surface on the concrete. For the massive structures, usually coarse aggregate is used. Concrete has been utilized for various things, including infrastructure and architecture. During the twentieth century, a steady rise in the strength of ordinary concrete is observed. The chemical processes and importance of ensuring the right condition of concrete fabrication became better understood. Knowledge about parameters that influences the durability of concrete successfully developed. On that time, calculation of concrete strength became necessary, especially for the large structures and it was measured by crushing a cube of a concrete. By the 1930s, typical concrete cube strength improved and raised. Afterwards, using special mixture led to production of higher grade concrete.

Along the years, not only demands for new and wider roads and bridges increased, but also technological developments required new materials with different properties. In order to respond these demands in the construction field, various concrete types created, such as High Strength Concrete (HSC), Ultra High Strength Concrete (UHSC) and High Performance Concrete (HPC). In the middle of the 1990s, utilizing of the quartz grain, silica fumes and superplasticizers provided UHSC [38]. Parallel to the increase in the application domains, these materials have been studied in wide range of loading from quasi-static loading to impact loading regimes. For instance, different types of concrete are tested by researchers under wide range of loading rates in the recent years [39, 40, 41].

However, applications of concrete in engineering structures increased in today's world. The technical information are more widely available and experiences are exchanged which leads to more publications and material developments.

2.2.2. Ultra-high performance concrete (UHPC)

In the current research, the second group of the studied composites is cementitious composite. Here, this material is briefly introduced and later the experiments on this type of composite material are described comprehensively. For engineering structures, important buildings and also specific structures it is vital to strengthen the structure through utilizing the new technology or new materials.

With developments in different industries, need of improved concrete appeared which led to production of Reactive Powder Concrete (RPC). Richard et al. [42] presented RPC by increase reactivity and fineness and very low water to cement ratio in 1993. On

year later, the term Ultra-High Performance Concrete (UHPC) is introduced by Larrad [43]. The world's first engineering structure which is made by UHPC, it's the Sherbrooke footbridge in Sherbrooke, Canada which is built in 1997 [44] and later application of this material in all continents is significantly increased [45, 46]. This material has been under fast development in recent years which provided several improvements. In 2005, ambitious research program started in German universities over the six years under guidance of the university of Kassel where published the obtained results [47, 48, 49]. After successful construction of UHPC, attempts have been made to optimize this material. In this respect, different types of fibers such as steel, carbon, glass and asbestos fibers with different geometries have been added to the UHPC and Ultra-High Performance Fiber-Reinforced Concrete (UHPFRC) produced and studied [50, 51]. It should be noted that, special curing such as heat and autoclave curing ply important role to produce material with higher strength. However, these materials show excellent capability of utilizing in nuclear facilities, explosion and penetration resistant structures [52, 53, 54]. Concrete, UHPC and their variants such as HSC, UHSC and UHPFRC are known to exhibit superior mechanical properties and unique response to the different loading condition [55, 56, 57]. In fact, UHPC as a new generation of concrete is material with favorable properties. The term UHPC reffered to very advanced cementitious based composite whose mechanical strength and durability surpass classical concrete. In Fig. 2.6 the most important properties of the UHPC compared with concrete are shown.
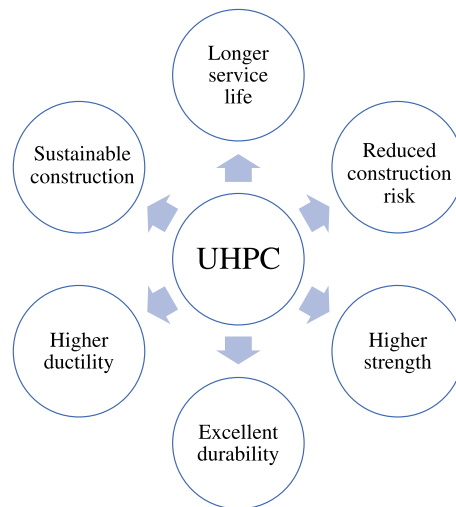
Figure 2.6.: The most important properties of UHPC compared with concrete.

With desired behaviors of UHPC materials under different loading conditions, applications of this material increased very fast. Although concrete and concrete-like materials has been somewhat in competition with other material like steel in the recent years, providing reliable data for future material development seems to be necessary. Currently,

special buildings such as military objects and cooling towers of modern atomic power stations are examples of UHPC consumption. UHPC indicate and proved that it is expand of consumption of concrete into new composition and formats that have been already nearly impossible. In fact, usage on nanotechnology is a result of higher performance material demands in cement and concrete industry. However, some structures made by concrete and UHPC might be experienced dynamic loading such as explosion, blasting or projectile-impact during their service time. Therefore, it is an interesting topic issue, and new perspective of UHPC material is one of the current topics in German committee for structural concrete (DAfStb). In this research, we conducted series of spalling tests and dynamic Brazilian experiments which are presented with the details in chapter 5.

3. Preparation of composite specimens and mechanical properties

To study effects of loading rate and influences of different environments on stability of the sandwich T-joints, knowledge about the concept of the sandwich composites is necessary. Moreover, at this point it is crucial to know details of the UHPC composition in order to determine material properties under dynamic loading regime, for future computational models and material developments.

In this chapter, all the parts of the sandwich T-joint which are the core, the face sheets and the adhesive are described and their mechanical properties are presented. Then, fabrication of the T-joint specimens is explained. It should be pointed out that in this research all the studied sandwich T-joint specimens are fabricated from the same composite materials as real aircraft interior. Furthermore, this chapter presents composition and preparation of the studied UHPC specimens.

3.1. Sandwich composite T-joints

Currently, the various parts in the aircraft interiors are being designed to take full advantages of composite properties. The extraordinary mechanical properties of various types of sandwich composites, converted them to favorable in aviation industry. In fabrication of sandwich composite components in commercial aircrafts, most of the structures must be assembled from individual components. Therefore, it is needed to chose proper method of the joining. This is more vital, when adhesive should be used, because optimal amount of adhesive must be utilized to avoid significant weight penalty. In fact, advanced technology should be employed to reduce weights to the minimum. Moreover, in design and preparation of the joints, avoiding local stress concentration is taken into account, because it can reduce the lightweight advantages. One important benefits of the adhesively bonded joints compared with some other types of the joints, is keeping structural integrity, specially in composites. This integrity is not preserved, when bolted or riveted composite joints are fabricated, because in these types of joints fiber are cutted and stress concentration is introduced. By usage of adhesive joints instead of rivet or fastened connections, fabrication of complex shapes are more applicable, while reduced

weight can be obtained. For comprehensive analysis of sandwich structures, complete understanding of material and details of the sandwich components is needed. In this regards, the used honeycomb core, GFRP skins and utilized adhesive are described in the next sections, respectively.

3.1.1. Honeycomb material and mechanical properties

Numerous researches are performed to study properties and behavior of sandwich composite with honeycomb core by considering different aspects and goals [58, 59, 60, 61, 62, 63]. Basically variety of types of sandwich structures depended on the configuration of the core. In general, core materials are divided to four following types: foam core, honeycomb core, corrugated core and web core. A honeycomb structure is the most efficient configuration to provide optimum mechanical performance per unit weight [17]. Nomex honeycomb which is presented extremely high strength to weight ratio is one of the most common core materials. Nomex paper is fabricated from short fibers called floc and small binder particles which are called fibrids [64]. In order to keep the effectiveness of the sandwich structure, the core must be strong enough to withstand the crushing or compressive loads occurred on the structure or part. Fig. 3.1 illustrated hexagonal honeycomb which is used in this project. L, T and W indices are referred to the length (ribbon direction), thickness (out-of-plane direction) and width (transverse to ribbon direction) of the honeycomb, respectively. Gluing the paper sheets on the manufacturing process produced double cell walls in L direction, see Fig. 3.1. In fact, the honeycomb core is composition of double cell walls and single cell walls.
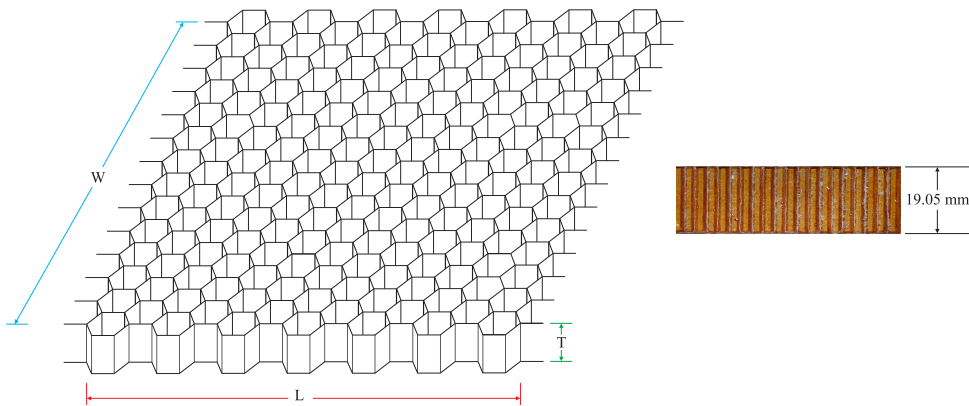
Figure 3.1.: The employed hexagonal honeycomb.

Nomex honeycomb is stable chemically and insulated thermally and electrically. It is also self-extinguishing which has high resistance on corrosion (against water, fuel and oil) and fatigue loading condition. Nomex which used here as core, is fabricated from ribbons of aramid paper which running in the longitudinal and ribbon directions. In the

production, they are glued together at intervals along the ribbons and then the stack of the ribbons is expanded into honeycomb by pulling in transverse direction. Two layers of aramid paper bonded together in double cell wall through adhesive [65, 66, 67]. Because of the mentioned construction method, unlike most of the sandwich foams, the honeycombs are anisotropic materials. The Nomex paper which is used in this study, is produced from fibers aligned in the direction of travel of the paper machine, and using corrugation and expansion processes provides directional dependence of mechanical properties. In detail of honeycomb production by expansion, firstly adhesive applied to the basic honeycomb material at right angles to the direction of expansion. Changes on width of the adhesive lines and distance led to changes in honeycomb cells. After that, web of the base material is folded into sheets which are stacked using a specific geometry. Length of the sheets determined width of subsequent honeycomb block. Also, number of sheets defined the length of expanded block. Large stacked block is produced by assembly of thousands of sheets. This block is then cured in heated press at high temperature and pressure. After curing process, the blocks expanded and finally dipped in suitable phenolic resins. It is provided the honeycomb core with proper mechanical properties and favorable density [68]. Both solvent-based and water-based phenolic resins are used in manufacturing process of honeycomb.

There are several different types of Nomex papers, while each type is for specific application. Nomex paper type 412 mostly used in honeycomb structures for aircraft and aerospace applications. In this study, the consumed core for the T-joint specimens is hexagonal Nomex honeycomb with cell size and the density of 3.2 mm and 48 kg/m^3, respectively. It should be noted that the basic material of the honeycomb core is phenolic resin impregnated Nomex aramid paper. As mentioned earlier, honeycomb is manufactured in expansion process. In detail, the used core is expanded from Nomex aramid paper (Nomex T412) which has nominal thickness of 0.054 mm. It has also weight and density of 40 g/m^2 and 0.74 g/cc, respectively. The relative density of the core without resin can be calculated 0.045 by following equation, [69]:

$$\frac{\rho^*}{\rho} = \frac{8}{3}\frac{t}{c} \rightarrow \frac{\rho^*}{\rho} = \frac{8}{3}\frac{0.054}{3.2} = 0.045 \tag{3.1}$$

where t is the thickness of the single cell walls and c is the cell size of the honeycomb.

The total weight of the Nomex T412 aramid paper without resin in 1 m^3 honeycomb block is 33.3 kg. Thus, the weight of phenolic resin in 1 m^3 honeycomb block is 14.7 kg. The density of the phenolic resin is about 1380 kg/m^3 [67]. Therefore, the volume of phenolic resin in 1 m^3 honeycomb block is about 0.01 m^3, which is indicated that the contribution of the phenolic resin to the relative density in the honeycomb block is about 0.01. Moreover, the relative density of the honeycomb core is 0.055. If we assume uniform distribution of resin on the surface of both honeycomb single and double cell walls, the relative density of the honeycomb core with a uniform wall thickness could be

27

calculated 0.016 mm from following equation, [69]:

$$\frac{\rho^*}{\rho} = \frac{2}{\sqrt{3}}\frac{t}{l} \tag{3.2}$$

where l is the edge of the cell. Thus, in each side of cell walls the thickness of resin layer is 0.008 mm. As the single cell wall is contains of two resin layers and one aramid paper layer, the total thickness of resin-dipped honeycomb single cell wall is 0.07 mm. Also, the double cell wall consists of two resin layers and two aramid paper layers, so the total thickness of resin-dipped honeycomb double cell wall is $[(2\times0.054)+(2\times0.008)] = 0.124$.

It should be mentioned that, the thickness of the resin and the paper layer in double cell wall are the same with the single cell wall. Some mechanical properties of the aramid paper are listed in Table 3.1. In the table E, S and δ represented elastic modulus, tensile strength and elongation at break, respectively. Also, MD and XD indices refer to machine direction and cross machine direction. The elastic modulus and strength of the phenolic resin are 5.8 GPa and 60 MPa, respectively [70]. Since aramids shows 5-10% higher mechanical properties compared to other synthetic fibers, they are displacing metal wires from high performance applications, like aircraft. Beside of the strength, the weight reduction and impact damage tolerance are vital factors in fabrication of aircraft composite parts. According to [71] aramid reinforced composites are able to absorb 2-4 times as much energy as carbon fiber material.

Table 3.1.: Some mechanical properties of aramid paper.

Material	E_{MD} (GPa)	E_{XD} (GPa)	S_{MD} (GPa)	E_{XD} (GPa)	δ_{MD} (GPa)	δ_{XD} (GPa)	ρ kg/m^3
Aramid paper	3.1	1.6	88	35	9.6	6.5	740

Aramid papers are interested by aerospace industry not only because of their elastic modulus, but also for their tensile strength and low density which is lower than glass fibers and even carbon fibers. The mechanical properties and behavior of the aramid papers should be understood prior to the undertaking the design of structures using this material.

In this project, Nomex honeycomb with thickness of 19.05 mm as the core of the sandwich T-joint specimens, is used. The properties of honeycomb core however are very different with and without the support from the face sheets. The honeycomb mechanical properties that are generally determined are bare compressive strength, and L and W plate shear strengths and moduli. It should be noted that the bare compressive test is just used for a quick quality assurance test while the stabilized compressive test (honeycomb with skins bonded on) is used for design purposes. Hexagonal cell honeycomb is orthotropic, thus the L or ribbon direction has much more shear strength and modulus as the W direction. According to the datasheet of the manufacturer [18]

some mechanical properties of the consumed core material summarised in Table 3.2. The compressive and shear moduli not change very much with thickness changes, but the shear strength decrease when the thickness increases. This change in properties is important and should be considered in design phase. Initially, such honeycomb products are used in high-tech products such as interior paneling of civil aircraft.

Table 3.2.: Some material properties of used Nomex honeycomb.

Compression	Plate shear			
Bare	L direction		W direction	
Strength (N/mm^2)	Modulus (N/mm^2)	Strength (N/mm^2)	Modulus (N/mm^2)	Strength (N/mm^2)
2.10	48	1.32	30	0.72

It should be mentioned here, Poisson's ratio of the core is equal to 0.2 and shear modulus of the consumed honeycomb is $G = 26.25 \, \text{N/mm}^2$. As it mentioned earlier, in process of Nomex honeycomb fabrication the paper substrate is dipped to suitable phenolic resin. The phenolic resins are large family of polymers and oligomers. They are used in large variety of applications from home to commerce and industry. Phenolic resin is a heat-cured plastic formed from a reaction of carbon-based alcohol and a chemical called aldehyde. In the previous century they used on cooking tools and decorative doors and in the current century extensively used for electronic circuit boards. Although epoxy resins have superiority over phenolic resins (because of better adhesion), the phenolic resins are applied in lots of specific applications. Indeed, the phenolic resins are consumed for the parts which should meet the fire safety, low flammability, low smoke development and special requirements for combustion and toxicity emission. If the resin exposed to extreme heat, very few toxic fumes distributed. This property which is key benefit of phenolic resin, converted it to desirable for consumption in aircraft parts. The resin could be brittle when cured, so the cured resin is usually mixed with small amount of natural or synthetic fibers to avoid breakage.

High heat and chemical resistance, also good thermal and dimensional stability are counted as specifications of cured phenolic resin. These parameters and also mechanical properties improved with level of cure and post curing process.

3.1.2. Face sheet materials and mechanical properties

The purpose of the composites utilization must be clear in particular usage, in order to choose proper material and composite constituent. In the present day scenario, applications of different composites has been significantly increased to a large number of aircraft components, both structural and non-structural, based on various factors such as in-service loading and environmental conditions. In this respect, choose the right type of structure is a crucial issue. In principle, on the sandwich structures with core and

face sheets, the face sheets are used to provide stiffness, thermal stability and to carry out in-plane and bending loads while applied to the sandwich part or structures. In this regard, several materials can be used as sandwich face sheet. The commonly used fibers for interior aircraft application are glass fibers.

Fiber reinforcement polymer (FRP) which is called also Fiber-reinforced plastic is composite made of polymer matrix reinforced with fibers. These fibers are usually glass, carbon and aramid. Also, polymer is usually an epoxy or polyester thermosetting plastic. The glass fibers are based on silica with additions of boron, calcium, sodium, iron or aluminum oxides. They are produced from raw materials and divide to two categories which are low-cost general purpose fibers and premium special-purpose fibers. FRPs are extensively used in different industries, such as aerospace and automotive [72].

In this project glass fiber reinforced plastic (GFRP) is used as face sheet. During the past years, application of this type of composite is increased from few small access panels to lots of parts, thereby weigh saving and improved performance are achieved. When this composite used for the panel, it gives a unique look. The most important factor is weight reduction, because it directly influences efficiency and the economy. In fabrication of the sandwich T-joint specimens, two different types of GFRP are used in each side of the honeycomb core. These types of composites, are light and fire-retardant aerospace material which are ideally suited for interior and structural components. For instance they used in galleys, floor panels, cabin lining, ceiling panels, side walls, partitions, overhead bins and air ducts. The phenolic prepreg which used are consisted of Gurit PHG 600-68-50 as inner layer and Gurit PHG 600-44-50 as outer layer. In Fig. 3.2 layup of the honeycomb sandwich panel is schematically shown.
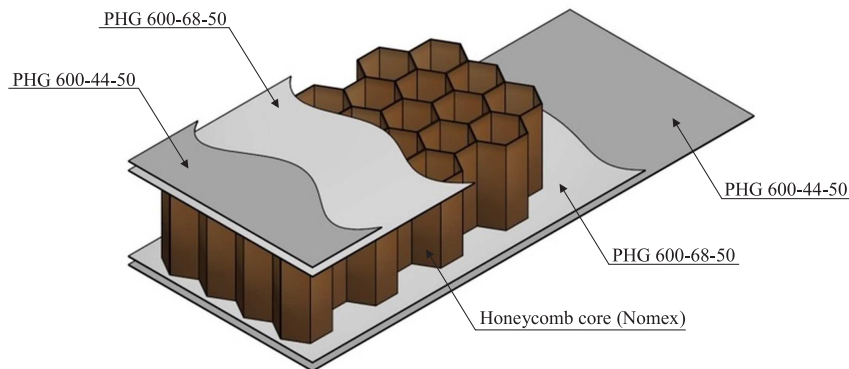
Figure 3.2.: Layers of fabricated honeycomb sandwich structure.

Thicknesses of the used face sheets for inner and outer layer are 0.19 mm and 0.09 mm, respectively. Also, resin content for both prepreg is $50 \pm 3\%$ and fiber areal weight for inner and outer layer of face sheets are $296\,\mathrm{g/m^2}$ and $105\,\mathrm{g/m^2}$, respectively. These types of phenolic prepreg are self-adhesive to core material, thus in fabrication no extra

adhesive is needed to connect the face sheet to the core. Mechanical properties of both GFRP are listed and presented later, in chapter 6. The GFRP are typically orthropic or anisotropic, so their analyses are much more difficult than traditional materials.

Outstanding adhesion to core material, adjustable tackiness, long shelf life and shop life are counted as properties of consumed GFRP. Moreover, both of the used GFRP have broad service temperature in the range of $-55°$C to $160°$C. Regarding to the data sheet of the manufacturer, some mechanical properties of the consumed GFRP material in two different temperatures and related standards are summarised in Table 3.3. It should be noted that all the data is based on mechanical testing of a single batch of material [73].

Table 3.3.: Some mechanical properties of used GFRP at different temperatures.

Mechanical properties at 21°C		
0° Flexural strength	470 MPa (68 Ksi)	ISO 178
0° Flexural modulus	19 GPa (2.76 Ksi)	ISO 178
0° Tensile strength	580 MPa (84 Ksi)	ISO 527-4
0° Interlaminar shear strength	15 MPa (2.18 Ksi)	ISO 65148
Mechanical properties at 80°C		
0° Flexural strength	320 MPa (46 Ksi)	ISO 178
0° Flexural modulus	16 GPa (2.32 Ksi)	ISO 178
0° Tensile strength	230 MPa (33 Ksi)	ISO 527-4
0° Interlaminar shear strength	12 MPa (1.74 Ksi)	ISO 65148

3.1.3. Two component polyurethane adhesive

Without doubt continuous developments in adhesive industry, is one of the most important reason of increases in adhesively bonded joints in various applications. In the words, achieved high-tech adhesives provided highly efficient adhesively bonded joints in engineering applications. This leads to many advantages from mechanical point of view, for instance lower structural weight, ease of components fabrication, improved design flexibility and lower fabrication cost are achieved. Another privilege of the adhesive utilization in the joints is stress distribution. By usage of the adhesive joints instead of the riveted or bolted joints, the stresses are evenly distributed in plane which can highly benefits the joints strength. Without adhesive bonding, certain applications could not exist. Joining of ceramic or elastomeric materials, joining of very thin substrates and also joining of thin face sheets to honeycomb are examples of these types of joints. Moreover, disability on some of the end products to accept shape which is required by mechanical fasteners, caused some more applications of adhesive on bonding.

Adhesive selection process is not easy as there is no universal adhesive which fulfill every application. Also, because of wide variety of available options, choose of appro-

priate adhesive is often complicated and partly daunting. Sometimes, selection of right adhesive is needed deal with large number of options in chemical engineering, due to a strong relationship between manufacturing process and the chemistry. In this regard several manufacturing processes such as temperature and pressure should be considered in fabrication of sandwich T-joints for aerospace industry. However, there are several guiding principles and computer-based selection system which can help in this adhesive selection process. Polyurethane adhesives are developed and adopted the latest eco-friendly international formula and advanced technology. Normally polyurethane adhesives are defined as adhesive which is contains a number of urethane groups in the molecular backbone.

Polyurethane adhesives are usually two-part and fast-curing. They provided strong resilient joints which are resistant to impacts. The market for high quality adhesives such as polyurethanes is grown faster than the market for larger volume commodity type products. Some reasons of this faster growth rate are as follows:

- developing new materials (e.g., composites, engineering plastics),

- new uses with different applications (e.g., sporting goods),

- higher standards of performance,

- lower level of pollutants.

The polyurethane adhesives are superior in performance and convenient in use. They have excellent adhesion properties due to the polar nature of the polyurethane polymer. Also, great flexibility and excellent strength are properties of polyurethane [74]. By consumption of two components polyurethane adhesive, fast cured is obtained and bonds with excellent physical and mechanical properties can be provided. Since two component polyurethane adhesives have fast room temperature cure, they should be properly mixed on-site prior to consumption.

For the connection of web and base plate of the sandwich T-joint specimens, two components polyurethane adhesive is used, namely Ureol 1356 A/B. Properties of both components are presented on Table 3.4. The full strength of this adhesive can be achieved after exposure to a temperature of 20°C during 5 days [75]. This adhesive is solvent free which is consumed for the assembly of different industrial substrates.

Table 3.4.: Some mechanical properties of the used polyurethane adhesive.

Name	Chemical base	Specific gravity (g/cm^3)	Viscosity (mPa.s)	Flash point (°C)	Mix ratio (weight)
Ureol 1356 A	Isocyanate	1.20-1.25	200	207	20
Ureol 1356 B	Polyol	1.50-1.55	45000-50000	190-200	100

Several polyurethanes are currently replacing or have replaced phenolic, polysulphide adhesives in different applications. Generally, in two component polyurethane adhesives, one component of adhesive acts as a resin and the second one act as a hardener.

World industry today is renowned for it is innovative products. In assembly applications, polyurethanes are replaced metal fasteners and some plastics and it's predicted rapid growth for this area. As it's mentioned on the Table 3.4 chemical base of two components of consumed adhesive are polyols and isocyanate. Many different properties of polyurethanes can be obtained in selection of these monomers. Indeed, this adhesive is used for aircraft interior panel and composite parts, because of the special properties. For instance, for the most part the polyols are either based on polyesters or polyethers and polyesters tend to have excellent heat and solvent resistance properties which are desirable properties in aircraft application. Moreover, polyesters showed excellent adhesion and abrasion properties. By the used two components polyurethane adhesives are developed and many of inconsistencies in cure rate and end usage performance are eliminated.

3.1.4. Sandwich T-joint specimens preparation

In the competition between various types of joints, adhesive joints overcome bolted and welded joints for application in aircraft interior. This success is due to numerous studies and optimizations along the last decade. There are various types of adhesively bonded composite joints, e.g., adhesive bonding of beams or plates, single-lap joints or double-lap joints, L-section and T-joints. Definitely, type of the joint must be adapted to the structure and required performance. In fabrication of different parts of the aircraft interior and also the galley, T-joint is favorable type of the joint which is designed and used. One of the most important aspect of designing adhesively bonded joint is geometry design, specifically the adherends with respect to the application type. Here, we used scaled T-joint which is used in aircraft galley. The recent design of aircraft galley provided adequate area to do the tasks which could not be taken lightly by the tiny galley. With the new design, the aircraft galley became more visible instead of to be hidden behind the closed doors. However, the studied T-joints are used for almost all types of the galley made from honeycomb sandwich composite which is most popular option for the galley fabrication by far.

According to the last three above sections which described components of the samples, T-joint sandwich specimens are made by honeycomb core, GFRP face sheets and two components polyurethane adhesive. The two component polyurethane adhesive which is explained previously, is used to connected web and base plate of sandwich T-joint specimens. In general, bonded joints may be subjected to tensile, compressive, shear or peel stresses and sometimes in combination. A bonded joint needs to be designed so that the loading stresses will be directed along the lines of the adhesive's greatest strengths.

In this research, all the T-joint specimens are produced by the material and manufacturing process which is used in many aircraft galley. Since the surface preparation

is critical on the durability of an adhesive bond, the surfaces have been prepared with special care. In fact, beside of the other parameters, the durability of joints depends on the conditions of the joint surfaces when the bond was made. Poor surface condition can be lead to low level of initial strength and reduced durability. Moreover, if it is needed a particular surface treatment should be carried out in order to increase the affinity for the adhesive. After applying adhesive, curing schedule (time and temperature) is performed to obtain strong adhesively bonded joints. The performance of the adhesive connection not only depends on the adhesive properties, but also on the thickness and on the uniformity of bonding. Here all specimen are glued with the same amount of adhesive which leads to a layer of about 1 mm thickness. The fabricated sandwich T-joint is shown in Fig. 3.3. The length of base plate is 180 mm and height of web part is equal to 80 mm, while the width and core thicknesses of these parts are identical, equal to 70 mm and 19.05 mm, respectively. After fabrication, all of the specimens and particularly the interface of web and flange are inspected visually.
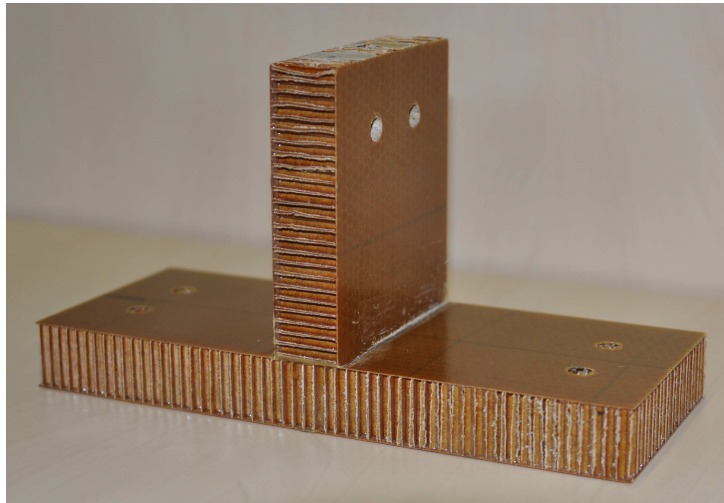
Figure 3.3.: Fabricated sandwich T-joint.

The described specimens used in the current study are kept at room temperature for about three months, they are named here 'unaged'. Several specimens are artificially aged which is described in detail below.

3.1.5. Sandwich specimens under accelerated ageing conditions

During the service life of the aircraft, different types of environmental conditions are experienced by the sandwich parts and the joints. Elevated temperature and high humidity are examples of the different environmental conditions. In some applications the operating environments is highly aggressive and it can be lead to reduction of struc-

tural integrity and service life. In order to understand an environmental effects, numerous researchers studied ambient effects on different types of composite materials [76, 77, 78, 79, 80, 26]. For instance, in [76] the response of aged composite joints is determined. The researchers tested T-joints made of a PVC foam core and fiber reinforced laminate skins. They concluded that material properties are reduced due to plasticisation as result of moisture absorption. Later, in work [79] adhesively bonded aluminum honeycomb sandwiches are exposed to ageing in the range of $-25°C$ to $75°C$ and then their fatigue strength is investigated. The structure was formed by bonding the honeycomb cells to the aluminum 5052 face sheets using an epoxy-based two-part adhesive. The researchers found that the fatigue strength increases with raising temperature and that the failure mode changes from local cracking to debonding at the interface for the aged specimens. More recently, ageing effects on static mechanical properties of carbon fiber reinforced composite are investigated in [26] the researchers fabricated specimens by laminated panels and exposed the specimens to an ageing temperature of $200°C$ which represents aerodynamic heating at the surface of the aircraft. By means of low velocity impact tests, variations in failure mechanism are determined.

Test procedure of the accelerated ageing on composites is described by several standard methods, but they are not explicitly specified for sandwich composite T-joints. Generally, suggested conditions on the test standards are material dependent. In this thesis, testing conditions are selected in an attempt to simulate service conditions in order to assessing service life time and durability of the T-joints. To this aim, ISO 9142 [81] is used as a guide for ageing conditions of bonded joints. Generally, damage in composite caused by ageing of structural components, can be result of a combination of processes.

In the current study, a natural environment is simulated and the related effects are examined by means of accelerated thermal ageing. For this purpose, two groups of the specimens are aged separately by a climate test chamber. The chamber was a floor standing model WK340 manufactured by Weiss Technik. It was large enough so that the volume of the specimens did not exceed 10 % of the free volume in the chamber. The set of the specimens was placed in the chamber in such a way that more than 30 mm distance between them and the sides of the chamber was always ensured. In order to keep the position of the web and the base plate during the ageing, each specimen is connected to a weight of 500 g to prescribe a certain tension and to avoid out-of-plane loadings and vibrations. The specimens under accelerated ageing condition are shown in Fig. 3.4.

There is no absolute rate in temperature reduction per meter, because each meter of atmosphere is different, but just by standard definition [82] the temperature reduced $1°C$ every 165 meter increase in altitude where commercial aircraft flies. As mentioned in [83] when temperature at ground is $20°C$, at 35000 feet as flight altitude of passenger aircraft, the temperature would be $-54°C$. In our research, the first group of specimens is artificially aged by 25 days of thermal exposure. The ageing temperatures were $-35°C$ and $70°C$, each temperature is kept for 12 hours. The temperature rate of change for
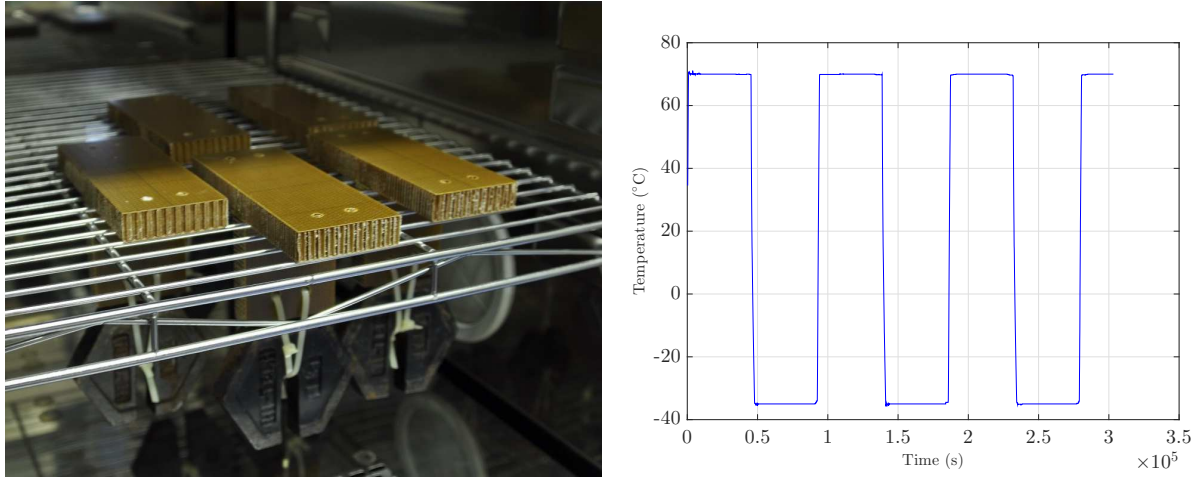
Figure 3.4.: Accelerated ageing of the composite sandwich T-joints in the heat chamber and the applied cycles of thermal ageing.

heating and cooling was 3°C/min. The thermal ageing cycles which are performed on the T-joint specimens are shown in Fig. 3.4 (right). It should be mentioned here, in determination of ageing temperature and exposure time, the flight condition is considered, which is made by three main states: temperature at altitude, duration of each exposure, and rate of heating and cooling during flight. Moreover, since the studied sandwich T-joints are employed in the galley of passenger aircrafts (e.g., Airbus A321), this part of the galley where the food is heated in convection ovens can experienced such a high temperature for a small period of time. Therefore, we considered this real application in order to determine the temperature range of the accelerated ageing.

For the second group of the aged specimens, 100 cycles of the same procedure and ageing temperature are conducted. After the ageing process, the specimens were cooled down to room temperature, kept for 10 days at room temperature and tested in the same way like the unaged specimen, which is described later in chapter 5.

Before testing the sandwich specimens were weighted with an accuracy of $\pm 0.001\,\mathrm{g}$ before and after the thermal ageing. A calculation of mass loss in percent was carried out by

$$\Delta W = \left[\left(\frac{W_A - W_0}{W_0} \right) \right] \times 100 \tag{3.3}$$

where W_A and W_0 are the weight after ageing and the original weight value, respectively. It should be noted here that length, width and thickness of the specimens were measured precisely before and after ageing. All the changes related to the weight and the dimensions are below 1% after thermal ageing. Furthermore, no type of failure was observed between the face sheets and the honeycomb core after ageing on the specimens. Accelerated ageing test and obtained reliable results can provide time and cost saving knowledge for future material design.

36

3.1.6. Mechanical properties of sandwich composites

In order to predict behavior of sandwich composites under quasi-static or dynamic loading conditions, many models have been developed by researchers. In work [84] extensive review of computational models of sandwich panels and shells is presented. Generally, honeycomb sandwich models are categorized into different two-dimensional models, three-dimensional detailed and also three-dimensional continuum models. This categorization is summarized in Fig. 3.7.

Figure 3.5.: Various models of honeycomb sandwich plates.
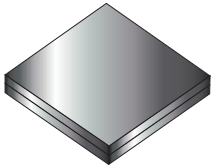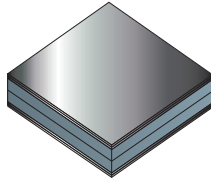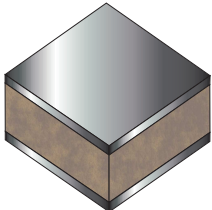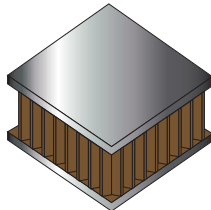
Two-dimensional approximation model, is also called equivalent single-layer model, and in this model the whole sandwich is replaced by a single equivalent layer [85, 86]. In the layerwise or zigzag model, the sandwich is divided to several layers, and modeled based on plate and shell theories, using Kirchhoff-Love, Reissner-Mindlin or enriched kinematic assumptions [87, 88]. Three dimensional continuum models are multilayer models, which plate or shell element have been utilized to model the face sheets, and also solid volume element used to model the core [89, 90].

The detailed three-dimensional finite element model (FEM) represents the actual geometry of the honeycomb core, adhesive and face sheet [91, 92]. In the current research, we used the detailed three-dimensional model in our FEM and it's comprehensively described later in chapter 6.

Advanced materials and new technologies leads to increase shift from solid metals to lightweight panels and sandwich structures. The I-beam presents a significant im-

provement over a solid metal for the same application. Also, it is provides much higher efficiency in term of strength to weight ratio. If we replaces I-beam with a sandwich panels made by core and face sheets, the highly efficient structure would be achieved. Fig. 3.6 show schematic of a solid metal (I-beam) and part of a sandwich panel.
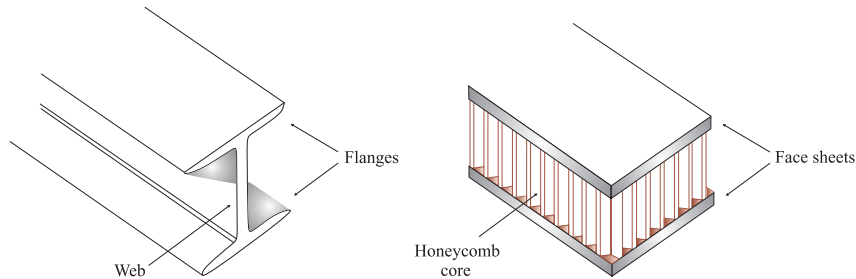
Figure 3.6.: Schematic of a solid metal (I-beam) and a sandwich panel.

The web and the flanges of the I-beam can be compared to the core and face sheets of the sandwich part, respectively. In comparison, the core and the web part of the I-beam, similarly resist the out-of-plane shear stress load. This core provides continuous support to the face sheet. The face sheets should carry the bending stress, like the flanges of the I-beam, while one of the face sheets is in tension and the other one is in compression.

One node and two free walls are the basic honeycomb elements. From this element various core relationships can be determined. Geometry of honeycomb core and detail of a cell are illustrated in Fig. 3.7.
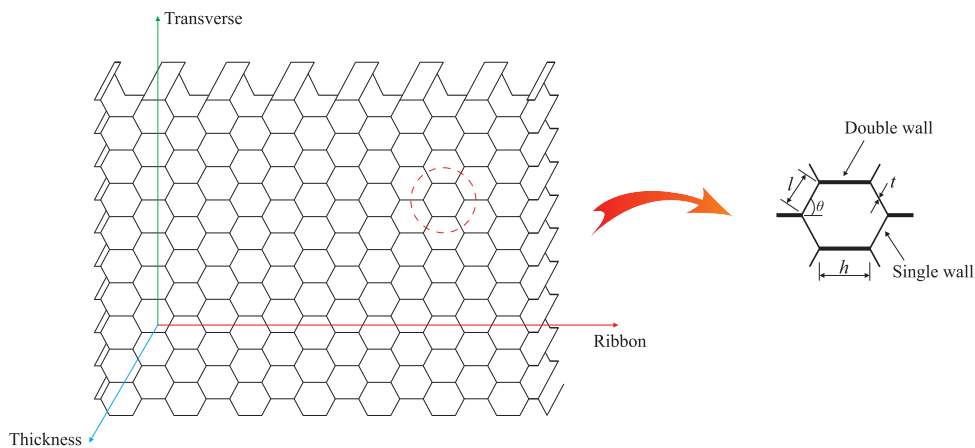
Figure 3.7.: Geometry of the honeycomb core.

In the hexagon equations a perfect hex cell was assumed with θ equal to 60°. This will not always be the case in actual honeycomb. The node may peel back slightly in some core types during expansion, therefore the node width is smaller than the free wall width. In the current study, both of h and l are equal to 1.847 mm and the angle of cell is $\theta = 30\pi/180 = 30°$.

As mentioned already in production of honeycomb core, Nomex paper produced from fiber aligned in the direction of travel of paper machine, therefore it has anisotropy defined. Also, by the previous experimental data and theory [93], it is proved that a honeycomb core can be classified as an orthotropic material. In [94] existing theories for the material properties of honeycomb estimation are reviewed and compared based on different methods. For the expression of the honeycomb material properties linear elastic deformation which is described by Gibson and Ashby [95] is used. The honeycomb equivalent orthotropic properties called effective properties and shown with star. The structure has three perpendicular mirror planes. This symmetry reduced further number of moduli and the orthropic material law depends on nine independent material parameters in their constitutive matrices. The orthotropic material law which is formulated in [96] is expressed as follows:

$$
\begin{Bmatrix} \varepsilon_x \\ \varepsilon_y \\ \varepsilon_z \\ \gamma_{yz} \\ \gamma_{xz} \\ \gamma_{xy} \end{Bmatrix} = \begin{bmatrix} 1/E_x^* & -\nu_{yx}^*/E_y^* & -\nu_{zx}^*/E_z^* & 0 & 0 & 0 \\ -\nu_{xy}^*/E_x^* & 1/E_y^* & -\nu_{zy}^*/E_z^* & 0 & 0 & 0 \\ -\nu_{xz}^*/E_x^* & -\nu_{yz}^*/E_y^* & 1/E_z^* & 0 & 0 & 0 \\ 0 & 0 & 0 & 1/G_{yz}^* & 0 & 0 \\ 0 & 0 & 0 & 0 & 1/G_{xz}^* & 0 \\ 0 & 0 & 0 & 0 & 0 & 1/G_{xy}^* \end{bmatrix} \begin{Bmatrix} \sigma_x \\ \sigma_y \\ \sigma_z \\ \tau_{yz} \\ \tau_{xz} \\ \tau_{xy} \end{Bmatrix} \tag{3.4}
$$

where the Young's moduli are E_x^*, E_y^*, E_z^*, Poisson's ratios ν_{yx}^*, ν_{zx}^*, ν_{zy}^* and shear moduli are G_{xy}^*, G_{xz}^* and G_{yz}^*. This analytical approach is extended by Gibson and Ashby to derive the nine orthotropic parameters in [95], that is currently a reference book in this field. It should be noted that the analytical solutions proposed do not take into account the double thickness walls in the direction of the ribbon (L), and are not match well with experimental results, therefore numerous researchers still continue working on improving the estimation of the effective parameters of the honeycomb core.

In order to evaluate failure mechanisms of a sandwich structure, stiffness and mechanical parameters of honeycomb core are needed. Here, regarding to the [97, 95], honeycomb properties are presented. In work [95] Gibson and Ashby assumed t and t' as thickness of cell wall and inclined cell wall, respectively, considered $t' \neq t$, and determined in-plane and out-of-plane (thickness) honeycomb core stiffness coefficients are as follows:

In-plane parameters

When all sides of a unit cell in the honeycomb are equal with the same angle and identical wall thickness, the in-plane properties are isotropic. For irregular hexagon or for the honeycomb with different wall thickness, the properties are anisotropic.

$$
E_x^* = E \left(\frac{t}{l} \right)^3 \frac{\cos \theta}{(h/l + \sin \theta) \sin^2 \theta} \tag{3.5}
$$

$$E_y^* = E\left(\frac{t}{l}\right)^3 \frac{(h/l + \sin\theta)}{\cos^3\theta} \tag{3.6}$$

For the regular hexagons, like the honeycomb we used $h = l$, the Young's moduli reduced to the same value equal to $2.3(t/l)^3$. The shear stress τ is $F/2\,l\,b\cos\theta$ gives the shear modulus:

$$G_{xy}^* = \left(\frac{t}{l}\right)^3 \frac{(h/l + \sin\theta)}{(h/l)^2(1 + 2h/l)\cos\theta} \tag{3.7}$$

For regular and uniform hexagons, like our honeycomb, this reduces $G_{xy}^* = 0.57(t/l)^3$. The Poisson's ratios are calculated by taking the ratio of the strains normal to, and parallel to, the loading directions:

$$\nu_{xy}^* = \frac{\cos^2\theta}{(h/l + \sin\theta)\sin\theta} \tag{3.8}$$

$$\nu_{yx}^* = \frac{(h/l + \sin\theta)\sin\theta}{\cos^2\theta} \tag{3.9}$$

which is $\nu_{xy}^* = \nu_{yx}^* = 1$ for the regular hexagons.

Out-of-plane parameters

$$E_z^* = \left(\frac{t}{l}\right)\frac{h/l + 2}{2(h/l + \sin\theta)\cos\theta} \tag{3.10}$$

$$G_{xz}^* = \left(\frac{t}{l}\right)\frac{\cos\theta}{h/l + \sin\theta} \tag{3.11}$$

and reduces to $0.577(t/l)$ for the regular hexagons.

$$G_{yz}^* = \left(\frac{t}{l}\right)\frac{h/l + \sin\theta}{(1 + 2h/l)\cos\theta} \tag{3.12}$$

again for the regular hexagons, reduces to $0.577(t/l)$. The Poisson ratios ν_{zx}^* and ν_{zy}^* are simply equal to those for the solid itself:

$$\nu_{zx}^* = \nu_{zy}^* = \nu \tag{3.13}$$

The honeycomb core moduli are very smaller than the face sheets and generally the core just moves with the face sheets and doesn't show resistance.

The effective stiffness of the facesheet, E_f, can be calculated using classical lamination theory. In this regards, face sheet materials should be assumed orthotropic, and each material characterize by four engineering constants E_x, E_y, G_{xy} and ν_{xy}.

3.2. Ultra-high performance concrete materials

In the past decades lots of advances have been made in the field of concrete and high performance concrete. UHPC exhibits superior and exceptional materiel properties, such as high strength and durability. This material can also resist freeze-thaw condition with no damage. Because of these properties, to date UHPC has been used in construction of numerous pedestrian and highway bridges and wide variety of other projects. Here, we prepared various groups of UHPC specimens for series of spalling and dynamic Brazilian tests to characterize the material behaviors and determine dynamic mechanical properties. In the following part, details of specimens preparation are described.

3.2.1. UHPC specimens preparation

Many researchers developed various UHPC all over the world. In the available UHPC which are developed over the years, there are several differences and also many overall similarities. Since concrete and UHPC are brittle materials with multi-phase composites, their response to the dynamic loading regime exhibits brittle behavior. Concrete and UHPC specimens with various diameter sizes are used in dynamic test by SHPB in the past. However, in [98] it is mentioned that test of the concrete on SHPB need relatively large specimen diameter to achieve reliable material properties. UHPC is a composition of cement, water, admixtures, additives and aggregates of different sizes, whose structure is mechanically almost homogeneous and as low-porous as possible. For all the specimens, fine-grain recipes were used, leading to UHPCs, in which the maximum grain size is defined by the size of the quartz sand. All the specimens are produced with a maximum grain size of 725 μm.

Cylindrical UHPC specimens for series of spalling tests

In this research, two groups of cylindrical UHPCs (specimen groups S_1 and S_2) were produced for series of spalling tests. As a reference for the material properties of the binder matrix in these UHPCs, a series of samples, only consisting of cement with a comparable water-to-binder ratio as in the concretes are investigated additionally (specimen group S_0). All compositions are given in Table 3.5 (mass proportions, normalized by cement). As cement, for all three specimen groups, a CEM I 52.5 R was used; high range water reduction was possible using a 3rd Gen. superplasticizer based on PCE (polycarboxylate ether) as additive. It should be noted here, that the static compressive strength and the static flexural strength are obtained using $4 \times 4 \times 16$ cm prisms by experiments according to DIN EN 12390-3 and DIN EN 12390-5 respectively [99, 100]. First the flexural strength was measured by three-point bending tests on the prisms (3 prisms for each specimen group). Then, both halves of each broken prism were used for measuring the compressive strength (total of 6 samples per specimen group).

The mixture S_1 refers to a typical and current UHPC recipe with a regular amount of

Table 3.5.: Composition and basic properties of cement and UHPC.

Composition	S_0	S_1	S_2
cement	1.00	1.00	1.00
quartz sand	-	1.46	0.94
quartz powder	-	0.53	0.34
microsilica	-	0.20	0.10
water	0.23	0.24	0.23
superplasticizer	0.03	0.05	0.03
water-binder ratio	0.23	0.233	0.230
water-cement ratio	0.23	0.28	0.253
Basic mechanical properties	S_0	S_1	S_2
static compressive strength (MPa)	160.2 ± 2.7	159.6 ± 1.6	186.1 ± 3.1
static flexural strength (MPa)	8.3 ± 0.6	17.2 ± 0.2	14.4 ± 0.3
raw density (kg/m^3)	2231.81	2382.71	2374.81

microsilica of 20 %. From the economical point of view such an amount is questionable, due to the costs of microsilica which costs a multiple of the price of cement. Furthermore, adding high amounts of microsilica to the concrete leads to a drop of alkaline reserves in the pore solution and therefore to a critical decrease of the pH value of the concrete. Because an alkaline surrounding of pH value 9.5 - 13 is necessary for the secure protection of steel reinforcements in concrete, the pH value cannot be excessively lowered through addition of microsilica to prevent corrosion in the system. By German standards the maximum amount of microsilica in concrete is therefore limited by 11 % according to DIN 1045-2:2008-08 [101]. For this reason a second UHPC was created (mixture S_2), optimizing the S_1 recipe to an amount of microsilica of only 10%. This leads to advantages in both economical and application-specific counts.

The recipes were adjusted in such a way that a good consistency and workability was ensured. Quantification provided the measured flow spread. The cylindrical UHPC specimen were produced by filling the concrete into specially designed, hollow copper tubes ($l = 25$ cm, open at both ends), allowing for an easy extraction of the samples after the first 24 hours of hardening. For filling, UHPC was horizontally injected into the single tubes by hand using a special syringe, applying very low and negligible ejection pressure. A concrete overflow was produced at the output of the tubes to cast off air bubbles in the concrete induced by the injection process. The tubes were then mounted vertically, closing the bottom, and each tube was fully filled with UHPC. Because densifying the concrete with a common plate compactor was not possible, a wire was used for manual densification and degassing after the filling process. Specimens were then stored under water at 20 °C for at least 28 days of hardening. Because the outer parts of the produced raw-samples could be impaired by sedimentation and air injection due to the filling and

vertical storage, all specimens were taken from the middle of the raw-samples. Precise cutting of the samples into their required lengths (200 mm and 20 mm) was realized by a linear precision saw with a diamond cutting disc. This ensured that all specimens have flat surfaces and that the free ends are perpendicular to the symmetry axis. To additionally plain the surfaces for the SHPB measurements, irregularities at both ends of the specimens were removed where necessary using a grinder and a $P180$ abrasive SiC-discs. It should be noted here, some of these cylindrical specimens have cut in length of 20 mm and used for tests on determination of dynamic elastic modulus. The hollow copper tubes and UHPC specimens are shown in Fig.3.8.

Figure 3.8.: Hollow copper tubes and prepared cylindrical UHPC specimens.

A comparison between the densities of the fresh concrete, calculated by use of the concrete volume calculation, and the measured densities of the hardened concrete served as an important scrutiny for the verification of the quality of the concretes. If both values are consistent, the theoretically assumed air pore content is actually present in the hardened concrete, which validates the concrete volume calculation. Current experiments showed a good correlation of both densities and therefore high concrete qualities and correct recipe calculations can be concluded.

Circular UHPC specimens for series of dynamic Brazilian tests

For series of the dynamic Brazilian tests, two groups of circular UHPC specimens are prepared. The composition of both groups are same as the S_2 group of the cylindrical UHPC for the spalling test, see Table 3.5. For the Brazilian tests UHPC disc specimens were produced by filling the material into a specially designed hollow die, allowing an easy extraction of the samples after hardening. In preparation of the first group of the specimens, circular discs with a diameter of 50 mm and a thickness of 15 mm are fabricated. Furthermore, in the second group, UHPC discs with the same diameter and

thickness but with two flat ends are fabricated. The flat end reduced stress concentration by replacing the point or line load on the cylinder's lateral surface with surface pressure. It also improves the contact between the specimen and the adjacent incident and transmission bars. The Brazilian specimens with plastic mold are iluustrated in Fig. 3.9.

Figure 3.9.: The fabricated circular (left) and flat end (right) Brazilian specimens.

All the specimens are constructed regards to the relevant standards. For instance, it is recommended in [102] that the specimens during the period between their removal from curing environment and testing, must be kept moist by means of a we burlap or blanket covering. Then, should be tested as soon as practicable. After extraction specimens were stored under water at 20 °C for at least 28 days of hardening.

Properties of concrete and concrete-like materials are closely influenced by characteristics and compositions of the utilized materials.

3.2.2. Mechanical properties of UHPC materials

UHPC materials are innovative class of cementitious composite materials that have been mainly developed in the last decade. Compared to normal concrete, high strength concrete, ultra high strength concrete and high performance concrete, the UHPC material shows better material properties which should be mainly attributed to the utilized materials in composition of UHPC. Indeed, not only mechanical properties, but also other parameters like durability, recycleability, workability and energy consumption indicate better performance of UHPC in between the above-mentioned materials. These properties, make them a reasonable alternative to traditional concrete for various structural applications.

One principle about the UHPC is that dense particle packing and also matrix homogeneity provides a higher compressive strength. This concept is applied by using small aggregates. Another concept is that UHPC contains very low water to cement ratio and behavior of concrete and cementitious composite material at early age highly depends on moisture content. By Ficks law, the overall moisture transport can be described which express the flux of water mass per unit time as a function of the spatial gradient of the relative humidity [103, 104].

The particle size distribution of all composed materials is crucial for mix design of the UHPC. In fact, behavior of UHPC at the fresh state and hardened properties of its mixture, both are affected by particle packing of all the utilized materials. Not only microscopic techniques, several methods are based on sedimentation of particles in suitable liquids or diffraction of light are currently used in this field [105]. Water demand and microstructure are also two crucial parameters which play important role in UHPC properties. The total water demand is significantly affected by layer of absorbed water to molecules around the particles, and additional water is required to fill the voids. The fine particles usually have specific surface area which can change the total amount of water demand, and finally behavior of UHPC material. In order to obtain superior mechanical properties, very limited water amount is normally used in UHPC material, thus evaluation of water demand amount of all the composed materials has important role in the properties and behavior of UHPC. In UHPC and cementitious composites, surface roughness and shapes of the particles directly change the flowability and bonding behavior. Investigations and scanning electron microscopy [106] showed that several spherical particles observed in fly ash and particles in the other powders have irregular shape. In this regards, when the spherical fly ash are added, flowability of UHPC is improved. On the other hand, bonding and strength between the materials is improved by the irregular particle shape.

UHPC as a cementitious composites is very brittle with high compressive strength and high tensile strength strengths which exhibits strain hardening in direct tension. This material becomes more brittle as the compressiev strength increases. Very dense packing of particles of UHPC material can provided high compressive strength in this material. In [107] uniaxial tensile tests are carried out on UHPC and regards to the tests tensile behavior of UHPC described in four phases: the first phase shows linear elastic behavior of uncracked concrete. The behavior is still somewhat linear elastic in the second phase and the first microcracks occurred in this phase. Propagation of these microcracks is limited and sometimes called the stable microcracking phase. This limited propagation leads to high tensile strength of UHPC. In the third phase the cracks propagates and multiple cracking happened. In the last phase, onset of strain-softening is observed.

It is well defined that two fracture criteria described cracking of concrete and concrete like-materials [108, 109]:

- energy criteria: crack extension requires energy release,

- stress criteria: crack extension needs stress to overcome the cohesive strength of material.

By consideration of the linear elastic fracture mechanics and Griffith criteria, the fracture stress (σ_f) can be controlled by the crack size (a) and fracture toughness (G_c)

of UHPC material:

$$\sigma_f = \sqrt{\frac{EG_c}{\pi a}} \tag{3.14}$$

UHPC material without fiber shows lower fracture toughness compared with UHPC reinforced with fiber. In the Eq. (3.14) three important issues of fracture process are considered. The first one is the material, since Griffith's original work dealt with very brittle materials, specifically glass rods. The second is size of the crack a, and the last one is critical strain energy release rate G_c. By this relationship, safe level of the stress can be determined. Thus, a UHPC structure can be seized to keep the working stress below this critical value.

From the theoretical point of view, concrete and concrete-like materials, such as UHPC and its variants are considered isotropic and homogeneous. As it is mentioned in [110] when response of the entire UHPC structure, isotropy is a reasonable assumption. By the isotropic damage models and numerical simulations there is possibility to predict the response and also failure mode of the concrete, UHPC and its variant. For the concrete and concrete-like materials which exhibits the same behavior in all directions, while subjected to the load, the stress and strain in three dimensional case are defined as [111]:

$$[\sigma] = \begin{bmatrix} \sigma_x \\ \sigma_y \\ \sigma_z \\ \tau_{xy} \\ \tau_{yz} \\ \tau_{zx} \end{bmatrix} \qquad [\varepsilon] = \begin{bmatrix} \varepsilon_x \\ \varepsilon_y \\ \varepsilon_z \\ \tau_{xy} \\ \tau_{yz} \\ \tau_{zx} \end{bmatrix} \tag{3.15}$$

where matrix $[C]$ is called the elastic modulus matrix, so $[\sigma] = [C][\varepsilon]$:

$$[C] = \left[\frac{E}{(1+\nu)(1-\nu)}\right] \begin{bmatrix} 1-\nu & \nu & \nu & 0 & 0 & 0 \\ \nu & 1-\nu & \nu & 0 & 0 & 0 \\ \nu & \nu & 1-\nu & 0 & 0 & 0 \\ 0 & 0 & 0 & \frac{(1-2\nu)}{2} & 0 & 0 \\ 0 & 0 & 0 & 0 & \frac{(1-2\nu)}{2} & 0 \\ 0 & 0 & 0 & 0 & 0 & \frac{(1-2\nu)}{2} \end{bmatrix} \tag{3.16}$$

46

For ν and E in terms of Bulk modulus (K) and shear modulus (G), the C is:

$$[C] = \begin{bmatrix} K + \frac{4}{3}G & K - \frac{2}{3}G & K - \frac{2}{3}G & 0 & 0 & 0 \\ K - \frac{2}{3}G & K + \frac{4}{3}G & K - \frac{2}{3}G & 0 & 0 & 0 \\ K - \frac{2}{3}G & K - \frac{2}{3}G & K + \frac{4}{3}G & 0 & 0 & 0 \\ 0 & 0 & 0 & G & 0 & 0 \\ 0 & 0 & 0 & 0 & G & 0 \\ 0 & 0 & 0 & 0 & 0 & G \end{bmatrix} \tag{3.17}$$

The difference between brittle and ductile materials in fracture behavior came from dimension and shape of the fracture process zone (FPZ), which is a volume of material engaged in formation of new surfaces. In order to explain development of microcracks in the FPZ, it is needed to formulate the matrix $[C]$.

The various difficulties in applying fracture mechanics to brittle materials like UHPC and its variants increased from the various toughening mechanism in the FPZ, such as micro cracking, crack deflection, crack branching, and crack face friction.

Currently, commercial finite element software packages are commonly used for numerical simulations of these materials. We also employed finite element method and modeled crack as a cohesive in our spalling tests on UHPC materials, also we utilized finite element software to numerically model our Brazilian experiments, which are all completely described in chapter 6.

4. Aritificial intelligence in fracture mechanics

Before we focus our attention to the experiments on composite materials, in this chapter we will review applications of artificial intelligence (AI) in fracture mechanics and its sub-domains. For this purpose, firstly we present definition of AI and related approaches briefly, and then fracture mechanics divide to four main sub-domains. Finally, applications of five branches of AI reviewed in the sub-domains of fracture mechanics, comprehensively. It should be noted here, most of this chapter has been published by us in [112] where Ms. Sara Nasiri as the first author discussed applications of the last approach of the presented AI methods, hybrid intelligent techniques and also future research direction. My contribution was a review and the comparison of the AI methods on the defined sub-domains of fracture mechanics. This review led to implementation of our prototypes to predict fracture and mechanical properties of the composites which are studied in this dissertation [113, 114]. These applications are explained in the last section of this chapter.

4.1. Concept of artificial intelligence approaches

Artificial intelligence began in ancient history, but from its appearance researchers have tried to use it in a wide variety Of applications. AI by definition of [115] is "the art of creating machines that performs functions that require intelligence when performed by people". AI is also defined based on the eight textbooks between human and rationality centred approaches which are organized into four categories: a) systems that think like humans, b) systems that act like humans, c) systems that think rationally, and d) systems that act rationally [116]. In fact, intelligent approaches and systems have been applied in wide range of industries and commercial fields. Expert systems performed in some limited domain such as failure analysis and mechanical fault diagnosis. Although there are different definitions for expert systems [117, 118, 119], it emulates work of human experts in computer model or program by five main components: knowledge base, working memory, inference engine, external inference and user inference [120]. Two decades ago, proficiency of AI approach and particularly expert system to solve problems in the area of fracture mechanics is discussed by [121]. The researchers described an idea

of creating an expert system on the domain of linear elastic fracture mechanics and the validity of the technique is also exhibited. At the same time, ability of knowledge based systems on determining of fracture characteristic of materials and structures are shown by [122], and twenty years ago, the author asked about the capability of handbooks to solve problems with the rapid change of technology during the next thirty years. Liebowitz predicted intelligent black boxes would be one of the substitutes for some handbooks. Now, after two decades, obviously it can be seen that AI and knowledge-based systems are developed and utilized in different fields of science and technology. It leads to users add knowledge to the existing applications and systems to make them smarter and more applicable. Despite some positive experiences of intelligent systems on failure identification, fracture mechanics and fault detection [123, 124, 125], because of some reasons, application of expert systems could not continue on this area. In fact, experiences show that knowledge extraction as a challenging and time-consuming process. In reality, lots of resistances from human experts are recognized when there is a request to import their expertise in an expert system. Indeed, the human experts are worry that be replaced by these systems. Moreover, the expert system has these limitations [126] common sense, inspiration or intuition and flexibility to apply in the semi-relevant field. Experts decide based on their overall view of the occurred problem, but expert system has not enough information. In the other hand, experts know their lack of knowledge and the limits of their information in dealing with new problems, but expert systems have narrow knowledge domain and just work when they are developed for specific or very specific problems. Therefore, they cannot generalize and still need the commitment of experts. Finally, for achieving the performed outputs and results require regular maintenance and update which has its costs. As an output of these systems is highly depended on the inputs, the above-mentioned conditions can be considered as major reasons which didn't allow them to grow. Thus, since the beginning of the 1990s artificial intelligence and machine learning methods are used significantly to develop such systems automatically [127].

Although AI has a long history, it is constantly used and actively grown. Over the years, AI applications indicated not only that AI can contribute major aspects to mechanical engineering, but also an investigation of AI on various domains can develop and improve in fracture mechanics. AI methods are applied in this field to reduce the failures and solve the problems. However, there are still unsolved problems and improvement opportunities. Therefore, our goals for this survey are as follows:

- describing the procedure and mechanism of reviewed AI methods,

- categorizing the existing systems and works,

- explaining the methodology of current applications and systems,

- analysing the advantages and limitations.

Investigations on fracture mechanics, including performing experimental tests and computational methods are not always an easy task and are quite time consuming, but also a high level of technical expertise is required. Indeed, fracture mechanics and failure analysis is one of the extreme complex engineering fields. There are many challenges for detecting failures and faults of mechanical machinery, parts and systems. The main issues based on the existing works in fracture mechanics domain are as follows:

- identifying failure mode,

- identifying fracture mechanism,

- monitoring of fault diagnosis process,

- monitoring of damage and failure diagnosis process,

- early detection of mechanical faults,

- early detection of damages and failures,

- predicting of fracture parameters.

Therefore, for achieving our goals and objectives in this survey, we have searched keywords in the scientific databases based on these challenges in fracture mechanics. According to these challenges, different AI methods are able to support solving the complex mechanical fracture problems. Material toughness characterisation, damage detection, fault diagnosis, failure mode identification and crack detection are various aspects of fracture mechanics which are surveyed by different approaches of AI. Here. we analysed literature based on a classification of five earlier methods and techniques of AI: Bayesian network (BN), artificial neural network (ANN), genetic algorithms (GA), fuzzy logic (FL) and case-based reasoning (CBR). In this section, the main concepts and mechanisms of these methods are highlighted.

During the past decades, many structural failures have been predicted by fracture mechanic approach. Research on fracture and failure showed that saving in time and cost can be obtained by focusing on two major areas which are materials and structures. In fact, predict and prevent failure load have been interesting topics of research in the past years. There are different AI methods which are applied in variety domain of mechanical engineering. In this section, five different intelligence methods with their definitions are counted. These methods are applied in the domain of fracture mechanics:

Bayesian Networks

In the late 1970's, Bayesian networks were developed in order to model distributed processing in reading comprehension [128] and now applied in a variety of fields where reasoning under uncertainty is required. Over the years, Bayesian network is applied in different domains of science [128, 129, 130, 131, 132, 133, 134]. Bayesian networks, also

known as belief networks (or Bayes nets for short), is a combination of graph theory and probability theory that consists of probabilistic relationships among the nodes. Kang et al. [135] presented the sample of faults diagnosis in a gear train system. It shows the network which combines with three nodes (O1, O2, O3) which indicate the different gear faults and three nodes (S1, S2, S3), which represent three statistical factors of vibration signals in the time-domain. The certainty of diagnosis results for untrained samples is calculated by probability theory in Bayesian networks.

the probability for evidence E giving providing information that the hypothesis H is true [135].

$$P(H|E) = \frac{P(E|H)P(H)}{P(E)} \tag{4.1}$$

where $P(H|E)$ is the posterior probability for H providing information that evidence E is true, $P(H)$ is the prior probability of H, and $P(E|H)$ is the probability for evidence E giving providing information that the hypothesis H is true. P is the probability which is the connections between the statistical factors of vibration in the time-domain as an input and gear faults as an output.

Artificial neural network

It is a computational model and based on the definition in [136] it's an interconnected assembly of simple processing elements, units or nodes, whose functionality is loosely based on the biological neural networks for engineering problems. During the past decades, variety types of ANNs are applied in the different area of science and numerous various systems. For instance, it is used in medicine [137], finance [138], marketing [139], mining sciences [140], civil and structural engineering [141], manufacturing technology [142] and mechanical fatigue [143]. It also has been applied for fault detection and failure analysis. ANN contains three main sections which are input, hidden and the output layers and they presented input parameters, learning process and solution of problem respectively.

In [144] back propagation ANN is utilized for faults diagnosis in a gear train system. All neurons are connected with different weights and weights are calculated as follows:

$$S = \Sigma O_i \, W_{ik} \tag{4.2}$$

where S is the collection of information from each neuron with an artificial neural input value, O_i is input value and W_{ik} is connection weight. Neural network models uses the numerous transfer functions which obtained the neuron output. These transfer functions can be linear or nonlinear functions and are used to obtain neuron output. For instance, it is calculated in [144] for fault diagnosis of train gears.

The capability of ANNs in direct learning is one of the most important properties of it. Moreover, it can regain and extract information from noisy, incomplete or poor data.

These properties make ANNs a powerful method for solving problems in area of fracture mechanics. Beside of the numerical analysis, application of ANNs also has received an increasing amount of attention from the researchers in the field of engineering fracture mechanics.

Genetic algorithms

John Holland developed GAs in the 1960s and the 1970s [145]. GAs have been utilized as optimization methods in various fields, and have optimized problems to find the optimal solutions in a wide variety of applications [146]. By utilizing the genetic algorithms, six basic issues should be considered: i) chromosome representation, ii) selection function, iii) genetic operators like mutation and crossover for reproduction function, iv) creation of initial population, v) termination criteria, and vi) the evaluation function [147].

The GA procedure with the four main steps is presented by [145] which starts with a randomly population of n chromosomes, which is the candidate solution to a problem (initial population). Then the fitness $f(x)$ of each chromosome x in the population is calculated. Therefore, in the selection step, the parent chromosomes for reproduction is selected based on a probability distribution which is defined by the user. With the probability of the crossover, chromosomes resembled to form two offspring. There are single point crossover and multi-point crossover in which the crossover rate for two parents in a single point and a pair of parents in the number of points respectively. Therefore, mutation of two offspring place the new produced chromosomes in the new population. In the last step, the current population is replaced with the new population. Therefore, the new generation is composed completely of new offspring and the first generation is entirely replaced and these steps are repeated till finding the solution.

Fuzzy logic

It is the theory of fuzzy sets. Fuzzy Set Theory (FST) was developed and applied by Lotfi A. Zadeh in 1965 [148] for making a better decision by dealing with the uncertainty of daily life decisions. The new logic for representing and manipulating fuzzy terms was called fuzzy logic and Zadeh became the father of fuzzy logic. A fuzzy logic system (FLS) provides a valuable flexibility of reasoning by utilizing the rules which are set in natural language. It is applied in different fields of fracture mechanics. For instance, in [149] it is applied in fault detection of a cracked cantilever beam. Moreover, when laboratory data exhibit scatter (like fatigue or creep tests) which leads to uncertainty on the result, the FL can be employed to obtain richer results. FLS process has three main phases which are fuzzification for gathering input data and creating fuzzy set, defuzzification for the resulting fuzzy output and a rule base contains a simple IF-THEN rules with a condition and a conclusion [150].

FL algorithm is initialized qualitatively by defining the linguistic variables and terms and it is initialized quantitatively by contrasting the membership functions ($\mu F(x)$).

Therefore, by utilizing these membership functions, the input data is converted to the fuzzy values. Afterwards, in inference engine, all the rules are evaluated and the results of each rule are combined, and finally the output data is converted to non-fuzzy values by utilizing the membership functions.

Case-based reasoning

It is the fifth AI methods which we reviewed in this chapter. Over the years, CBR approach is applied in different fields of science and technology. For instance, it is applied on technical diagnosis and maintenance, medicine and health science, classification, law, planning, intelligent sales support, decision supporting system, engineering design and software development [151, 152, 153, 154, 155, 156, 157, 158, 159, 160, 161, 162] and demonstrated good potential for wide range of applications in the real world.

It is an intelligent technique for solving new problems by finding previous similar problems based on the previous experiences and cases which have similar solutions. Core components can be grouped into the following areas by CBR: (1) knowledge representation, (2) retrieval methods, (3) reuse methods, (4) revise methods and (5) retain methods [163]. The CBR is usually divided into two different classes: (a) interpretive CBR and (b) problem-solving CBR. Previous cases are used as reference points for classifying new situations by interpretive CBR, while previous cases are used to recommend solutions for new problems and conditions by problem-solving CBR [164, 165]. As a description, in interpretive CBR, cases are classified already and new cases will be judged and categorized by comparing and contrasting arranged cases [166]. In CBR, the knowledge cases are structured and stored in a case base. After present a new problem, CBR generate a description for the problem and search for similar problems. In retrieval step, the solutions of similar problems are used by CBR. To apply the solution, adaptation techniques may apply if it is necessary. Finally, when the process is successful, the results are stored to use in future. For instance, General Electric used CBR for gas turbine diagnostics [167], which contains retrieve, reuse, revise and retain steps. When a turbine trip report is received, a nearest-neighbor technique is used to retrieve some number of cases with the input case. The CBR Engine is responsible for executing all modules for diagnosing new incidents and monitoring the system.

4.2. Fracture mechanics in different sub-domains

For technology in mechanical engineering, not only supervising of processes, but also study, investigations and analysis of different sub-domains of engineering fracture mechanics of the systems are important. These parameters are able to improve process and system performance. As it can be seen in Fig. 4.1, the five mentioned AI methods are reviewed which are applied in sub-domains of fracture mechanics. These sub-domains are:

- failure mode and mechanism identification (FM),

- damage and failure detection and diagnosis (DD),

- fault and error detection and diagnosis (FD),

- mechanical fracture and fracture parameters (MF).
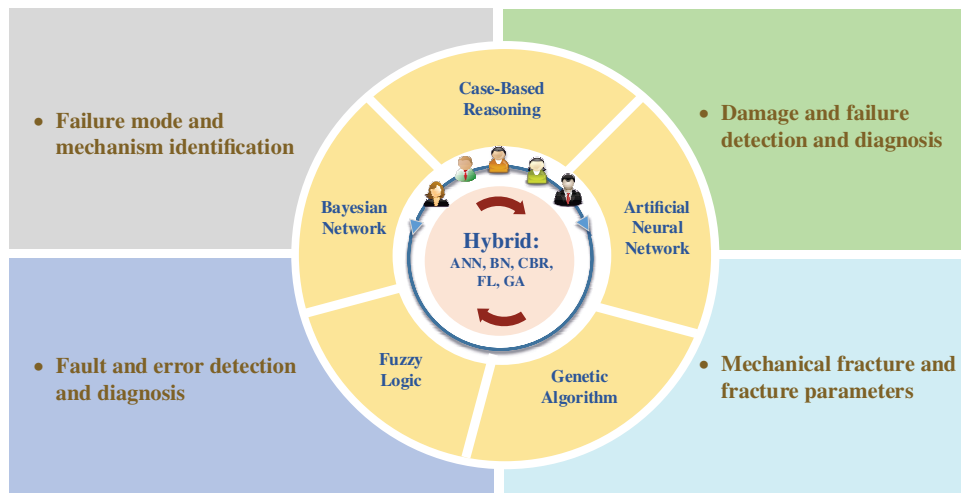
Figure 4.1.: AI applications in fracture mechanics.

The mentioned four sub-domains of fracture mechanics had been active research areas in the past years which are also the research domain of AI applications. The definitions of these sub-domains are recited as follows:

- Failure mode and failure mechanism: A mechanical failure mode is defined as physical process or processes that take place or combine their effects to produce a failure [168]. In this regard, failure mechanism is defined as a detailed description of a failure mode.

- Damage and failure: Mechanical damage is a characterization which presents existed defect on the object. Damage could be in micro, meso and macro scale and led to the mechanical failure.

- Fault and error: On the mechanical components or system, fault and error are defined as loss of ability to do required mechanical action. In other words, they are a deviation from the normal (expected) value and an occurred.

- Mechanical fracture and fracture parameters: Fracture mechanics deal with solid containing planes of displacement discontinuities (crack) [169]. Fracture is the separation or fragmentation of a solid body into two or more parts [170]. Several parameters such as crack propagation, fracture energy, fractography and fracture toughness are concerned on mechanical fracture.

4.3. Applications of AI on sub-domains of fracture mechanics

In this part, comprehensive literature study is carried out about AI methods which are used in the above mentioned sub-domains of engineering fracture mechanics.

4.3.1. Applications of Bayesian network

BN is a tool for modeling complicated problems in probabilistic knowledge representation and reasoning. Since 1990's it has also been applied in fault detection and diagnosis of mechanical systems such as a fault in combustion engine, automobile and gas turbine engine [171, 172, 173]. Probability reasoning is an approach which considers uncertain information and BN as a technique that brings it into reality. BN is a technique for uncertain knowledge and limited information in fault diagnosis. Mechanical fault diagnosis based on BN contributes to the probability of possible ranking failures, handling simultaneous failures and uncertainty symptoms of certain faults.

Bayesian network in fault and error detection and diagnosis

For fault detection and diagnosis as a sub-domain of fracture mechanics, application of BNs in fault diagnosis is presented by [171, 172, 135, 174]. In [171] dependency between exhaust gas contents and fault in injection system is modeled. The fault is modeled in a four-cylinder engine. Three ranges of variables are defined as low, normal and high for injection of little fuel, faultless operation and too much injection respectively. Also, for other variables in exhaust gas content, the same ranges are considered. It was claimed that the case is well suited, because it could be extracted from the network and handled as a small three-node network without loss of generality. We continue to review BN applications in fault detection in current century. The use of BN in mechanical fault detection is explored by [172]. They used Bayesian network to model the temporal behaviour of the faults and proposed a fault diagnosis system. In the design of the system, Markov assumption is used which stated that the future is conditionally independent of the past given the present. The implemented BN based system tested for car handling system. In this respect, classic bicycle model of vehicle is considered and steering angle to deviation rate and sideslip angle is calculated. The researchers used experimental data from a car factory which is obtained by standard sensors. Although the accuracy of the diagnosis depends on the magnitude of the faults, results showed that the developed system diagnosed the faults with small magnitudes. The researchers in [135] implemented fault diagnosis by using BN based on statistical parameters of vibration signals in time-domain for gear train system. They considered and defined several statistical parameters of vibration signals in fault diagnosis. Corresponding gear faults of experimental rotor-bearing system is simulated to produce the training samples. In detail, tooth breakage fault and wear fault are considered and several training samples

for each fault are studied. More over the BNs, they used back-propagation neural network and probabilistic neural network in fault detection of the same system. Finally, it is concluded that there are no wrong diagnosis results by using Bayesian Networks. By [174] an intelligent system is developed which is based on Bayesian belief network for fault inference of rotating flexible rotor. The researchers employed human expert's knowledge and three layers configuration of Bayesian belief networks is implemented. The first layer presented running and environmental conditions, second layer composed faults which should be investigated and the last layer contained those which are caused by the faults directly. Some data of the layers could be provided by human expert and technician. The constructed Bayesian belief network is employed for diagnosis of the flexible rotor and different machine faults are considered. In this respect, single fault and composition of the machine faults are considered. The results of implemented Bayesian belief network in fault diagnosis for rotating flexible rotors demonstrated good agreement with experiment results. It should be noted here, in comparison with the traditional BN, the developed Bayesian belief network considered the information not only from the fault systems but also from the machine running conditions and it could be counted as an advantage of implemented system. In the same year, application of BN in fault detection of fixture is explored by [175]. Different reasons could cause dimensional deficiency like the fixture failure. The proposed system is able to quickly detect the fixture fault which is used in the assembly process. Construction of BN from data consists of two tasks which are learning from network structure and the parameters. In fact, it involves optimal sensor placement for network node selection and structure learning algorithm based on mutual information tests. The researchers used commercial software Netia for the network conditional probability table learning and belief updating. The proposed BN could be more accurate by updating with more measurement data and knowledge. According to the results it is concluded that the developed model is robust and practicable.

Bayesian network in damage and failure detection and diagnosis

As reported by [176] BN is applied for categorizing different damages in jet turbine aircraft engines. A specific engine is selected and different possible fault categories identified. Moreover, additional faults added which could occur within single fault category. In order to differentiate between the occurrences, three different magnitudes (small, medium and large) and three flight phases (take-off, climb and cruise) are considered. Initial tests of BNs indicated that fault detection is much easier in the cruise region, than the other two regions. By this method, the correct identification is occurred. In fact, BNs worked well for the points which have been designed. Recent evidence proposed Bayesian damage diagnosis approach for bearing failure by [177]. Damage detection of bearings is important issue as bearing plays an essential role in some applications and it's needed to be predicted at an early stage. The researchers collected acceleration data and energy of vibration of the bearing which is used on a rotary machine. Generally,

the bearings are destroyed due to the long duration of usage and for the acceleration on the damage process some external particles with certain diameter are added to the lubrication. For the test the device worked eight hours per day and stopped for the rest of the day. A first order autoregressive moving average model is used to characterize the vibration level of the bearing, and also in the procedure of the prediction, they used last available points of observations while training data are not sufficiently available. The researchers used data filtering and the prediction without any influence from the uncertainty on the real data is achieved. The obtained results proved that the Bayesian approach could be used to determine remaining useful life while condition monitoring data is utilized.

Fault detection and diagnosis in engineering based on BN, combined graph theory which provided more knowledgeable and probability theory that provided very well representation of uncertainty. Recently, with development of data mining techniques, the inference and learning capabilities of BN have gained more attention. Although BN is applied to model diagnostic systems, but there is no structured way for building BNs (as there is for another method like fault tree). In fault detection by Bayesian network, it is not possible to identify a fault which the system has not been designed. So, all possible fault types which could be reasonably occurred should be taken in the early stage of process design. On the other hand, estimation of conditional probabilities network is involved. For these reasons, BN is mostly combined and integrated with CBR which is applied in other fields [178]. In this case, the probabilities achieved by training a network structure with data on past fault situation.

4.3.2. Applications of Artificial neural network

As a branch of AI, the ANNs are introduced and applied in various mechanical engineering problems, as well as fracture mechanics. They deal with problems which are difficult to analyse by the help of other methods. On the optimization, identification and damage detection, the ANNs applied in fracture mechanics.

Artificial neural network in failure mode and mechanism identification

The ductile fracture could occur in cold forming process, so prediction of fracture process is able to improve the production quality significantly. Another application of neural network on fracture mechanics is presented by [179]. The ANN is used in the prognosis of fracture in steel cold forming operations. The developed ANN received input data on stress and strain histories and predicted fracture for wide range of bulk forming operations. In fact, the system is trained by stress and strain data and the prediction of fracture occurrence was defined as an output of the system. The researchers are collected experimental data on fracture occurrence of chosen material which is produced by different forming processes. With the aim of best performing architecture, the ANN was carried out on MATLAB environment. Different configurations are tested for the

network to obtain a satisfactory result which is contained of four hidden layers. This architecture prepared successful training performance which means square error is very little. The later performance of the system is tested by set of data which are not contained into the training data set and achieved result predicted fracture in acceptable range of error. Although there are advantages in adhesive bonding on composite materials which are capable to joint dissimilar materials, the disadvantages influenced the mechanical failure behaviour of these joints. Failure load on adhesively bonded composites was predicted by the neural network and discussed by [180]. They fabricated specimens which are bonded in five different angles and five different bonding types. After that tensile tests are conducted and ANN analysis performed to predict the failure load. The researchers used back-propagation algorithm as supervised learning algorithm. MATLAB ANN toolbox is used and obtained results with low values of mean error proved that ANN method could be used effectively to predict failure load of bonded joints.

Artificial neural network in fault and error detection and diagnosis

Since ANN found comprehensive acceptance in many fields for modelling complicated real world problems, [181] used neural network for fault detection on helicopter rotor system. Single and multiple faults are considered on the damaged blade and neural network detected and quantified both types of faults. Maintenance cost of a helicopter rotor is high, but usage of health and monitoring systems reduced it. The researchers developed a neural network-based approach for rotor system fault detection. In detail, two neural networks consist of input, hidden and output layers which are used to categorize the type of fault and also to characterize the level of damage. For the fault detection of helicopter blade, it was important to train neural network with noise-contaminated response data. For this reason, three representative rotor faults are used and training data started form undamaged rotor and increased damage intensity on damage blade. the advantage of system was capability of the developed system in case of more damage types. One year later, it has been suggested by [182] to use high order neural network for fault diagnosis of rotating machines. In this research, theory and the structure of the higher order neural networks are reported. The standard feedforward neural networks has some limitations, but higher order neural networks are suggested for the fault diagnosis. Since large rotating machines have complex structure, different types of fault might occur. The researchers proposed a Hierarchical Diagnostic Artificial Neural Network (HDANN) based on ellipsoidal unit networks. Various fault data of a motor is used and frequency feature of the vibrational signal are obtained. On the system, new fault data are utilized which is has not been used in the training program. Based on the achieved results, it is proved that the HDANN is more accurate. HDANN could also be used for real-time condition monitoring of the large scale rotating machines. Also, this research showed that the proposed method is easier to retrain than the single network which is very applicable in the online training process.

Lots of mechanical failures on the parts of machinery showed warnings in advance. These warnings are usually a physical condition which specifies that a failure is near to occur. As it is reviewed, changes on natural frequencies and mode shapes are example of these warnings which used on ANN-based system for fault and damage detection. Based on the conducted investigations, it can be concluded that the significant advantage of the ANNs among other methods is capability of predicting crack growth direction on the sheet of material under the influence of second or more cracks. Another advantage is that while ANNs is used, it is not necessary to make prior assumptions about the concerned material behaviour. Also, in structural damage identification, ANN has been shown that the local damage could be better identified when the structure is divided into sub-structures and each sub-structure analysed separately.

Many types of machinery are used rotary parts such as different types of bearings, gears, motors and shafts. Over the past few decades, ANN extensively adapted to use in fault diagnosis of rotating parts and machinery and have been applied in different types including Back Propagation Feed Forward (BPFF), Feed Forward Neural Network (FFNN), Back Propagation Neural Network (BPNN), Multi-layer Perceptron (MLP), Radial Basis Function Networks (RBF), Recurrent Neural Network (RNN) and Learning Vector Quantization (LVQ). All the above mentioned neural network methods are applied for fault detection of rotating parts and machinery which are listed in table format and we already published in [112].

Artificial neural network in damage and failure detection and diagnosis

In different investigations, ANN is used for damage detection on beam-like structures. In [183] vibration data is analyzed by ANN in order to detect the location and severity of the damages in beam-like structures. In fact, natural frequencies and mode shapes are used as input data of ANN to predict damage in beam-like structures. In this regards, modeling and simulation is performed and vibration data which are first three natural modes for damaged and undamaged beams are obtained. To find most effective ANN, they designed different neural networks by MATLAB toolbox. To check the robustness; the researchers generated artificial random noise numerically and added to the noise-free data during the training of the ANNs. In the experiments, modal parameters are obtained by surface-bonded electrical strain gauges which are connected at the tip of the steel beam. By the achieved results, increasing in the noise level led to predict the damage location more accurate than prediction on the severity of damage. Moreover, it is claimed that experimental procedure and measuring devices have important role in prediction of location and severity of the damage. Application of ANN for damage detection in beam like structures is developed by [184]. In fact, crack damage in cantilever steel beam is predicted by ANN. In this respect, undamaged and damaged beam are modelled and first three natural modes are obtained as necessary features for crack detection. In the experimental test, several steel beams are used which are equipped with strain gauges and accelerometers. The proposed system predicts

location and severity of the crack damage.

Later, in [185] ANN approach is used for fault diagnosis of cracked cantilever beam. The proposed system is made by six input parameters which are first three natural frequencies and first three mode shapes, while the output parameters are depth and location of the crack. A beam made of aluminium is used to do experimental setup and determine natural frequencies and mode shapes. Very good agreement is obtained from the comparison between experiments and the proposed system for cracked and uncracked beams. Later, vibration data and ANN are used in damage diagnosis of beam-like structure by [186]. The first four natural frequencies of the beam are predicted on free vibration condition by neural networks in the first part. In the second part, crack parameters are determined while natural frequencies and mode shapes are used as input of the neural networks. In order to obtain lower error estimates, different hidden nodes are tested and the optimal method to predict crack parameters in presence of the noise is determined. At the same time, it has been demonstrated that ANNs is a feasible solution for fault diagnose and predict crack growth on the beam-like structures and metal sheets as well. [187] designed neural network architecture to predict crack growth direction on an aluminium sheet and showed that ANN is able to predict crack initiation direction with good accuracy. At the same time, as presented by [188] fault is diagnosed by ANN on a beam-like structure. In [187] aluminium alloy with different crack positions are used and tests are performed under static loading condition. In multiple cracks analysis by ANNs not only material properties (for instance modulus of elasticity, yield strength), but also wide range of crack position parameters (such as crack size, crack offset distance) could be used as input. The network structure and their operational parameters are selected mostly by using trial and error method. It is concluded that, best prediction by ANNs is recognized while sigmoid activation function with two hidden layers are used. Although different fracture criteria for determination of crack initiation direction are introduced, but obtained results from the ANNs showed good agreement with experimental results. For the I-beam structure, two different damage points are studied by [188]. Finite element model (FEM) is implemented and combination of natural frequencies and mode shapes are used as a dataset for training and as an input parameter of ANNs as well. Modal testing and experimental modal analysis performed on both undamaged and damaged I-beam. The ratio of damage depth to the height of the beam and ratio of damage location to the length of the beam are defined as damage severity and damage location indices respectively. Both mean square error and absolute error are considered to evaluate the designed ANN. Achieved results showed that the ANN is feasible and efficient technique for damage identification on I-beam structure.

Artificial neural network in mechanical fracture and fracture parameters

Due to catastrophic failures, mechanical engineering design criteria are consequently developed based on fracture toughness. In fact, developments are performed to increase safety in structures design by prediction the fracture toughness on the working condi-

tions. Fracture toughness is a fundamental material property which is influenced by the microstructure of the material. Study, investigation and prediction of fracture toughness of different materials have been subject of considerable research interest for many years. [189] demonstrated prospect of neural networks applications on fracture mechanics. Indeed, they adapted computational fracture analysis methods to neural network computing environment. In detail, three following problems considered which are (a) a crack with classical interface condition, (b) cracks with detachment and (c) parameter identification problem for a cracked body. For the mentioned problems, neural network approach is applied and the 4th- order Runge-Kutta method is applied to achieve numerical solution of the system. Due to the appearance of the inequality subsidiary conditions, problems are in different levels of difficulty in the classical sense and the applied neural network has shown good convergence. From the obtained results and the numerical experiments, the researchers concluded that in inequality problems the ANNs method is superior compared to the trial and error approaches and classical optimization.

Later, the possible application of ANNs in the field of fracture mechanics by prediction of fracture toughness is showed and proved by [190]. They used experimental data from [191] which contains uniaxial and biaxial tests on beams and plates with straight and surface cracks. ANN is used to predict fracture toughness of special aluminium alloy. Also, a relationship is developed between fracture toughness and the crack geometry, specimen dimensions and operating temperature. For the training process the NeuroShell simulator is used and after some adjustments the prediction of trained model was in good agreement with the actual gains. One important property of developed ANN is ability to determination the contribution of parameters which are an influence on average of the fracture toughness.

In the work done by [192], ANNs are used to predict fracture parameters of concrete. To predict fracture parameters, a fracture model based on ANN is presented. The fracture parameters are critical stress intensity factor and critical crack tip opening displacement. The used data are taken from literature which obtained from different test methods in several laboratories. Fracture parameters of concrete influenced by four material parameters. One of these material parameters was not available in the literature and for this reason the researcher used other three parameters as an input. Two fracture parameters (as mentioned above) are the output of the ANN. Data is presented to the ANN and the trained system showed the results which are very close to the experimental results. The obtained results have an accuracy which is acceptable for most design consideration. In addition, as a parametric study effects of compressive strength and maximum aggregate size on fracture parameters are investigated. This study proved that ANN could be used to perform parametric studies in the area of fracture mechanics. From the evaluation of the AI methods, it's foudn that the ANN can be built directly from experimental data without simplifying assumptions and using the self-organizing capabilities. Another advantage of this system is that results of ANN could be easily adapted to the other fracture models which also propose two parameters for modelling of fracture.

4.3.3. Applications of Genetic Algorithm

Application of GA in engineering domain is developed by [193]. Different measured responses could be used to determine structural damages. For instance, strain mode shapes, natural frequencies and mode shapes are measured and used in detection and identification of different types of structural damages. Like other AI methods, genetic algorithm also applied in the area of fracture mechanics. In this part, engineering applications of GA in damage and failure detection which is a sub-domain of fracture mechanics is reviewed.

Genetic algorithm in damage and failure detection and diagnosis

Genetic algorithm has also been applied on mechanical damage identification like to the ANN approach. Damage detection and particularly determination of location and intensity of damage in mechanical systems or structures by utilize the measured vibrational data on GA. Several application of GA in damage detection in engineering structures are documented [194, 195]. Identification and location of damage in elastic structure is determined from measured natural frequencies and mode shapes data based on GA by [194]. They implemented a method with the concept of residual force vector which is GA-based and tested on truss-type structure and cantilever beam to detect microscopic structural damage. For the truss-type structure, they simulated in finite element model and GA operated with exact mode shapes and natural frequencies. Also, they assumed three different problems and random noise added to the value of natural frequencies and mode shapes in order to simulate experimental analysis. The cantilever beam is also simulated numerically by FEM. There is possibility to formulate the damage evaluation problem as an optimization problem or objective function. Different numbers of modes are used to compute the value of objective function. The robustness of GA with respect to the effect of noise on measured data is shown. The obtained results show that the proposed technique is more capable compared with conventional methods which are used residual force vector for damage identification. Furthermore, accurate identification is recorded while multiple damage presents in the structural model. Since modal parameters of the structures are functions of the physical parameters, presence of any type of damages could be proved by changes in the modal properties of the engineering structures. In [195], measured displacements are used and GA is employed in damage detection to find the location and extent of structural damage. In detail, the method is applied for one skeletal structure which is truss bridges and vehicle transfer on the bridge is considered as series of static test. They suggested two different methods based on GA for structure condition monitoring. In the first method, just measured displacements are used and GA is employed to minimize the measured and corresponding computed displacement. The second method is performed by encoding the unmeasured displacements. In both methods, the truss bridge with same size of the span and different number of elements are considered. The obtained results indicated that suggested method based on GA

is able to determine location and magnitude of damage on the structure for measured static displacements. Moreover, the capability of proposed technique in determining unmeasured nodal displacements is proved. One advantage of the proposed technique is application on various types of structures. Also, ability in determination of unmeasured displacements which is avoiding the complete finite element analysis can be considered as a second advantage of the proposed method.

Later, in [196] modal data and GA are used to determine damage on the engineering structure. in fact, technique based on GA is proposed and natural frequencies and mode shapes are used in damage identification on engineering structures. Since small differences in natural frequencies can be result of significant damages, the mode shapes usually present a better solution in localized damage identification. In [196] researchers verified the suggested method with variety simulated damage scenarios. The different scenarios defined with different locations and degree of the damage. On the FEM, decrease on stiffness of each finite element presented damage in the structure. For the validation of proposed technique, experimental data is used. The capability of the implemented method on damage detection is proved by the achieved results. At the same time, crack location and depth in a shaft is detected by GA in the work done by [146]. The localized additional flexibility near to the crack presented by lumped parameter model according to the linear fracture mechanics theory. The researchers modelled the cracked shaft to obtain the frequencies and used in crack detection process. They performed experimental tests on different shafts which have fatigue cracks (cracks are produced by four point bending method) to check accuracy of the implemented intelligence system. By the achieved results, capability of the system in crack detection of the steel shaft is proved.

In the work done by [197] bi-dimensional and three dimensional models are presented with transverse breathing crack and GA is used as an optimization method in damage detection. They simulated the crack as a notch or a wedge in a finite element model. For the crack detection, the GA optimization method and dynamic response of damaged points are compared with obtained results from FEM. The optimization algorithm is developed in MATLAB environment which is in cooperation with FEM. In parallel, they also performed experimental tests and the results are used as an input in the detection algorithm. In comparison with [195, 196] in the research by Buezas et al. [197], the technique is applied for arch with a 2D model and for a blade-like structural element through a 3D model as well. Since this model could present a wind turbine blade, the proposed technique has high capability in damage detection in such engineering parts. In most of the researches, like the research by [197], achieved results are compared with two-dimensional FEM and experimental measurements for the validation. Moreover, usually the proposed approaches are verified by various examples with different damage scenarios and cracks with different configurations.

According to the applications of GA in damage detection on the engineering structures, it is concluded that this method is an effective method which is easy in implementation and due to the formulation, this technique can be used in several engineering structures

such as two-span continuous beam and frame structures as a damage identification technique. Moreover, experiences showed that no special requirement regarding to the initial values of unknown parameters is needed. Also, it should be noted that the quality of the measurement has important role in the success of this method.

Over the past years, some researchers suggested combination of GA with compatible method to produce a hybrid computational method in order to accelerate convergence and obtain more accurate results. Application of GA in hybrid intelligent techniques for fracture mechanics and fault and failure analysis is discussed later in this chapter.

4.3.4. Applications of Fuzzy logic

For the first time, fuzzy set theory presented by Lotfi A. Zadeh [148]. It is more general than traditional logical system. As it is explained, the FL approach is aimed at a formalization of modes of reasoning which are approximate rather than exact. During the decades, it is applied in many engineering and scientific applications and achieved results increased the amount of interest of this AI method. It is also used in different areas of mechanical engineering such as design, modelling and optimization. From the past century this technique is applied in the area of fracture mechanics which is reviewed as follows.

Fuzzy logic in failure mode and mechanism mechanism identification

In the recent years, different knowledge and experience are utilized and applied to characterise and predict mechanical failure on oil and gas pipelines. In this respect, FL approach is also used for prediction and estimation of failure on oil and gas pipeline by [198, 199]. In [198] fuzzy based model is developed to predict failure type on oil pipelines. They used historical data which covers European cross-country oil pipeline to develop the model that is able to predict mechanical and operational failures. In details, the researchers used MATLAB fuzzy logic tool box and not only different parameters such age and diameters of pipes, but also critical factors affecting failure are considered. The prediction effectiveness of the model is validated mathematically. Moreover, they compared the obtained results with models which are developed in some previous studies by different methods. It is claimed that FL approach predicted failure correctly the same as the other techniques. More recently by [199] corrosion failure of oil and gas pipelines are estimated by novel model based on fuzzy logic technique. The researchers defined two different types of corrosion which are corrosion cracking and corrosion thinning for the corrosion of oil and gas pipeline. Furthermore, some related factors of each corrosion type are considered as influence factors for prediction corrosion failure on the pipeline. To implement the system, fuzzy rules generated based on engineering knowledge using logic rules which are provided by experts and some standard specifications. Finally, on the real application the system is applied on carbon steel natural gas pipeline. The results showed that accuracy of the influence factors play important role to reach success

in this application. As it is concluded, this method can be used as an effective method in maintenance plane of the pipelines.

Fuzzy logic in fault and error detection and diagnosis

Fuzzy set approach is used for mechanical fault classification by [200]. They experimentally studied feasibility of fuzzy sets theory on integrated machine fault diagnosis. In detail, to provide information related to the dynamic behaviour of the machine, vibration sensors are installed on housing of gearbox and bearings support. The rotating parts produced unique frequency and change on this frequency is defined as a fault. Complete information about the dynamic condition of the machine is defined data which are collected and then Fast Fourier Transform Spectrum (FFTS) is utilized to extract useful information from sample data and convert into frequency domain. Fault clustering and fault assignment as two stages for fault diagnosis are considered. The output of fault clustering is set of classified cluster and the fault assignment appointed incoming data set to an existing pattern cluster. Fuzzy relations are defined and regarding to the fuzzy-sets theory, equivalence class under certain threshold is founded. The algorithm is implemented in FORTRAN programming language and the main menu is presented and explained. It is demonstrated that the proposed method is not very sensitive to the small changes in frequency.

FL approach is applied to classify different faults on the rolling bearing by [201] and to diagnose motor bearing fault in [202]. In [201] different fuzzy set shapes are used to process the frequency spectra. The data from low speed rolling element bearing tests is used which represented different bearing conditions and different error types. In signal analysis, the basic FL concept which is simplest fuzzy set is employed as a fault diagnosis tool. Variation within a group of spectra which presented the same type of fault was often significant, so upper and lower fuzzy membership function domains used to match standard deviation at each frequency. The ability on correct classification of frequency spectra which represented different fault classes is proved. However, it should be noted that generally various frequency spectra have similar characteristics, but it is depended to the data collection procedure and machinery and mechanical parts operating condition. In the research by [202], vibration signals of the bearing are analysed by FL approach. The researchers used fast prototype motor simulation (MotorSim) to generate appropriated motor data which is needed to indicate algorithm of motor fault detection. This software is also developed by the same researchers on the MATLAB-Simulink environment. Capability of the implemented system is tested by data which are generated by MotorSim. The obtained results proved that the developed system is able to diagnose the bearing faults accurately.

Mechanical vibration signals are comprehensively used in fault diagnosis by different methods. The main reason could be high understanding of vibration mechanisms of the machinery and mechanical parts and related changes. It could present different types of the fault. Applications of FL technique on fault diagnosis of mechanical rotary parts

and machinery is shown by [203, 204]. In [203] the FL technique is used for railway wheel fault diagnosis. They presented a new technique based on FL and vibrational data of healthy and damaged railway wheels. For the data collection, the new rails without any defect are used and measurements are performed on both healthy and faulty wheels. Defects on the wheels are presented by the changes on the measured vibration. In detail of the experiment, accelerometers are positioned on the special place where wheel-rail interaction produced vibrational signals. The damage on the wheel could be started and grow during the time, so it is considered as a matter of degree. The researchers implemented fuzzy decision system which is able to detect the degree of the damage. Three parameters (peak level of vibration, frequency and train velocity) are assumed as input to obtain wheel condition as an output. Four different levels of wheel condition are considered as outputs of fuzzy system. The achieved results proved capability of the introduced technique in description of rail-wheel conditions. FL technique is applied in mechanical fault diagnosis of pump by [204]. In fact, uncertainties are described by FL approach as mathematical tool. Fuzzy information analysed and frequency spectra are classified which are presented various types of pump faults. In this respect, firstly the diagnosis features are extracted from frequency spectra and secondly the fuzzy membership function established and finally fault diagnosis is realized. The used data are frequency spectra of vibration signals which are gathered from five-plunger pump. To determine fuzzy membership function of the fault diagnosis, converting the frequency spectra is used and for data gathering accelerometers are mounted on the housing of the pump. In case of the fault in the pump, changes in overall energy content occurred and this led to increase or decrease in general spectrum level. The obtained results provided confirmatory evidence on capability of the FL approach on identification and classification of the pump faults.
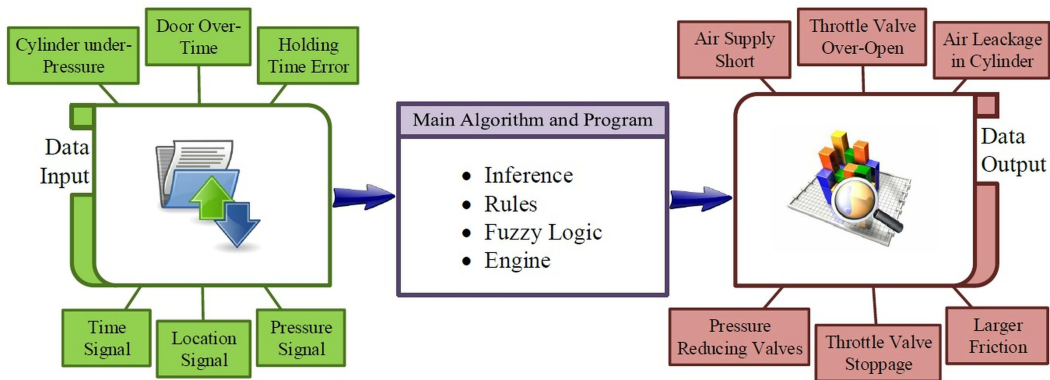
Figure 4.2.: Fuzzy-based fault diagnosis system for pneumatic press.

Fault diagnosis of pneumatic press based on fuzzy inference is implemented by [205]. In fact, feature factors of the press such as output pressure and run time are analysed. The fuzzy inference rule is employed to extract the fault signs and fault causes and finally

a fault diagnosis system is implemented. In detail, the fault symptom and fault causes expressed as set and membership function is accepted by experimental results. According to the calculation and the requirements of the systems, trapezoidal membership functions adopted. By analysing the information and working mechanism, all essential faults are determined. Furthermore, relationship factor between fault symptom and fault cause is defined based on the analysis and experimental results. The accuracy of the system is evaluated by experimental tests and it is claimed that the implemented fuzzy fault diagnosis system is a beneficial choice not only for the pneumatic pressure, but also for the complex pressing process. In Fig. 4.2 schematic of the fuzzy-based fault diagnosis system based on [205] is shown.

Fuzzy logic in damage and failure detection and diagnosis

Since failure on the engineering structures could led to irreversible damage and fatality, structural damage detection by AI methods is a critical issue for the research. So, the research in this field was carried out by [206] to show ability and accuracy of FL in mechanical damage detection. They modelled a Euler-Bernoulli beam and natural frequencies are determined by FEM. The reduction on the element stiffness is presented damage on the structure. Input of the FL system is the measurement displacements and outputs are location and size of the damage. In this respect, fuzzy sets with Gaussian membership functions are used for the input variables. Also, fuzzification of the numerical values which are achieved from the finite element analysis, are used to obtain rules for the fuzzy system. The proposed FL system is tested by measured data and high percentage of success is achieved. Sometimes in the real situation, some parts of measurements are missing or faulty. The researchers considered this issue and tested the implemented FL system while modal vector is missing. It is found that the proposed damage detection algorithm is quite accurate in damage classification with missing measurements as well.

Damage in engineering structures is also an important theme, which is still research topic of interest. Recently, damage of cracked beam is detected by FL technique [149]. In fact, FL approach is used to find location and depth of crack on a cantilever beam. On the fuzzy mechanics in crack detection, the researchers used FL control method which is used on their previous researches [207, 185]. In detail, fuzzy controller which used the hybrid membership function is formulated. As existence of cracks is able to change the modal data, this data could be used to determine crack parameters. So, first three natural frequencies and first three mode shapes are employed and defined as input parameters of the system. Then, desired parameters of the crack are defined as an output of the system. Experiments are conducted and the results are saved. On the other hand, MATLAB toolbox is used by the researchers and several fuzzy rules are trained to achieve the results. The obtained results from MATLAB and FEM are compared and this comparison proved that the implemented fuzzy system is able to estimate location and depth of the crack accurately.

The review of the published papers indicated that in the researches which are used FL

approach for damage diagnosis based on experimental data, achieving higher precision is possible by more measurement tests and results. It should be noted that, environmental noise or incorrect locations of the sensors have high impact on modal parameters like mode shapes and accuracy of the results. Furthermore, it is concluded that the FL is beneficial in the decision safety systems while response time is important.

4.3.5. Applications of Case-based reasoning

Over the last years, CBR is an intelligent approach which is used in area of mechanical engineering. Several researchers are applied CBR on different fields of mechanics. For instance, CBR approach is used for design of micro electro-mechanical systems by [208]. It is claimed that many designers of micro electro mechanical systems suffer from insufficient computer aided design tools. Moreover, some recent published papers such as [209, 210, 211, 212, 213] shows advanced and developed CBR systems which are used in the domain of mechanical engineering, but as it mentioned earlier, in this paper we focused on review of CBR applications on fracture mechanics. Although, lots of researches and studies have been performed to develop computerized techniques for the mechanical fractures, but to the best of our knowledge, comparatively few researches are conducted to apply and develop CBR in fracture mechanics. Like other reviewed AI methods, applications of CBR in the area of fracture mechanics is reviewed here.

Case-based reasoning in failure mode and mechanism identification

Since identifying failure mode of components, structures and parts, is the most important step in the whole process of failure analysis, different intelligent approaches by several researchers have been used in mechanical failure mode identification and analysis. In lots of domains, failure mode identification not only needs specific knowledge and expertise, but also it is usually complicated and time consuming issue. It should be noted here, CBR is an approach which is able to reduce this dependency to the extensive knowledge and information in the failure analysis. Human experts often use knowledge of similar cases in identification of failure mechanism and it is motivation of the researchers to use CBR and develop computerized system for failure mechanism. As reported by [214] CBR system is implemented to identify failure mechanism. They used experience of human experts and also the hand books and finally failure cases are represented in nine major groups of attributes. Two groups just described the case information and the rest are used for reasoning process and the final answer. It is mentioned properly that the case base cannot cover all kind of failure cases. Actually, when a limited number of cases are available in the case base, the failure mechanism of the most similar case can be inappropriate for a target case. Moreover, sometimes the target case is similar to more than one old case in the case base. They proposed a method by considering the next level of similarity values. In fact, they provided a mechanism for user to choose this adaptation if it is needed. Different CBR tools are available and can be used to

conduct CBR system, but similarity measuring methods in CBR tools might not be adequate and acceptable for mechanical failure analysis and it cannot be easily modified. For implementing CBR system, they used ACCESS as a database-management system which is user friendly and provided integrated development environment. One of the advantages of ACCESS is programming ability and moreover Visual Basic Application (VBA) as a powerful language is installed in ACCESS. Genetic algorithm learning module and CBR functions like adaptation and retrieval are created by VBA. By the help of a company, the researchers gathered 477 actual failure cases which divided to standard and exceptional cases, also fifteen failure mechanisms which are frequently occurred are considered. A case is standard if it supports induction of if-then rule, otherwise it is assumed as exceptional case. To evaluation the implemented CBR system, all failure cases were tested. The calculated accuracies for standard cases is more than exceptional cases. Moreover, two other methods such as rule-based system and multi-layer perception neural networks are also tested for the same data. By comparison of the results, it was concluded that CBR perform better than two other techniques. The amounts of information have effect on performance of implemented CBR and it was tested by reducing numbers of available information. In this case, accuracy reduced and it shows that more accuracy is obtained while more information is available. Also, it was confirmed that CBR system have incremental problem solving capability.

Case-based reasoning in fault and error detection and diagnosis

Fault detection in mechanical systems, different equipment and parts are still complex problems and several researchers applied CBR for this purpose. In [215] CBR is applied on acoustic signals of the industrial robots to diagnose faults. Comparison between normal and abnormal acoustic signals of industrial robots shows mechanical faults. They proposed CBR to collect, preserve and reuse in the fault diagnosis. The case library is made of normal and faulty sounds and the robots diagnosis results and sounds are recorded on the realistic conditions. There is ability to decide the fault class of the new case while unclassified sound signal is given. In the experiment, they have shown that identification is performed by one recorded sound and it's sufficient. The proposed technique accepted by technicians and supports them to achieve better results. Later, CBR is applied by [216] for fault diagnosis in maintenance of injection molding machine. In fact, the researcher developed a web-based fault diagnosis system which is based on CBR. The system is implemented for injection molding machine by application service provider which is in cooperation with ACCESS database. The machine is used to produce blank compact disc and the fault identification is a time-consuming process, if the users are not familiar with the machine. Original maintenance data are provided by a factory and the researcher determined seven possible fault types which are derived from fault tree analysis. Also, different symptom attributes are defined that can be useful to help in calculation of cases similarity. One advantage of such an intelligent system is application for other types of equipment. It is possible to do some modifications on the symptom

attributes and use the system for other mechanical equipment. Another advantage of CBR systems is updating case library which is continuously enlarged while new cases are saved.

For the fault diagnosis of gas and steam turbines, CBR is used by several researchers during the years [167, 217, 218]. In [167] CBR approach is employed for gas turbine diagnosis. This CBR system is helpful for the turbine producer while they want to reduce maintenance cost. Similarly, in [217] CBR is used to help users in decision making in the case of diagnosis and maintenance of gas turbine. Required information is gathered by the researchers from books, handbooks, operators and experts of the gas turbines. The researchers used Protégé which is an open-source platform for knowledge modelling and validated the system by human experts. Later, Dendani et al. designed and implemented CBR system for fault diagnosis of steam turbines [218]. In the implementation, they used jCOLIBRI which is a framework to make CBR systems. For the ontology domain, like [217] Protégé is used. In fact, they used domain ontology Onto-Turb which is built with Protégé to save steam turbine diagnosis cases. It is claimed that the implemented system is user-friendly and it is shown a rapid prototyping of CBR application. The achieved results from troubleshooting of steam turbine indicated that the system can be used for larger case base as well. All of the above-mentioned researches are applications of AI techniques in real-world problems, several issues such as accuracy and robustness are considered in the design and implementation stages.

Any particular AI technique has specific advantage and disadvantage. As an example there is no automatic structure to learn or improve the efficiency on the expert systems while they are used, but this problem is solved in CBR approach. To overcome the shortages of intelligence techniques which are applied by researchers and knowledge engineers, hybrid intelligent systems are developed. Combination of AI methods is generated hybrid intelligent systems that its applications on the sub-domains of fracture mechanics is reviewed here.

4.3.6. Hybrid intelligent techniques

Similar to any particular intelligent approach, hybrid intelligent systems are also used in a wide variety of applications [219, 220, 221]. In an intelligent hybrid system, two or more AI methods are combined to overcome the limitations of individual method. In other words, hybrid intelligent systems are computational systems which integrated different intelligent approaches. Here, hybrid system is the combination of the five reviewed AI methods in the last quarter-century. This review of literature indicated that GA combined with ANN, FL and CBR in the last two decades. FL also with ANN and CBR made a performed hybrid system. We have also hybrid system which utilized ANN, GA and FL to obtain appropriated and higher performance. Furthermore, ANN is combined with FL, GA and CBR to make a hybrid system which is reviewed later, here.

The benefits of hybrid intelligent systems for different applications are increased. For

example, rule based reasoning doesn't perform very good in learning and in working with poor or noisy data, but it's very good for explanations of the reasoning process. On the other hand, artificial neural networks are not very good on explanations of the reasoning process, but they act very good on learning and in working with noisy and poor data. Therefore, a hybrid intelligent system combined from rule based reasoning and ANN has advantages of the individual approaches. However, lots of attempts are performed to predict and consider all the possibilities at design stage. Here, in this section we reviewed hybrid intelligent systems which are employed for mechanical fault detection and diagnosis.

In the early current century, neurofuzzy network is proposed by [222] for application on vibration monitoring. In fact, the implemented system is made by input, hidden and output layers based on standard FL system and if-then rules are reduced by using neural network. For the evaluation and illustrate the performance of the proposed hybrid system, Fisher's Iris data set and Westland vibration data set are used which are famous benchmark data set. For the Westland vibration data set, several accelerometers are mounted on different locations on power transmission of helicopter. These data are recorded for different types of fault and one correct (no fault) condition as well. On the Westland vibration data set, two classifiers are used and compared with the implemented neurofuzzy classifier. The obtained data showed that proposed neurofuzzy network has higher accuracy and performance compared with other used classifiers.

Neuro fuzzy technique has also been employed to crack identification on the engineering structures. In the early current century, neuro fuzzy technique is employed for crack identification on the structure by [223]. Since crack properties such as location and depth of the crack have significant influence on dynamic behaviour of the structures, identification of these parameters has been widely investigated. The researcher presented a method based on fuzzy inference system to identify location and depth of the crack on the structures. In order to predict the size and location of the crack in the structure, Continuous Evolutionary Algorithms (CAEs) is employed based on the Adaptive-Network-based Fuzzy Inference System (ANFIS) architecture. ANFIS used depth and location of the crack as an input and structural eigenfrequencies as an output. To evaluate the proposed method, a clamped-free beam is considered. The crack parameters can be determined from measured eigenfrequencies of the structure. The neuro-fuzzy-evolutionary technique estimated size and location of the crack with high accuracy. Also, it is concluded that the method could be generalized for general boundary conditions and structures.

Hybrid intelligent systems made by CBR developed in different scientific and engineering areas. In the continuous of the previous study, capability of hybrid CBR technique on identification of failure mechanism was investigated by Liao [224]. He integrated CBR and multi-layer perception (MLP) neural network to obtain better results and identify failure mechanism automatically. The author utilized the data which are used in his previous study [214] and again in the similar way the Cases are divided to standard and exceptional cases. In detail, the implemented approach covered fifteen failure

mechanisms such as fatigue, creep, hot corrosion, brittle overload, ductile overload and thermal damage. Attribute weights are obtained by MLP neural network. To see the performance, MLP neural models firstly appointed on the training data and after that used to test unseen data. Moreover, to achieve good training results, the failure mechanisms with fewer cases are not considered for the training data. In order to evaluate the performance of the hybrid method, several sets of attribute weights are achieved. For testing each data set, the leave-one-out technique was followed. According to the results, it is claimed that activity measures which is used for attribute weighting, gives higher accuracy than other measures. The author believes that proposed method which is integration of MLP and conventional CBR sometimes leads to obtain better results instead of using each of them alone.

At the same time, in combination of two branches of AI with application on fault diagnosis, the CBR approach and ART-Kohonen neural network (ART-KNN) are integrated by [225]. Since machine breakdown leads to significant decrease in industrial production, the fault detection and diagnosis have been become critical in this domain. To understand machinery fault diagnosis, theory of ART [226] is combined with Kohnen's learning strategy [227]. ART-KNN is formed by attentional subsystem and orienting subsystem. The researchers build diagnosis system which could provide diagnosis results depend on measurement condition and signal. The proposed system, could be updated online and experts are also able to add new cases. In fact, the procedure of the developed system can be summarized as a case base, feature description and ART-KNN. As a description, case base is used to collect learned cases from case history as one uniform pattern. The researchers gathered cases from troubleshooting reports which experienced in industrial fields. Furthermore, feature of diagnosis procedure is consists of different categories which are extracted from the case base. Finally, classification of new cases is carried out by ART-KNN. For the experimental data, the researchers used several electrical motors with different motor defects such as bearing faults, rotor damage, stator faults and misalignment. The obtained result shows possibility to achieve high rate of success. It should be noted that the employed ART-KNN is able to solve the plasticity-stability dilemma of conventional neural networks and it can carry out online training that is different from most of the networks which carried out only offline.

In the area of fault detection and diagnosis [228] and [229] proposed hybrid systems. As maintenance in aircraft could be matter of life and death, reliable and effective maintenance is very important issue to avoid any problem or accident and also improve flight safety. In [228] the researchers proposed CBR system and implemented three different GAs procedures. To construct the trouble-shooting system, they used three hundred electric ballast maintenance records from one major airline and seven features identified as highly related to abnormal electric ballast operations. In fact, two hundred maintenance cases were used for training and the rest for the testing. After evaluation of all approaches, the best one which has minimum error is determined. It is suggested to use the proposed GA for other components of aircraft which leads to shorter repair times and lower maintenance. In [229] a hybrid intelligent system has been suggested

to detect the gear fault. The system was implemented by ANN and GA. Both normal and defective gears on the rotating machine are considered and time-domain vibration signals are extracted. The ANN trained with experimental data and GA is employed to select most suitable feature. The difference on process of feature extraction from time-domain signal is the main difference between the research by [229] and the work which is done by [230]. In fact, GA is employed in selection and optimization of input data in [229]. Several accelerometers are used to measure vibrational signals. For training and implementing of the ANN, the MATLAB neural network toolbox is used. The researcher investigated effects of signal pre-processing and also effects of load and sampling rate. The ANN with and without GA-based feature selection is used and it is found that on the ANN with GA-based selection of feature, the performance and accuracy are increased.

Application of thin-walled composite parts is significantly increased in engineering structures and due to their important role damage detection on these parts by different methods is interesting research topic. In this respect, a hybrid intelligent system is used by [231] to detect matrix crack in thin-walled composite beam. The implemented system combined specification of uncertainty representation form FL approach with the learning capability of GA method. Theoretically, the cracks in the matrix provided changes in natural frequencies and the researchers developed a hybrid intelligent system to determine location and level of the damage. They modelled a thin-walled hollow circular cantilever beam consists of composite laminates. One dimensional finite element analysis is conducted for dynamic analysis. The midpoints of the fuzzy sets are obtained by data from finite element analysis. The input of the system is measured frequencies. By the fuzzy system and the learning ability of GA, the size and location of the damage are obtained and optimized. The research showed that success rate of the hybrid system is depended to several parameters while noise is existed. The results also indicated high accuracy of the hybrid intelligent system, but it might be confused to determine damage location due to the high level of noise.

In the same year, by [232] CBR is combined with GA in order to identify the failure mode in aeronautical components. On the data collection, failure analysis cases of aeronautical parts have been collected by the researchers from failure analysis reports and journals, so three failure modes are considered. For the similarity measuring between new case and saved cases, they used adapted K Nearest Neighbours (KNN) algorithm, also attribute vector determined by weight learning process via GA-based training. For the training policies, a mixed training policy is proposed and used which is made by two different training policies. For the validation of training effects, both training policies and also the proposed mixed training policy are tested separately on the whole training set in the case base. It was observed that mixed mode policy gives better training effect. The results proved success of the implemented hybrid intelligent system with high accuracy in all three failure modes.

The hybrid intelligent systems which used in the area of mechanical fault detection and diagnosis in the last ten years, are summarized in table format and presented by us in [112].

4.4. Discussion and future of AI in fracture mechanics

The various types of researches are conducted to monitor the mechanical parts and engineering structures and predict failure load, crack direction and detect the mechanical faults. They diagnosed the mechanical faults at the earlier possible time and stage. Results of the researches proved that by using AI approaches, prediction time for fault detection and diagnosis is reduced compared with other methods such as experimental tests and computational methods. In the following sub-sections, advantages, strengths and limitations of the research works are discussed, and also important factors in implementation of AI systems are suggested. Moreover, our ideas about implementations of assistant systems to predict fracture of sandwich composites and mechanical properties of UHPC are explained.

4.4.1. Limitations and suggestions

Around twenty years ago expert systems also applied in the area of fracture mechanics and fault detection, but their application is limited. In fact, experiences showed knowledge extraction as a time consuming process. In real applications, lots of resistances from human experts are recorded when it was needed to import their expertise in a computer based system.

Bayesian network is used for mechanical fault detection, but it doesn't apply in so many cases in model-based approach, because specifying the conditional probability table of BN is a time consuming process and great attempts from the experts is essential. If instead of the experts, the data used in generation of the probability of the networks automatically, some weakness are unavoidable. In this case, a generated network is assumed to be demonstrated the distribution of data entirely, which could be counted as a restrictive assumption. Moreover, other factors such as inaccurate data values or absence of one type of the fault could lead to the failure on the data set and should be considered as a weakness of this method. In contrast, if machine faults divided to single faults and composite faults, identification of the composite faults of the machines is an advantage of Bayesian diagnosis network. However, several damage detection techniques are applied for different applications, but when some uncertainties are involved, the early damage detection turn into a challenging issue. In this case, the Bayesian damage detection techniques indicated successful applications in the last quarter around 8% besides the other AI methods.

Despite of reduction on popularity of ANN in the late of 1990s, but more recently ANN revived again and so far it is applied 46.5% in the area of fracture mechanics. Due to their abilities and properties to work with complexity, uncertainty and poor or corrupted data, they have been widely used. When experimental investigation of the parameters is not possible, some of the ANN techniques can be applied. For instance, as discussed ANN was applied and failure load on the joints was predicted accurately in the recent years. It should be mentioned here that changes which are performed in

techniques, application methods and the tools have big role and provide new opportunity which leads to success in this field. As researches showed, modal data and ANN are used and applied to detect the mechanical damages. Although changes on natural frequencies and mode shapes are investigated by ANN methods in order to detect the damages and diagnose the faults, it should be noted that damage in structures is a local phenomenon and might not be affected significantly the mode shapes of the lower modes. This case occurred more on the large structures. Moreover, in the gathering data from the experiments, number and position of the sensors plays important role on the accuracy of fault diagnosis system. It should keep in mind that intelligent prediction systems based on ANN have some advantages compared with traditional prediction methods. Nonlinear mapping properties, self-adapting, adapting to different environmental conditions and parallel processing capabilities are advantages from application point of view. Although ANN is applied for detection of mechanical faults on lots of cases in recent decades, it is suffered from some disadvantages such as low convergence rate and lacking sufficient generalization when number of fault samples is limited. Difficult extrapolation behavior is a problem in usage of MLP networks on fault detection applications. Since data sets are not complete and comparatively sparse in fault diagnosis applications, the diagnosis system should work outside of the trained symptom domain and it is created a problem in MLP networks. As a solution, radial basis function networks could be applied instead of MLP, because extrapolation behavior is a major difference between them. However, this ANN method also could not be applied in all fault detection and diagnosis cases, so other AI methods are hired in this area.

As it is reviewed, GA is also applied for mechanical fault detection and it is applied 8% during last 25 years. The evaluation of the systems shows that it is a great method, because search on the whole solution space is not required. Comparison of the performed researches and projects proved that combining GA with other AI methods, significantly increase the performance of the system. For instance, in mechanical fault detection when ANN is used and GA employed for selection of input features, the performance considerably increased and higher accuracy is achieved. In fact, combining GA and ANN presented better results than most of trial and error approaches. As it mentioned, GA is used as optimization method in damage detection. In this case, it is operated better than other optimization methods and it's more robust. According to the reviews on performed researches, it is concluded that intelligence systems such as ANN and GA have ability to adapt to the changing environment which is counted as an advantage. On the other hand, these approaches required especial training part that is considered as a weak point. Another disadvantage of these systems is that they are data oriented. In fact, they modelled the relationships that are contained in training data set. Thus, if the used training data set is not representative selection from problem domain, results are differed from real problem area.

Like other AI techniques, different performance criteria such as implementation aspects, accuracy and time must be considered while FL based system is used in mechanical damage detection. According to the performed researches and obtained results, applied

FL contribution around 10.5% in mechanical faults and damages and showed appropriated performance and highly reliable classification. This classification required very large training set and large number of parameters to obtain accurate results. Since, availability of this amount of numbers and parameters is not possible for some cases it could be counted as a disadvantage of this AI method in this particular application. By the performed reviews, it can be concluded that the FL and ANN are somewhat complementary to each other while one is lacking and the other could be useful. So, by the researchers they often used together and neuro-fuzzy systems are provided. In this case, two different categories of combination of neural networks and FL are available. In the first category, individual properties of both techniques are preserved and they work independently. In the second category, one of these AI techniques is attracted by the other one. However, application of neuro-fuzzy systems in the area of fault detection and damage diagnosis extensively developed in the current century. In fact, the neuro-fuzzy based systems have advantages of both techniques and as showed more efficiency than other fuzzy adaptive systems, their applications in mechanical fault and damage diagnosis increased. It should be mentioned here that the reviewed neuro-fuzzy systems are not very different in their structures and learning algorithms.

CBR applications on mentioned sub-domains of fracture mechanics shows 7% of total AI application in this field. In the area of mechanical damage and fault detection, human experiences are counted valuable property and it is more valuable if it saved and reused for other cases later. This demand is possible by CBR approach. It is a fact that some AI approaches do not used prior knowledge and this limitation is solved in the CBR approach. All types of results from successful solution and costly mistake experiences could be collected. It is clear that large amount of time and money would be saved if these experiences collected. This type of human thinking, intelligence and reasoning model could be provided in CBR technique. Indeed, by CBR technique the new users have access to not only local, but also distributed database which is covered previously stored experiences from other sources. In the area of fracture mechanics, all experiences can be stored by CBR in the form of fault and damage database which describe steps, signs, activities, reasons and detection of different type of failures modes which might be occurred on various mechanical parts. The conducted researches and obtained results indicated that implementation of intended knowledge base is a difficult and time consuming process and that is solved by CBR technique. It is really difficult while problem domain covered a broad range of knowledge, but explicit domain model is not needed in CBR and extraction is defined as a task of data collection for the case base. CBR is implemented based on defined features which are created the cases. This is more appropriate than create an explicit model by other AI techniques. Moreover, CBR has ability to learn and increase the knowledge from new cases. This ability and application of database technique provided convenient maintenance for a large-scale information. However, in application of CBR, retrieval and adaptation knowledge is still needed and it can be considered as a difficulty of CBR technique.

Beside of development of any particular AI method, the researchers found that dif-

ferent types of processing are required for complicated problems which are made by different components. Therefore, the researchers combined AI methods as a hybrid system to overcome to the deficiencies of any individual AI method. Hybrid systems with 20% contribution are in the second position besides the other five AI methods. According to the reviews, it is found that design and implementation of hybrid intelligent system in some cases is very difficult, because they have lots of parts, components and many interactions. Thus, it makes hybrid intelligent system complicated procedure. The problem is that interactions might be occurred between unpredictable parts at unexpected times and reasons. Lots of existing software development techniques are not able to manage these complicated interactions effectively and efficiently.

Since hybrid intelligent systems are made by different AI methods, choosing appropriate AI approach is an important part of the design stage. Indeed, in some cases different AI methods can be exist for any section of the hybrid intelligent system, but it is vital to select the most appropriated one. With the correct steps in the construction of a hybrid intelligent system, simulation of human-like intelligence is provided.

It is concluded that combination and integration of AI approaches provided a better solution than ones considered a single method which is applied in all of these sub-domains. Although implementation of integrated intelligent system is complicated procedure, the progressing developments opened new possibilities to investigate problems of fracture mechanics with an appropriate hybrid intelligent system. However, there are lots of things to be learned and models, techniques and methods should be adapted and improved to be more beneficial in dealing with complicated fracture mechanics problems in real world applications. Here, we suggested important factors, parameters and attributes that should be considered in the implementation of an intelligent systems in discussed sub-domains. These recommendations are described as follows:

- Method development

In order to utilize AI methods, the requirements and efforts of programming should be noted. On the other hand, it should be considered which available software packages are computationally efficient and can be used in the desired AI method. In this respect, an appropriate decision not only reduced cost of operating, but also time can be saved. Moreover, any attempt and strategy in design and implementation stage should be considered to reduce the computational cost.

- Capability on multiple faults

In some mechanical parts and cases multiple faults occurred. The implemented AI based system should have the capability of detection and classification of these multiple faults accurately. In some cases, mechanical faults are difficult to recognize, but the implemented systems based on AI approach should be able to detect the damages to maintain the diagnostic performance.

- Applications design

The implemented and established system should be friendly and readily usable for the engineers who are not deeply familiar with any particular AI technique and sophisticated statistical method. Moreover, in the design stage of AI damage detection system it should keep in mind that the physical necessities (such as memory and storage requirements) must meet the conditions of the application. For implementing a specific system, firstly the faults should be identified. Afterward, the method of implementation should be selected and the procedure of detection is designed based on diagnostic features and algorithms. The user interface of the system is one of key aspects in these applications while experts need the flexible and easy interface.

- Maintenance and update

Continuously decision support, defined as activities which have to be done to train the implemented AI system into designed operation conditions or return the order to these circumstances. The maintenance sometimes is expensive and needs investment on cost and time, but it is a vital activity which could increase the performance. On the other hand, update of designed AI system looks necessary to obtain better and more satisfactory results. For instance, by an update in an intelligent hybrid system containing CBR system, the performance and efficiency could be significantly increased. This update includes changes in design, required features and components standardization.

- Efficiency and economical aspect

Like other scientific fields, there is attracted interest in saving time and cost. The implemented systems based on AI approach are operated as a non-destructive method to detect mechanical faults and damages. Indeed, if the proposed and implemented system, correctly designed, well optimized and reached to high accuracy, it can provide significant economic benefits. The increase in usage of mechanical parts and machinery in the different industry leads to a collection of modern problems. Based on the reviewed literature on the performed projects and the researches, it should be noted here that AI methods have potential to convert difficult fracture mechanics problems into simpler. AI methods are utilized significantly, to reduce cost, saving time and enhance reliability of a system

- Accuracy, evaluation and performance

The high accuracy could be achieved by using one AI method, but the minimum number of feature and parameter should be used. In other words, beside of accuracy, attention has to be paid to robustness and simplicity of the system. So, in some cases higher accuracy and capability could be achievable by a combination of AI methods and use the hybrid intelligent system. In reality, uncertainties are inevitable. The system should be designed with high robustness in the measurement of uncertainties and increase the accuracy, reliability and effectiveness of the system.

4.4.2. Applications of intelligent system in studied composites

As our future works in the field of engineering applications of AI, it was contemplated and planned to apply CBR in the composites which are studied in this research. To this aim, two artificial intelligent systems based on CBR methodology are implemented. Development of these systems are in progress [113, 114]. The first systems is implemented to predict fracture in sandwich composite joints. The goal of the second system is prediction of UHPC mechanical properties. The details of these systems are presented here.

- Prediction of fracture in sandwich composite joints by an intelligent system

The evaluation of composite joints under various loadings is a fundamental issue in investigation on material behavior. Experimental practice and numerical simulation are two methods for this evaluation. However, precise knowledge about fracture occurrence and behavior of composite joints is crucial for design of structural elements. Beside of the mentioned methods, intelligent systems can also presents information about behavior of composite joints. Different AI approaches are employed for prediction of composite materials behavior, but CBR has not been used for prediction of fracture in sandwich-structured composite joints. Although fracture of a composite joint is not a deterministic property, accurate prediction of this fracture is achievable with an intelligent system. To this aim, we implemented a system based on CBR approach which is capable to predict response of the sandwich composite joints to the various loadings, and determine behavior of the joints under different environmental conditions. Moreover, the system is able to predict fracture occurrence in various sandwich composite joints. Implementation of this intelligent system requires detailed knowledge on composite materials and artificial intelligence approaches. The combination of these expertises leads to prediction of the behavior of composite joint as a function of loading and environmental conditions.

In our system, experimental data of literature studies are stored on the case base. This data is covered a wide range of sandwich composite joints which experienced various loadings from quasi-static to dynamic loading conditions. Moreover, on the case base of the system we saved data of sandwich composite joints which tested at different environmental conditions. This data are used for characterization of the joints and its performance under load and environmental condition.

Record of the documented failures is the first step in implementation of the system. Analysis of this data, helps to determine the key cause of the fracture occurrence in the joints. An implemented system consists of four main components. They are (a) parameters selection, (b) weight calculation of the parameters, (c) case representation and (d) prediction. In the first component, parameters of the sandwich composite joints should be selected. These parameters are related to the composite materials. Moreover, loading and environmental conditions should be specifically determined in this step. In the second phase, relationship between the parameters and behavior of the composite joint is extracted. To this aim, it is needed to define influences of each parameter to

the strength and performance of the joint. Also, weight of each considered parameter is calculated in this section. The third component is case creation which contains joint geometries, environmental conditions, fracture and behavior of the sandwich composite joint. The last component consists of case retrieval and prediction. In this part, fracture probability and response of the joint to the various environmental conditions are presented. Fig. 4.3 shows the structure of the system. This intelligent system, determined the long-term behavior of sandwich composite joints subjected to loads and exposed to various environmental conditions.
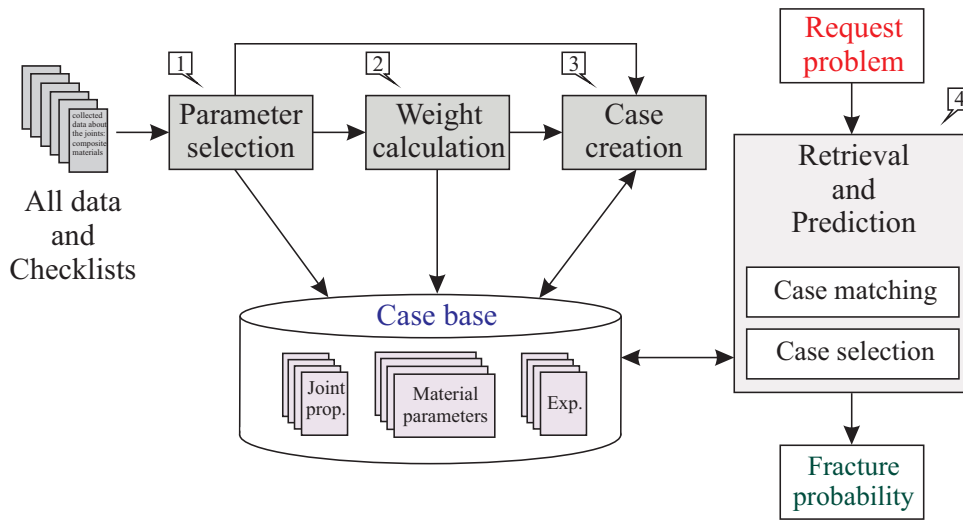
Figure 4.3.: Structure of the system for prediction of fracture in sandwich composite joints.

The output of the implements system are evaluated by experimental results which are achieved by the performed tests on studied composites. This evaluation proved that the implemented system can be effectively used instead of numerical simulation or experimental test, to predict fracture and behavior of sandwich composite joints.

- Intelligent system for prediction of UHPC mechanical properties

Since demands of engineering cementitious material are increased, investigation on mechanical behavior of this material is interesting topic in today's research programs. However, determination of mechanical properties of concrete-like material under dynamic loading is still a complex issue. Particularly, due to the difficulties in applying uniaxial tension in a concrete-like specimen, obtaining mechanical properties by other techniques is favorable. In this respect, it is aimed to predict HUPC mechanical properties by an intelligent system. Although different AI methods such as ANN and FL are used to predict some mechanical properties of concrete specimens, CBR has not been utilized to estimate mechanical properties of UHPC specimens. In our implemented system, CBR is applied to predict dynamic behavior of UHPC materials with various mixtures. To

this aim, data from the performed experiments which determined dynamic mechanical properties of UHPC are gathered and stored in a knowledge bank. These experimental data are acquired from existing publications. Furthermore, case base of the system is enriched by data of previous researches which discussed numerical simulations on UHPC under dynamic loading. Some of the utilized data which presents dynamic properties of various UHPC are summarized in Table 4.1. As can be seen, in the reviewed researches different mechanical parameters like elastic modulus, compressive strength and tensile strength, all under dynamic loading conditions are determined which we used on our case base.

Table 4.1.: Some of the stored data in case base of the system.

Reference	Experiment	Studied parameter	Result
[233]	compression	dynamic compressive strength	204.8 MPa
[234]	tension	dynamic tensile strength	24.9 MPa
[235]	compression	dynamic compressive strength	208.4 MPa
[236]	spalling	dynamic elastic modulus	55.3 GPa
[236]	spalling	dynamic tensile strength	45.6 MPa
[237]	compression	dynamic compressive strength	200 MPa
[238]	compression	dynamic compressive strength	160 MPa
[239]	Brazilian	dynamic tensile strength	19.3 MPa
[240]	compression	dynamic compressive strength	174.8 MPa
[241]	spalling	dynamic tensile strength	37 MPa
[242]	Brazilian	dynamic tensile strength	18 MPa

In the data collection, numerous researches are considered which have been tested various UHPCs. Throughout the years, UHPC specimens with various mixtures have been constructed. In these constructions, several types materials with different aspect ratios have been utilized. In UHPC recipes, fibers with different geometries made of steel, glass, polyethylene and carbon have been used. Literature investigations indicated that not only type of fiber material, but also the aspect ratio of the fiber should be carefully considered in the engineering constructions. Indeed, it is found that specimen size, mixture, fiber material and geometry influences response of UHPC to dynamic loading. In our CBR system, all these factors have been considered.

The implemented system is based on different phases which covers core components of the CBR. In practical application of the system, in the first step, a new incoming case should be refined by information about UHPC specimen. In the last step, the required dynamic properties in a range will be recommended to the user. The system is able to works, even when all the required input parameters are not given to the system properly. In this case, the recommended values will be presented mechanical properties with less accurate range. It should be noted that, when the current case is similar with a less

similarity degree, adaptation mechanism should be considered to obtain more accurate solutions.

The implemented system is utilized to predict dynamic properties of UHPC with various recipes and the outcome of the system compared with the values which are obtained from the experiments. The results of the system indicated its capability to determine dynamic mechanical properties of UHPC in a strikingly good agreement with experimental results. It is concluded that this intelligent system can be used for investigation on stability and safety of UHPC with different mixtures and time consuming experiments can be avoided. By considering more data, enriching case base and utilizing experts opinions, some modification can be done in the future, concerning various important parameters which influences behavior of UHPC material.

5. Experiments, results and analysis

This chapter focus on experimental tests on both groups of studied composite materials. Since obtained materials properties will be used for future computational models and material developments, the experimental test should be carried out precisely. In other words, material properties, and also response of the studied materials to various loading and different environmental conditions must be determined accurately to provide reliable data.

In this chapter, the details of quasi-static and dynamic loading tensile tests and also influence of environmental effects on sandwich T-join are presented. Excerpt of this chapter related to the experiments on sandwich T-joints is already published by us in [243]. Moreover, this chapter explained spalling and dynamic Brazilian tests on UHPC material under high strain rate conditions. In [244, 245] we already published essential parts of these tests on UHPC material which are presented in this chapter.

5.1. Characterization of sandwich composite T-joints

New engineering product design presents problems on prediction of the durability and behavior of an adhesively bonded structures at the early stage, before it is even built. Utilization of adhesively bonded composite joints in aviation and automotive industries, indicates this material is in direct human contact. Despite of these applications, the fracture behavior of these materials under static loading is still under study, because of the multitude of possible failure mechanism. Since, adhesively bonded composites structures have been subjected to various loadings, assessment of their fracture behavior and response to the loadings are crucial for design, dimensioning and production.

There are variety methods to test and measure the mechanical performance of the adhesive bond. The standards provided ways to identify mechanical properties of adhesive bond or joint which can be included strength, fracture, fatigue and creep. In detail, more than 30 standards are suggested test methods to measure the mechanical properties of an adhesive bonds. Most of the tests are mainly based on quasi-static or fatigue loading. Peel test, wedge test, shear loading test and tensile lap-shear strength are examples of available standards in evaluation of adhesive bonding. Standard agencies, for instance The American Society for Testing and Materials (ASTM), the International Organiza-

tion for Standardization (ISO) and the Comite Europeen de Normalisation (CEN) are the main reference for the standard tests. Although there are standards on design and manufacturing of adhesively bonded composite joints and the they can be adapted by the standard agencies to the specific test requirements, there is no standardized procedures on experimental fracture testing of the sandwich T-joints under quasi-static and dynamic loading regimes. The variety of pultruded products, provides a large range of different types of adhesively bonded composite joints, and this variety is one factor that makes standardization of tests for such joints difficult. Although T-joint is a structural element, the relatively large variety of basic T-joint design in engineering applications, and also different cross-section of composite products, clearly can be counted as another difficulty in standardization of fracture and fatigue fracture tests.

In work [246] sandwich plates made of carbon-fiber reinforced laminates are investigated and the major fracture types of adhesively bonded joints are classified. For a sandwich T-joint under tensile loading, three types of failure are schemtically illustrated in Fig. 5.1. In an adhesively bonded composite fracture can show as: (a) *cohesive failure:* The crack initiates in the adhesive and propagates in it till final fracture; (b) *adhesive failure:* On the adhesive or interfacial fracture, debonding takes place between the adhesive and the adherent structure whereby all of the adhesive remains on one side of the separated materials; and (c) *adjacent failure:* in this failure mode, adhesive and bonding area remain intact and the fracture occurs in the adjacent structure.
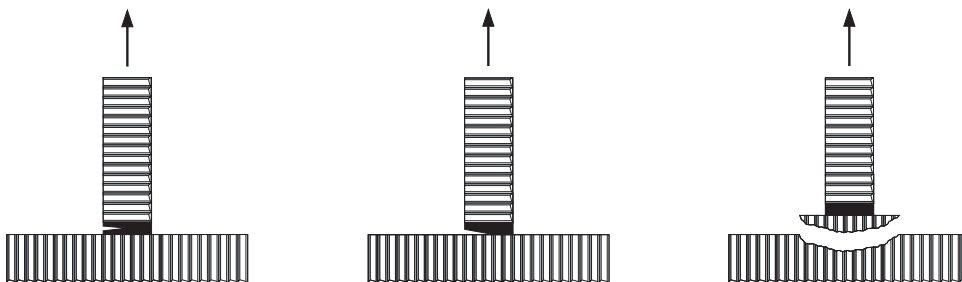
Figure 5.1.: The sandwich T-joints under static tensile loading.

Here, in this chapter experimental procedure of tensile tests under different loading conditions for both aged and unaged sandwich T-joints is presented, and the obtained data can be used to predict the service life of these parts. For this purpose, the achieved results can be used as an input in one of the AI approaches which are described in the previous chapter, and employ the proper AI technique to estimate the life time or damage initiation time.

5.1.1. Experiments under quasi-static loading conditions

The focus of the present part is on the tensile tests under quasi-static of aged and unaged sandwich T-joints which are employed in aviation industry. Analysis of the static loading

can be starting point of any engineering design process, specifically if the component holds mainly static loads. Actually, in many structural components and especially in aerospace adhesively bonded structures, constant force for an extended time can be observed. Therefore, static loading tests should be considered during the design process of the bonded components. This attention can be lead to prediction of failure load and also determine maintanance program details and increase safety by changing the joints before exceeds its residual strength.

All the static tensile tests on unaged and aged specimens were carried out by using the hydraulic machine fitted with 15 kN load cell and speed range of the machine is 0.01 mm/s to 30 mm/s. Electronic control unit allows monitoring the applied load and movement of the top cross head. The series of our static tests performed under displacement control at constant cross-head movement of 0.25 mm/s provided a strain rate of $1 \times 10^{-2} s^{-1}$ which is in the range of quasi-static loading conditions. All the test are carried out on the room condition $23 \pm 3\,^\circ\mathrm{C}$ and $50 \pm 5\%$ temperature and relative humidity, respectively. A rigid fixture was fabricated and used for the experimental setup not only to fix each specimen on the test position, but also to minimize non-symmetric effect, cf. [243]. The fixture keeps top and bottom of the base plate at both ends. A sandwich T-joint specimen under static loading is shown in Fig. 5.2. Combination of the sandwich structures from core and face sheets with different mechanical properties provides a coupled mechanical response which leads to difficulty in behavior prediction.
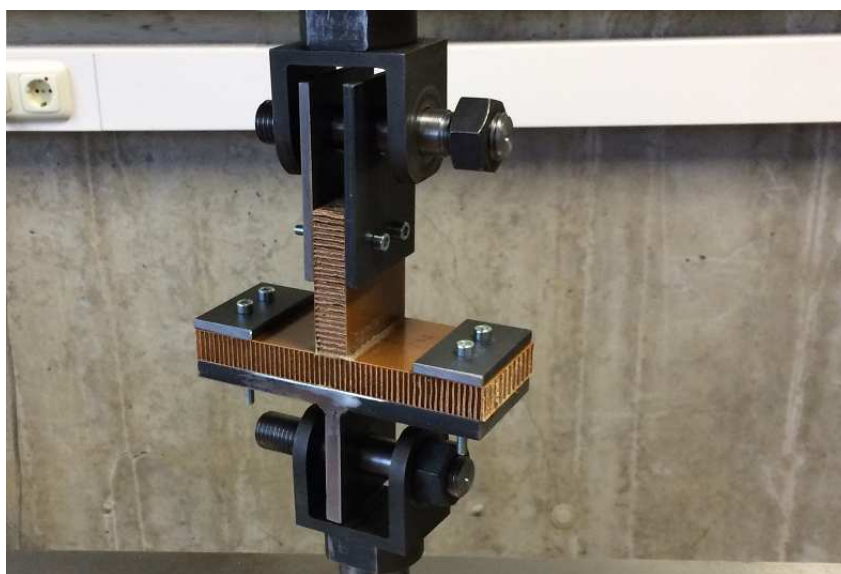
Figure 5.2.: The sandwich T-joints under static tensile loading.

Series of the experiments with the same conditions are performed and average of the load-deflection curves for the unaged specimens and the two groups od aged specimens under static tensile loading are shown in Fig. 5.3. The displacement controlled loading

leads to an almost linear rise until it reaches the peak load of 1550 N at a displacement of about 2.1 mm (averaged values for the unaged specimens). As can be seen in Fig. 5.3 the tensile load continues and debonding appears on the web/base interface, leading to the final rupture. The load drops rapidly and the test is finished.
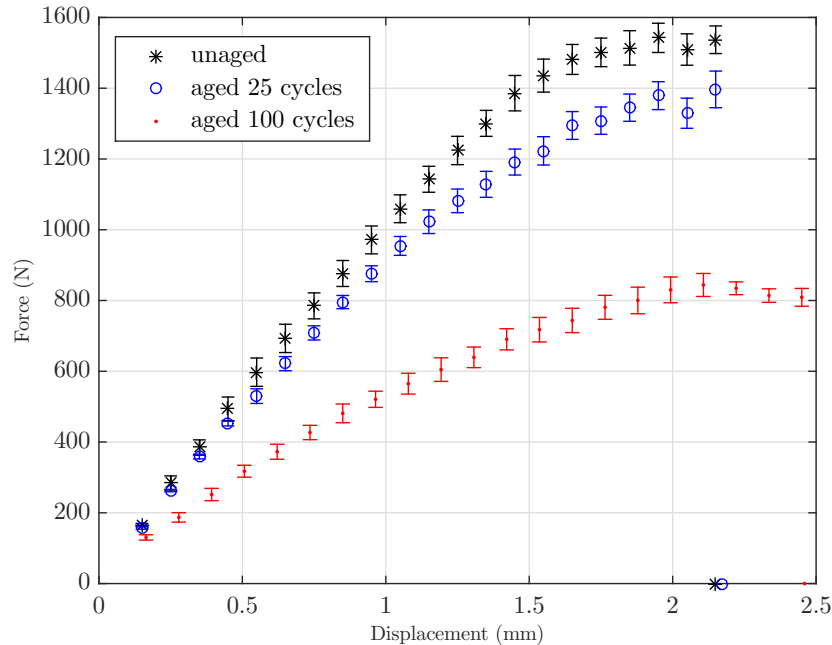
Figure 5.3.: Force-displacement curves of unaged and aged groups of sandwich T-joints.

The two groups of aged specimens experienced 25 and 100 cycle of accelerated aging. They are also subjected to a tensile load which is increased almost linearly. For comparison, the averaged of the failure loads of the unaged, 25 cycles aged and 100 cycles aged groups of sandwich T-joints are 1550N, 1395N and 835N, respectively. Clearly, the accelerated ageing causes a lower fracture load. Due to the ageing, adhesive network is plasticized, it leads to lower strength after ageing and stiffness reduction. Residual stress developed by temperature cause the initiation of cracks under loading. For all specimens the separation of the web from the base plate shows the features of brittle fracture. We need to mention that the thickness of the core and the thickness of the face sheets play a major role for the rigidity of the sandwich composite which affects the mode of failure. In our series of the tests the skin thickness remains unchanged, without any type of failure.

Visual inspection of the fracture surface of the unaged specimens showed that here cohesive failure had occurred, cf. Fig. 5.1. The crack grows in the center of the adhesive layer and also near an interface for some T-joint specimens. In cohesive failure, both composite bonding surfaces are covered by fractured adhesive after debonding. Regarding most quality control standards, cohesive failure is considered as a 'good' adhesive

bond because it shows suitable adhesive curing conditions and good cohesive strength. In other words, it is the desired mode of failure. For all the test specimens that experienced accelerated ageing, however, adhesive or interfacial fracture is observed. Indeed, the accelerated ageing changes the mechanical response of the adhesive. The changed failure mode can be attributed to a loss of adhesion or surface curing of the utilized adhesive in the course of thermal ageing which has also been observed in [247] for epoxy bonded CFRP.

The corresponding stress-strain curves are shown in Fig. 5.4 for the averaged values. Considering a step-by-step loading the observed zones are: (i) initial loading with linear-elastic deformation, (ii) loading with a (minor) softening; (iii) crack initiation and failure by separation. The achieved results indicate brittle fracture in all groups of specimen. For the unaged specimens it was observed that unloading can almost recover to the original configuration, i.e. the structure behaves mainly linear-elastically. The reason is that the core material (aramid paper) does not break in the initial stage of loading nor does it show any plastic deformation. For the specimens which are experienced ageing we have a certain reduction of stiffness in the course of loading.
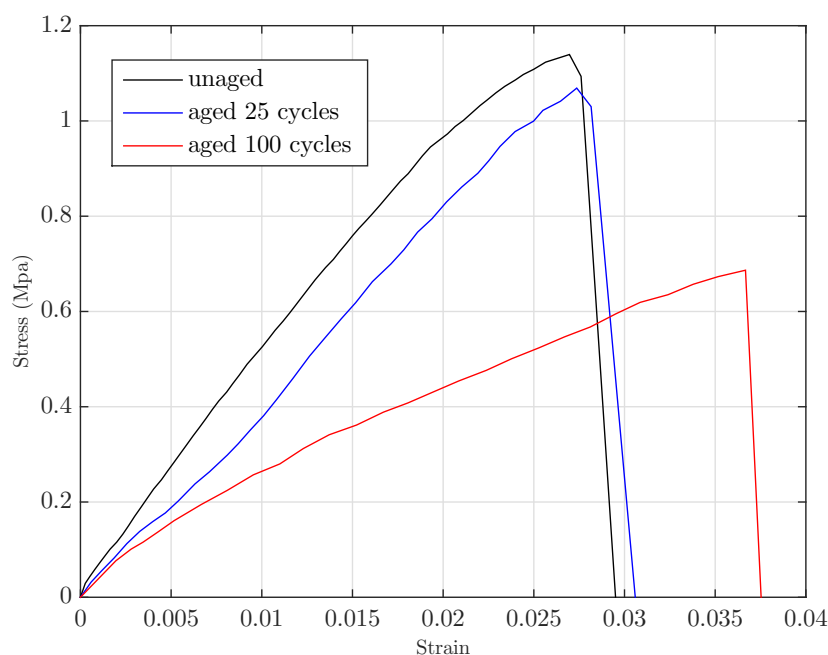
Figure 5.4.: Stress-strain curves of aged and unaged sandwich T-joints.

Notably, the failure load is significantly reduced in the specimens that are aged 100 days compared with specimens which experienced no or 25 days of ageing. It shows the influence of environmental conditions on the strength and the load-carrying capability of the sandwich T-joints. Although weight and thickness of the honeycomb core are not changed by the performed thermal ageing, behavior of the T-joint is changed.

The material shows an overall damage in the sense of the continuum damage theory of Kachanov [248], who first introduced a variable d with $d \in [0, 1]$ to describe a reduced elasticity,

$$K_N = (1 - d)K_0 . \tag{5.1}$$

The limit case $d = 0$ defines the material to be free of any damage and, on the opposite, $d = 1$ corresponds to a material which has completely lost its load carrying capacity. Fig. 5.5 illustrates the meaning of the damage variable d in the special case of a bilinear elastic material were no permanent strains remain after unloading. The slope of the unloading/reloading path reduces with relation (5.1).
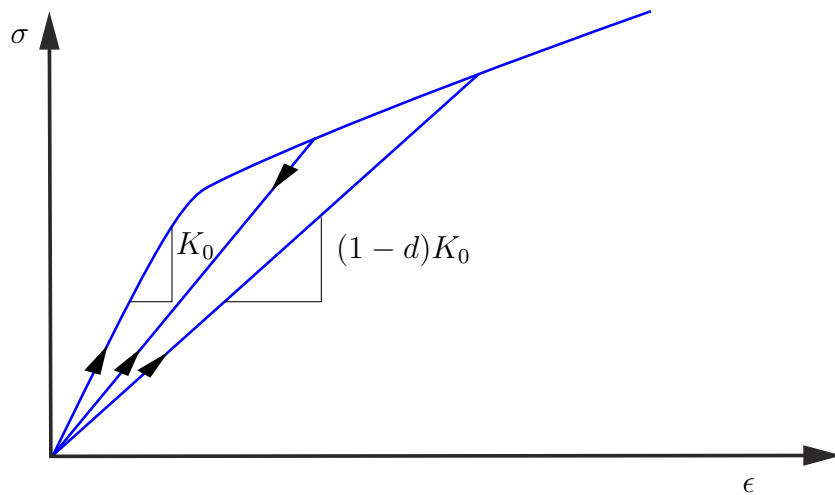
Figure 5.5.: Typical stress-strain relation for a damaged material [3].

For the the T-joints the difference in the slope of the curves shows such a loss of rigidity. From the experimental data we deduce an effective stiffness of the studied specimens of $K_0 = 43.42\,\text{MPa}$, $K_{25} = 42.95\,\text{MPa}$, and $K_{100} = 17.05\,\text{MPa}$ for the unaged and the two groups of aged specimen respectively. This corresponds to $d_{25} = 0.011$ and $d_{100} = 0.607$ with the indices referring to the number of aging cycles. Please note that this effective elasticity is a structural one and does not correspond to the material's elastic modulus. The degradation d, however, can be determined this way as we will prove by our finite element simulations.

5.1.2. Experiments under dynamic loading conditions

Some parts of developments in the commercial aircrafts are driven by customer desires. In this respect, possibility of manufacturing complex parts by the sandwich composites show positive and significant impact on the aircrafts interior. In designing sandwich-structured composite in transportation applications that experiences short-time dynamic

loading, information about effects of loading rate is necessary. Moreover, replacement and repairing the composite parts are difficult, expensive and time consuming, therefore provide reliable data become an important issue in composite structures and joint design in order to reduce time and cost during the design phase. This technical data can be used in basis of safety assessment procedure. The materials employed in aircraft are similar regardless of aircraft types. By far, largest composite applications are sandwich components made with honeycomb core, utilized for ceilings, flooring and galley. Despite of occurrence of dynamic loading in transportation structural applications like aircraft, marine and train and provided damages on composite sandwiches, these damages on the service life are not well documented. In this part, details of dynamic tensile test on sandwich T-joints are explained.

As mentioned before, there is no specific standard procedure on experimental setup for assessing sandwich T-joint under dynamic tensile loading conditions. In the current study, to investigate the structual failure characteristics, dynamic tensile tests are performed. In this respect, series of dynamic tensile tests are performed on servo hydraulic high-speed testing machine with maximum piston speed of 20m/s. A steel fixture was fabricated and used on experimental tests. It's supported the specimens on it's edges. Dynamic testing of the composite sandwich T-joints conducted with a constant crosshead speed of 5 m/s and provided strain rate of about $5000s^{-1}$ which present dynamic loading condition. Fig. 5.6 shows experimental setup for dynamic tensile test on the studied sandwich composite T-joint.
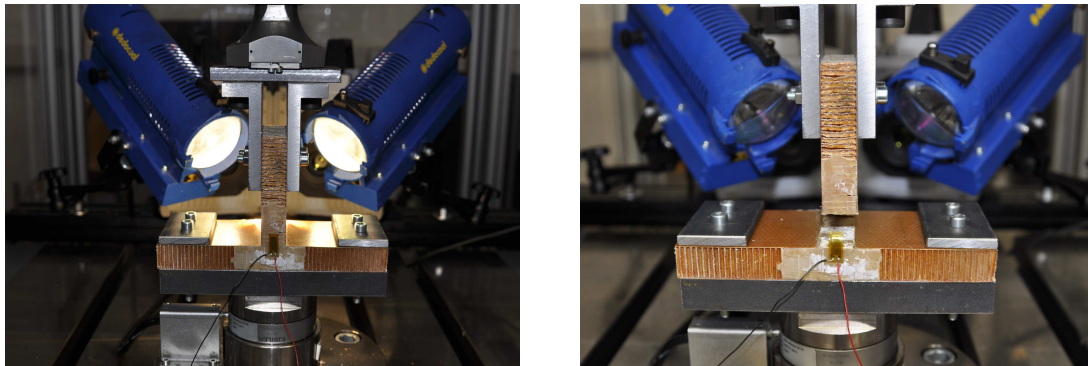
Figure 5.6.: Experimental set up on dynamic tensile test (left) before and (right) after applied load.

Since strain measurement plays critical role in reflecting the state of the structure, strain history recorded accurately during the experiments. In the tests, the strain gauge is mounted on the area which is interface of base and web part and it was repeated by new strain gauge for each specimen.

The average of force-displacement and strain history of the dynamic tests are illustrated in Fig. 5.7. Series of the tests, showed same failure process on both loading

conditions, just higher fracture load is occurred on dynamic loading regime. As it is depicted, the fracture load in dynamic loading condition is reach to 3000 N which is roughly double compared with quasi-static loading test. This is result of the rate dependency of the aramid paper honeycomb. As can be seen, slope of the force-displacement curve is increased over the time, concerning strain stiffening effect until reaches fracture load at peak of the curve. Regarding to the presented strain history and by comparison of latter parts of the curves, it can be concluded that stiffness increased while increase in strain rate is observed. The behavior produced by dynamic loading regime is fundamentally different from linear behavior for static loading condition. In contrast with static loading condition, there is non-linearity on the force-displacement curve on dynamic loading. Increase in tensile strength, stiffness and displacement with increasing loading rate is achieved for studied sandwich T-joint specimens.
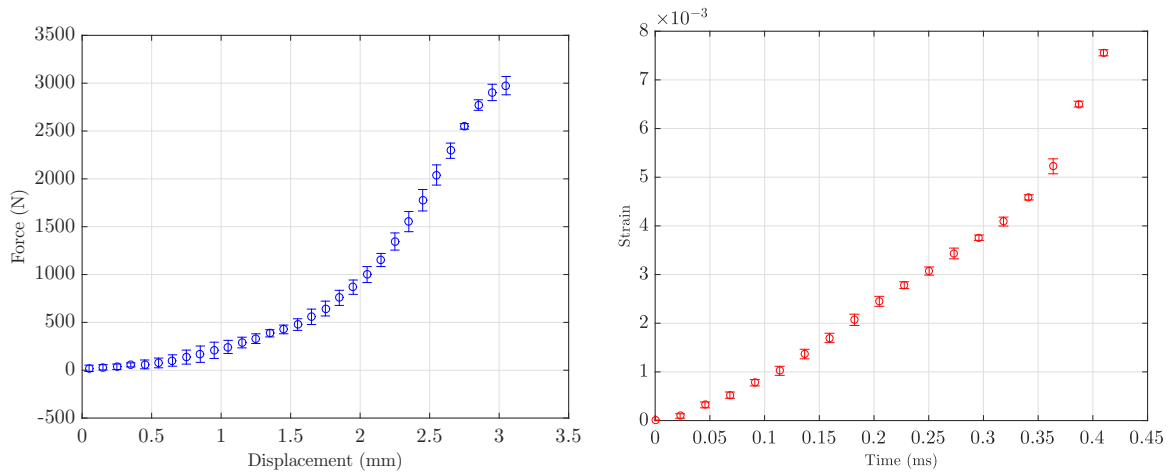
Figure 5.7.: Mean values of load-displacement (left), and strain history (right) of the dynamic loading tests.

By comparison of the quasi-static and dynamic tests, it is observed that failure strain is increased when the loading rate increased. Indeed, evolution of maximum failure strain as a function of strain rate is proportional to the strength. As it is shown in strain history of the tests, the strain reaches to the failure strain in about 450 microseconds. The failure strain is defined as the highest recorded strain before failure. Strong dependence of tensile strength to the loading rate is detected. Relationship between degradation of the strength with loading rate is observed. In quasi-static loading condition, more time is allowed to develop the crack which finally provided reduction in tensile strength of the T-joint. In dynamic loading condition, tensile behavior of the T-joint strongly influenced by loading rate and the strain increased rapidly until failure strain and fracture. In compare with the temperature effect (ageing), the strain rate effect considered minor. Indeed, tensile failure strain is changed significantly with the temperature.

5.1.3. DIC, crack propagation and fractographic analysis

Generally, in fracture mechanics there is assumption of crack existence. This crack can be available form the very begining, because of material defect and can be result of the component manufacturing process. However, cracks oftenly caused by operational loading that is an important issue in service strength of materials and components. With development of advanced image processing methods, Digital Image Correlation (DIC) technique became an appropriate and common method for study material behavior in field of fracture mechanics. Basically, it compare the random patterns on the surface of the tested specimen before and after deformation. The DIC technique can be used to provide quantitative results and also validate data of the tests. It can also visualize the response of the components under different loading regimes. By the help of developed high speed camera with high resolution, the DIC can be applied to wide range of loading rates.

Digital Image Correlation

In the tensile tests on sandwich T-joints, we employed two high speed video cameras (Photron FASTCAM SA5) with capability of clear recording in low-light and with a maximum rate of 775000 frames per second (fps) are used to record the process till specimen failure. Here, we set the cameras to 262500 fps which provides images of 128×128 pixels. These high frame rates cameras were able to record clearly for dynamic motion analysis. To obtain high quality movie and images, a specific lighting system is used. In this regards, a pair of COOLH dedocool Tungsten light head are used which is designed for high speed videography. It provides a record of dynamic deformation fields in real time. The recorded movies are used for the DIC technique. In our experiments, full-field strain measurement on the desired area of the specimen under load is provided by the DIC technique. It should be noted that elaborate surface preparation of the specimen was performed. Random speckle pattern of spray paint was applied on the T-joint specimen surface to obtain good contrast of the images. Since the random speckle pattern has significant influence on measured data, this high contrast random pattern is fabricated accurately to achieve most accurate results. When ideal pattern on the surface of the specimens created, the specimens are fixed on the tensile machine, and the cameras and the pair of the lights are placed in an optimum distance. The cameras are triggered from the arrival of the pulse generated by a strain gauge mounted on the specimen. By the DIC technique images are captured and the subsequent correlation of features within the images to track changes in strain. In this study, movies are recorded for all the tests which are composed by more than one thousand images for each test. The movement is used for the strain measurement and for every camera pixel strain components are calculated. Fig. 5.8 shows full measurement of strain by the DIC technique. It show crack development and strain values on the tested specimens.

Strain distribution in the structural components is and incresingly important part
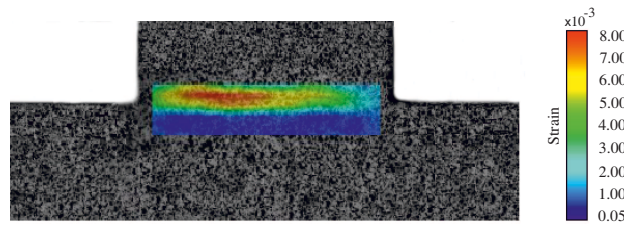
Figure 5.8.: Crack propagation and mesured strain by DIC technique.

of material design. The recorded video data loaded into ARAMIS system [249] which is a non-contact and material-dependent measuring system based on DIC. The strain distribution that occurred in the T-joint specimen is obtained. The determined strain is different with the position in the specimen and with the crack propagation. According to the picture obtained by DIC technique, the crack initiation position is corresponds to the where the maximum strain is occurred, and then it's propagated to final fracture.

The achieved results by the DIC technique are compared with the data achieved from applied strain gauges on the specimens. The described strain gauges are used for all the tested specimens. By the comparison of the strain gauges, good agreements are observed.

Crack propagation

In the conducted tensile tests, time-series images of the fracture process were acquired using the mentioned high speed cameras and the lighting system. The crack detection is clearly possible by the sequence of the images. A sequence of the sandwich T-joint fracture process under static loading condition is depicted in Fig. 5.9. The utilized lighting system enabled the acquisition of clear images of the fracture zone.
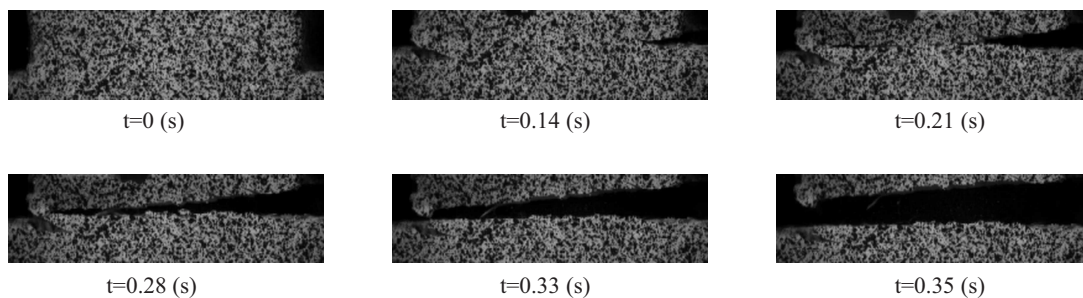
Figure 5.9.: Crack sequence viewed from the front of the T-joint specimen.

A comparison of the recorded high speed video showed that the quantity of applied adhesive on the web/base interface plays an important role on the failure modes and the locus of crack initiation. Mainly cohesive fracture was observed as failure mode on the tested sandwich T-joints with 1 mm thickness of the adhesive on the web/base

interface. When the amount of adhesive is increased in the manufacturing process of the sandwich T-joints, interfacial failure is observed. Therefore, the amount of adhesive on the web/base interface affects the bonding capability of the joints. There are several theories which tried to explain this issue and this subject is still controversial. For instance, in [250] it is explained that the probability of an internal imperfection in the joints could be increased by higher bonding thickness. Moreover, in [251] it's indicated that thicker joints have a lower strength by considering plasticity of the adhesive. The performance of the adhesive not only depends on the adhesive properties, but also on the thickness and on the uniformity of the bonding. An insufficient treatment of the composite surfaces may also be a possible reason of failure which, however, would only affect single specimen and not the full set. Although the effect of the adhesive thickness on single-lap joint is well documented [251, 252, 253], there is no documentation or standard for the thickness of the adhesive layer. For the tested composite sandwich T-joints the highest strength is observed with an adhesive layer of 1 mm thickness.

Fractographic analysis

The fracture modes in composites are complex and effected by various factors. For instance, number of plies, loading direction and environmental condition influences the failure mode. Furthermore, different types of manufacturing defects are able to significantly change the behavior of the sandwich parts. In [254] it is indicated that the failure load is affected by the existing voids in the interface of fillet and composite sandwich panels. Recently, influence of manufacturing defects on modal properties of truss-like core sandwich panels investigated in [255]. Generally, brittle fracture or brittle with fiber pullout can be occurred in composites which are subjected to the tensile load [256]. As it's mentioned, we have seen the brittle fracture in all of the tested sandwich T-joints.

To study the details of web/base interface, a fractographic examination is required after mechanical testing. Currently, fractography is widely used in both academic and industrial applications that provides reliable data which are beneficial in characterization, material development, numerical simulation and production. In the current research, the tested composite sandwich T-joint specimens are visually investigated by a 3D laser microscope (KEYENCE VK9700K) and also by a free-angle observation system (VHX-S90 BE). The used microscope employs a laser confocal technology with a short wave laser light source and white light source, which provides focused images for all depth of the surface. The failure mode is a good indicator of adhesively bonding performance under different loading and ambient conditions and a precise and careful microscopic inspection on the fracture surface is needed to identify the fracture initiation point.

The fracture surfaces of an unaged and a 100 cycle aged specimen after static rupture are shown in Fig. 5.10. As can be seen in Fig. 5.10 (left), in the unaged specimen a cohesive failure occurred. The interface is covered by fractured adhesive after rupture. When the specimens are aged and tested by same loading condition, the failure mode changes to an interfacial failure which is shown in Fig. 5.10 (right). In this case, debonding is

between the adhesive and the adjacent plate. It is assumed that the ageing process of the adhesive is responsible to the transition in failure mode. An effect of thermal ageing on the deterioration of the adhesive properties was observed in particular for the second group of aged specimens. Here an enormous loss of strength is recorded which shows the influence of the thermal cycles on the strength. Uncontrolled changes in the properties and softening of the adhesive layer concurrently with a loss of adhesion are results of the applied thermal ageing. Also, in [257] it had been discussed that the environmental conditions shifted the failure type from cohesive to interfacial failure.
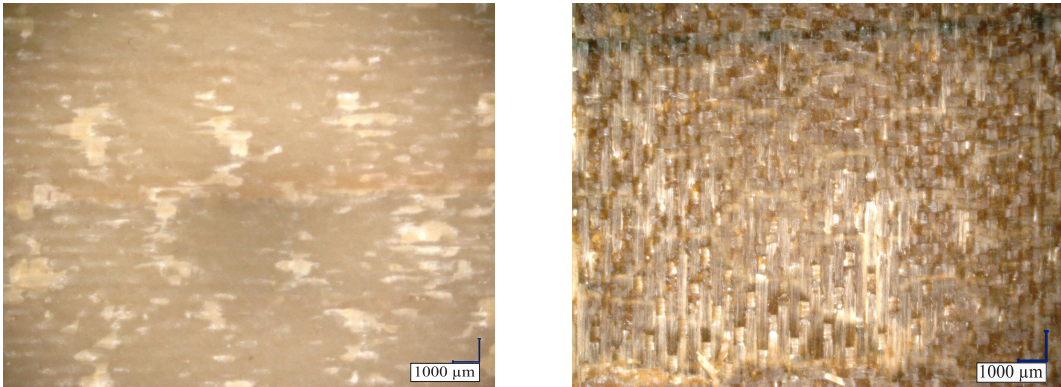
Figure 5.10.: Fracture surfaces of unaged (left) and aged (right) sandwich T-joints.

Fig. 5.11 shows tensile fracture surface of T-joint as result of static (left) and dynamic loading (right) conditions. Regarding to the applied loading regimes, the debonding are looks different in the same location of the composite specimen. As it is illustrated in Fig. 5.11 (right) in the dynamic loading regime the fibers are detached completely on the interface and there is no fiber fracture like static loading tensile test.
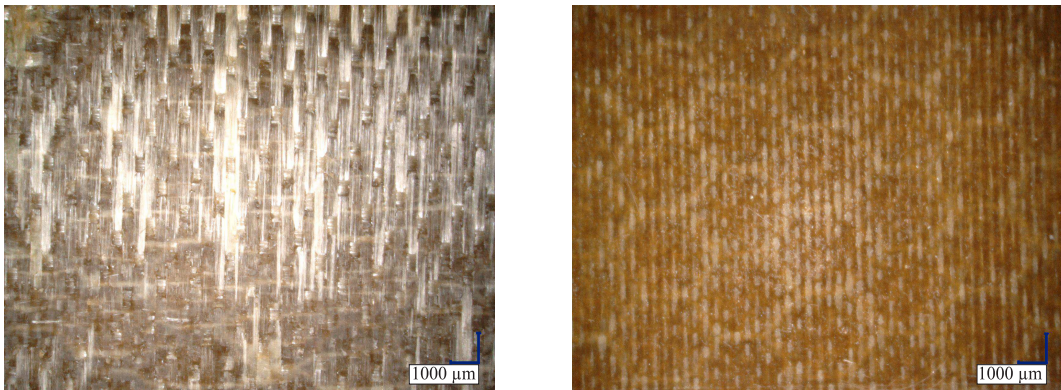
Figure 5.11.: Tensile fracture surfaces of T-joint from static (left) and dynamic (right) loadings.

Over the years, European exchange forum GARTEUR focused on developing standard nomenclature for fractographic analysis of composites. As a result, in [258] the guideline for fractographic analysis of composites is documented.

In sandwich-structured composites, the geometrical dimensions such as cell size play crucial role in strength of structure. Because of various reasons, voids (bubble) can be made in the adhesively sandwich-structured composites. They might be introduced during surface preparation, manufacturing conditions, moisture content, mechanical treatment or because of material chemical composition. The voids can reduce the stiffness of the structure. In [259] has been claimed that the relationship between the voids and the stiffness of the carbon epoxy structure is non-linear and the stiffness can be decreased significantly when the voids content is more than 5%. By the conducted fractographic analysis, we conclude that it provides key information about the failure mode and also failure location in adhesively bonded sandwich T-joints. It is important to collect all the information from the fractured surface before dissection. Moreover, for easier comparison it is needed to use standardised magnifications.

5.2. Behavior of UHPC materials under dynamic loading conditions

With increase in applications of UHPC and its variants, investigations about this materials also increased and fundamentals of UHPC materials with different examples are presented in [260]. Various types of UHPC materials examined under quasi-static loading [261], explosive and blast loading [262, 263], projectile impact [264, 265], and drop weight test [266, 267]. However, structural capability is considered issue in safety assessment of the structures. Concrete and cementitious materials are highly sensitive to the strain rate under tension, compression or flexure. Therefore, the mechanical properties which are obtained under quasi-static loading condition cannot be used for design of the structures under dynamic loading regime. Due to the lack of accepted standards and limitations on the testing methods, some challenges appeared. However, experiment under dynamic loading condition is much more complicated than quasi-static loading, and the parameters can be affected by the test setup. To obtain reliable data, researchers employed Split Hopkinson Pressure Bar (SHPB) which is a most widely used method for study materials behavior under high rate of loading. The SHPB experimental setup is used in various researches to study different material under dynamic loading condition [268, 269, 270]. SHPB is utilized to evaluate numerus materials and run compression, tension and also torsion dynamic loadings. The high strain rate in the experimental test on the concrete can be obtained by direct impact on the specimen, dropping of weight, explosive charges against the specimen or utilizing SHPB device. However, experiment under dynamic loading condition is much more complicated than quasi-static loading, and the parameters can be affected by the test setup.

Concrete and cementitious materials exhibits strong strain-rate sensitivity and SHPB is most popular dynamic testing technique to investigate the behavior of these brittle materials. Since, here in this thesis series of spalling tests and dynamic Brazilian experiments are carried out by SHPB, in the following lines a brief historical background of the split Hopkinson bar is presented and then the basis of SHPB is described.

Numerous accepted experimental tests by SHPB proved that this technique is most reliable measurement method in material characterization under high strain rate. The Hopkinson bar experimental setup is a developed version of stress wave experiment in iron wires which is performed by Hopkinson [271] and later the experiments by his son [272]. Ten years later, in [273] the pressure bar is developed which is well-known today as SHPB in order to determine the pressure produced by an explosive. About three decades later, electrical condenser units in conjunction with the oscilloscope are used by Davies in order to record the wave propagation in the SHPB for the first time [274]. Shortly after that, in 1949 the split bar system developed by Kolsky to determine dynamic compression stress-strain behavior of various materials [275]. In 1964, previous modifications are combined by Lindholm and an updated version of Kolsky bar system designed, which become a template of current SHPB [276]. The details of this historical background are reviewed in [277, 278]. However, during the two decades till 1970s the SHPB systems were not widely used, but with development of Hopkinson bar in tension [279] and torsion [280] the Hopkinson bar become a standard method and its application significantly increased in the late 1970s to study materials under dynamic loading and its still one of the most common method in measuring dynamic mechanical properties of materials.

A classical SHPB is consists of a gas gun, a striker, two long cylindrical bars, called incident and transmission bars and a damper at the end of transmission bar. Also, data acquisition system used to collect the data. Usually striker and the bars are made by same material and same cross-section area. The specimen to be tested is sandwiched between the bars. A schematic of SHPB is shown in Fig.5.12. The striker is launched by gas gun and impact the incident bar. This impact produces a compressive stress pulse which travels through the incident bar. On the experiment, the loading pulse propagates in the incident bar, and then loads the specimen which is placed between the bars and finally propagates in the transmission bar. Part of the pulse through to the transmission bar and some part of the pulse is reflected back to the incident bar at specimen-incident bar interface. The amount of this reflected pulse is not only depend on the bar materials, but also affected by contact configuration.

The most common measurement method in SHPB is employing strain gauge. Beside of this method, other measurement techniques such as laser extensometer [281], digital image correlation [282] and optical measurement [283] are used in SHPB tests. Strain gauges are mounted on incident and transmission bars to record the strain history during the test. The impact velocity of the striker determines the amplitude of the incident wave. The stress, strain and the strain rate of the specimen are calculated from the
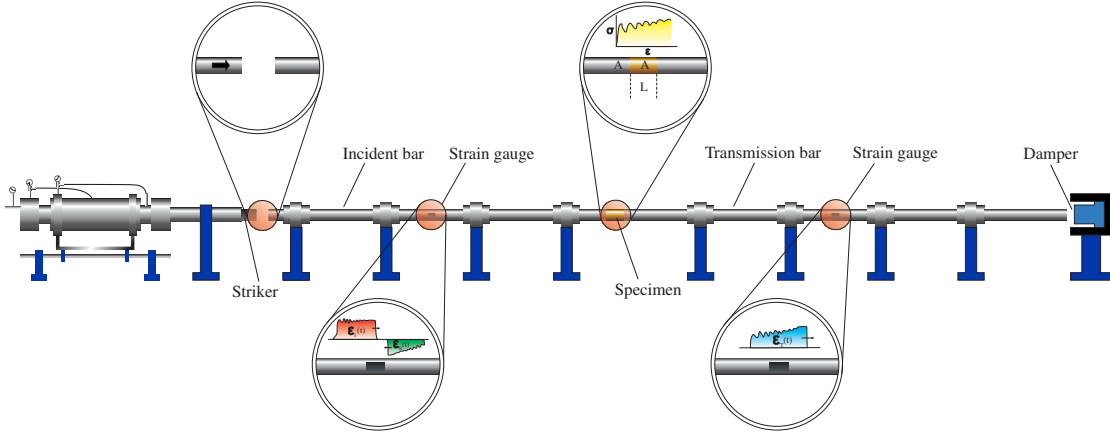
Figure 5.12.: Schematic of split Hopkinson pressure bar (SHPB).

recorded strain history and following equations:

$$\frac{\partial \varepsilon}{\partial t}(t) = -\frac{2c_0 \varepsilon_R(t)}{l_s} \tag{5.2}$$

$$\varepsilon(t) = -\frac{2c_0}{l_s} \int_0^t \varepsilon_R(t) \mathrm{d}t \tag{5.3}$$

$$\sigma(t) = \frac{E A_b}{A_s} \varepsilon_T(t) \tag{5.4}$$

where σ and ε denote stress and strain as function of time, E is the elastic modulus of the bars; A_b and A_s are the cross-sectional area of the bar and the specimen, respectively. Here and later, the indices R and T are used to show reflected and transmitted wave accordingly. Moreover, l_s and c_0 denote specimen length and wave speed in the bar, respectively.

The experiments by SHPB are based on several idealized assumptions which are discussed by different researchers [284, 285, 286, 287]. Two assumptions are fundamental and validity of the experiments depends to verification of them. The first one is the assumption of one-dimensional wave propagation theory which describes the wave in the bar and is only valid when the stress wave propagates in both bars without dispersion [288]. The second assumption postulates an instantaneous equilibrium of forces in the loaded specimen and basically states, that the reaction force on the specimen-transmission bar interface is the same as the incoming force on the specimen-incident bar interface. This assumption corresponds to an axially uniform state of deformation within the specimen [289]. On the basis of this assumption, which is often named stress equilibrium condition, the relations (5.2) to (5.4) are deduced.

For dynamic stress equilibrium in the specimen the following relationship between

incident, reflected and the transmitted strains holds:

$$\varepsilon_I(t) + \varepsilon_R(t) = \varepsilon_T(t) \tag{5.5}$$

In the experimental setup, utilizing pulse shapers in SHPB test is prerequisite to extend the rise time in the incident pulse and to provide a constant strain rate. In this regard, usually a very thin piece of deformable material like copper or aluminum should be connected to the impact side of incident bar. In our tests, we also used pulse shaper which is described in this chapter on the details of spalling and Dynamic Brazilian experiments.

The equilibrium condition needs to be to established in order to get reliable stress-strain data from SHPB tests. For conventional SHPB tests this is achieved when the specimen deforms nearly uniformly, so the specimen's response is averaged over the volume which is a good representative of the pointwise material behavior. Criteria for stress equilibrium base on a comparison of forces or stresses at both ends of the specimen. Based on incident, reflected and the transmitted stress waves, in [285] a stress equilibrium factor is defined as

$$\sigma_{EQ} = \frac{\sigma_T}{\sigma_I + \sigma_R} \tag{5.6}$$

where $\sigma_{EQ} \approx 1$ indicates equilibrium. In work [290] another parameter $R(t)$ is proposed for the evaluation of equilibrium. When the specimen is sandwiched between the bars, the forces at the begin and the end of the specimen are

$$F_1 = EA_b \left(\varepsilon_I + \varepsilon_R \right) \tag{5.7}$$

$$F_1 = EA_b \, \varepsilon_T \tag{5.8}$$

When the dynamic load between specimen and incident bar (F_1) and that between specimen and transmission bar (F_2) are equal, the specimen is in equilibrium. Thus, the parameter

$$R(t) = \frac{\Delta F(t)}{F_{\text{avg}}(t)} = 2 \left| \frac{F_1(t) - F_2(t)}{F_1(t) + F_2(t)} \right| \tag{5.9}$$

accounts for the force difference and the specimen is considered to be in stress equilibrium when $R(t)$ approaches zero. Wu used this method for our dynamic Brazilian test which is mentioned later in this chapter in explanation of experimental setup.

It should be pointed out here, some other assumptions such as inertia and friction effects are also considered on the SHPB experiments. For instance, the inertia of large diameter specimens can provide serious errors on the force history. It is proven that the assumptions can be fulfilled approximately by utilizing long bars with a large length to diameter ratio. Since some of the assumptions are not satisfied automatically, additional

effort is required in designing the experiments. For example, the interfacial friction effect can be significantly minimized by a proper lubricant at bar-specimen interfaces. Also, it is vital to optimize the specimen length and diameter. The length should be minimized in order to reasonably justify the assumption of stress equilibrium along the specimen. The specimen radius should be minimized to ensure the effect of radial self-confinement is limited.

The experimental errors on SHPB test can be minimized by careful attention to the critical parameters including stress-wave propagation effects, inertial effects, uniformity of stress and strain along the specimen length, specimen geometry and frequency response of the measurement system. However, in the test by SHPB, all the above-mentioned conditions are not fully satisfied, but ignore of these effects might lead to determine incorrect material properties.

Dynamic mechanical properties of concrete and UHPC materials and also their variants under high rate of loading are mainly determined by means of two experiments namely spalling and dynamic Brazilian tests both via SHPB. These experiments are carried out in this thesis, and presented in the following parts.

5.2.1. Spalling tests on UHPC via split Hopkinson bar

The high strain rate in the experimental test on the concrete can be obtained by utilizing SHPB device. Spalling test is one of the most noticeable experiments by SHPB at high rate of loading. To provide an overview, mechanical properties of concrete material which are obtained from saplling tests by split Hopkinson bar are summarized and presented in Appendix A. To conduct the spalling test, the classical SHPB should be modified and the specimen is connected to the single Hopkinson bar. The impact generates compressive pulse on the incident bar which transmitted to the specimen, propagates on it and reflected as tensile pulse on the opposite free end of the specimen. The incident and reflected superimpose within the specimen and when it reaches ultimate tensile strength of the specimen, spall is occurred. By series of the spalling tests on UHPC samples, we determined:

- Dynamic elastic modulus

- Dynamic tensile strength

- Dynamic fracture energy

UHPC material and its variants are widely employed in engineering specialized facilities such as nuclear power plant and high rise buildings. One the one hand, possibility of extreme loading events in these engineering structures should take into account, which generate large stresses with high strain rates on the material. On the other hand theses three above-mentioned parameters are sensitive to the strain rate. Therefore, understanding the behavior of material and reliable data about these mechanical properties can avoid catastrophic consequences.

Calculation of dynamic elastic modulus

The spalling experiment is limited to the brittle materials that their compressive strength is much higher than tensile strength. Otherwise, the specimen experienced pre-damage via the compression. Throughout the spalling experiment, the stress field in the specimen continuously evolves in space and time. This evolving of the stress field can be recorded by the strain gauge. The wave speed in the bar is obtained by

$$c_0 = \sqrt{E/\rho} \tag{5.10}$$

From the Eq. (5.10) the dynamic elastic modulus of the specimen calculated

$$E_{dyn} = \rho \, c_o^2 \tag{5.11}$$

For the strain in the specimen it holds

$$\varepsilon(t) = \frac{u_2(t) - u_1(t)}{l_s} = \frac{c_0}{l_s} \int_0^t (\varepsilon_I(\bar{t}) - \varepsilon_R(\bar{t}) - \varepsilon_T(\bar{t})) \, d\bar{t} \tag{5.12}$$

where u_1 and u_2 are the axial displacements at the specimen-incident bar interface and the specimen-transmission bar interface, i.e, the begin and the end of the specimen. Alternatively, by combining Eqs. (5.2) and (5.4) the dynamic elastic modulus on the specimen can be calculated

$$E_{dyn} = \frac{\sigma}{\varepsilon} = -\frac{A \, E \, \varepsilon_T \, l_s}{2A_s \, c_0 \int_0^t \varepsilon_R \, dt} \tag{5.13}$$

These relationship are particularly useful for the calibration of the SHPB setup. Fig. 5.13 shows cylindrical UHPC specimen sandwiched between the bars.
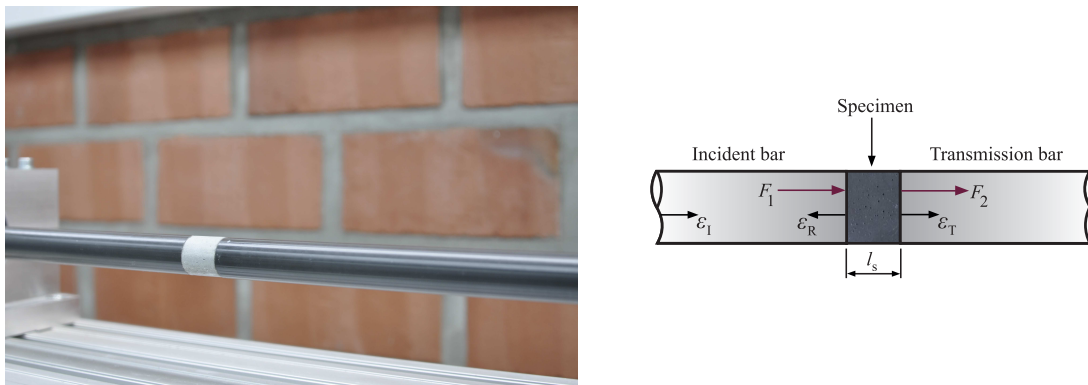
Figure 5.13.: Cylindrical UHPC specimen sandwiched between the bars (left), and illustration of incoming, reflected and transmitted wave with reaction forces at the interfaces (right).

Typically, the dynamic elastic modulus is higher than the corresponding quasi-static value, an effect which is at least partially attributed to lateral inertia of the specimen in a SHPB experiment [291, 292]. In our research, to measure the incoming and passing impulses, strain gauges are mounted in the middle of incident and transmission bar, respectively. Our strain gauges have a resistance of $120.0 \pm 0.1 \, \Omega$ and gauge factor of 2.07. All data are acquired by a HBM GEN7t system with a 1.0 MHz band pass through Wheatstone bridges. In our tests, incident and transmission bars, both are made by an aluminum with length, diameter and density of 1800 mm, 20 mm and 2710 kg/m^3, respectively. The cross sections A of incident bar and specimen are identical.

The 20 mm long cylindrical UHPC specimens with diameter of 20 mm are positioned between the incident and the transmission bar and very thin layer of the grease is used on the bar-specimen interface to reduce friction during the test. To avoid the inertia effects in the classical SHPB setup, a length to diameter ratio of 0.5 to 2.0 is recommended in [293], we use a ratio of one. Here, four different specimens of each material group have been tested multiple times on classical SHPB in order to determine the dynamic elastic modulus. All the experiments are performed at strain rate of $30s^{-1}$. Details of the strain history is shown later, in calculation of dynamic tensile strength. Using Eq. (5.13), an average dynamic elastic modulus is obtained, the average values are shown in Table 5.1. We see a stiffness raise of about 8 % for the modified UHPC mixture S_2 with a microsilica content of 10 %. This tendency is in accordance with the static strength values, which are mentioned in Table 5.1

Table 5.1.: Dynamic elastic modulus measured in the SHPB at a strain rate of $30s^{-1}$.

Material	E_{dyn} (GPa)
Cement S_0	44.2 ± 0.3
UHPC S_1	48.6 ± 0.2
UHPC S_2	51.3 ± 0.5

Alternatively to the above calculation, the dynamic elastic modulus is also determined from the wave speed, Eq. (5.11). The The determination of the UHPC's wave speed bases on the time shift of the signals measured at a specified distance. It should be noted that, this requires a longer specimen for sufficient accuracy. We obtained in this way an averaged elastic modulus of second group of UHPC equal to $E_{\mathrm{dyn}} = 52$ GPa which is very similar to the value calculated from Eq. (5.13).

The strain rate dependency of concrete and cement-based materials is investigated by several researchers throughout the years. On the other hand, by summarizing the available experimental results on UHPC (without additional reinforcing fibres) it can be stated, that different investigations about its static behavior report a typical elastic modulus of 43-50 GPa [110, 294, 295]. Comparing the elastic modulus in quasi-static loading condition to the value we obtained from dynamic loading test, shows the strain rate dependency of UHPC's elastic modulus.

Calculation of dynamic tensile strength

The apparent dynamic tensile strength R_m^t, i.e., is the maximum tension a material can sustain and it's can be determined by spalling test on modified SHPB. When the superposed wave exceeds this value the specimen will fail and two fragments result. Brittle materials like UHPC have a low fracture energy and break by cleavage, i.e., the fractured surfaces are flat, unstructured and almost perpendicular to the axis of the specimen. Therefore, only a portion of the stress wave's energy is dissipated and the process of wave propagation and superposition will continue within the fragments. Depending on the energy of the incoming wave, additional cracks may occur. A modified SHPB that used for the spalling test is schematically shwon in Fig. 5.14.
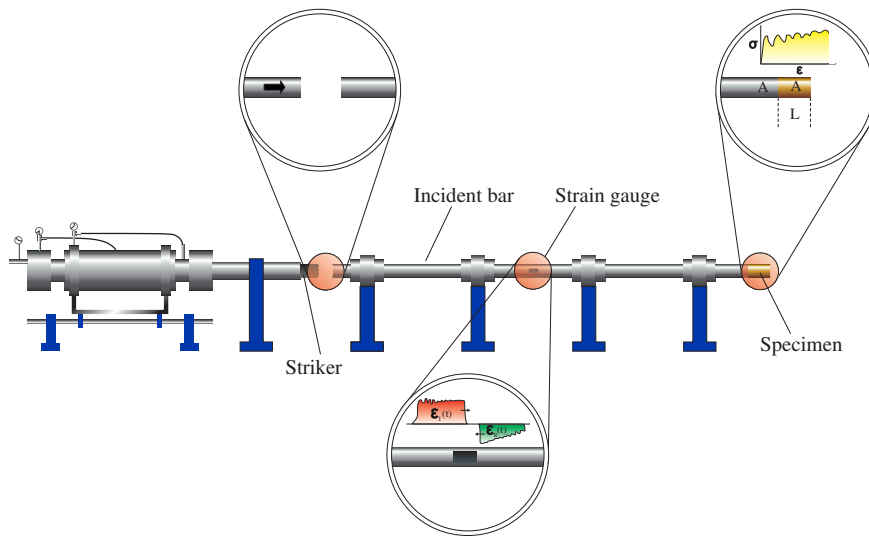
Figure 5.14.: Schematic of modified SHPB used for spalling tests.

The impact of the striker generates a compressive stress pulse traveling through the incident bar. When this pulse (σ_I) reaches the interface between incident bar and specimen, one part (σ_R) is reflected back, and another part (σ_T) is transmitted through the specimen. At the free end of the specimen the stress (σ_T) is reflected as a tensile pulse. The transmitted wave portions

$$\frac{\sigma_T}{\sigma_I} = \frac{2z_2}{z_1 + z_2} \tag{5.14}$$

depend on the acoustic impedances $z_1 = A\rho_1 c_1$ and $z_2 = A\rho_2 c_2$ of the two materials, where c_1, c_2 are the corresponding wave propagation velocities and ρ_1, ρ_2 are the material densities. In order to obtain a sufficiently transmitted wave, an aluminum incident bar is used and from (5.14) a transmission number of $\sigma_T/\sigma_I = 0.76$ is calculated.

The impact velocity of the striker determines the amplitude of the incident compressive wave σ_I. In order to measure incoming, reflected and transmitted stress pulses, strain gauges are positioned in the middle of the incident bar as well as on the specimen with distances of 15 mm from the free end. All gauges are bounded by Z70 adhesive (cyanoacrylate). The data are acquired by the data acquisition system with the maximum sampling rate of 100 megasamples per second. Using a dual rate recording principle, long term observations can be continuously recorded while rapidly occurring events can be captured concurrently.

In order to obtain experimental conditions with a constant strain rate the incoming pressure wave needs to be shaped. The ideal incident pulse rises to its maximum with a long rise time to have a reproducible and well defined strain rate. To this end we modified the incident wave by circular paper sheets with a thickness of 0.8 mm, placed at the impacted end of the incident bar which is stricken by the striker. The paper pulse shaper realizes after about $45\mu s$ a waveform with a constant strain-rate, which is a clear improvement to the wave obtained without pulse shaper. A typical strain history which is measured at the incident bar during the test is displayed in Fig. 5.15.
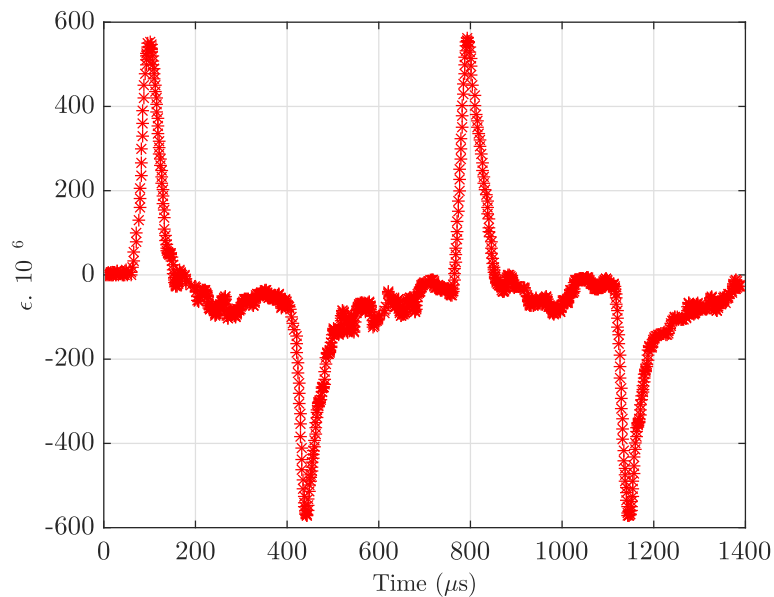
Figure 5.15.: Strain history on the incident bar.

In the experiments by modified SHPB, the stress pulse travels from the incident bar into the specimen, where it is reflected at the free end. The phase inversion now causes tension and a superposition of incoming (compressive) and reflected (tensional) wave leads to a non-homogenous stress state. The specimen will fracture if this tensile stress exceeds the material's strength. The situation in the specimen is illustrated in Fig. 5.16 for a compressive pulse with a tension tail. The incoming wave is reflected at the rear face
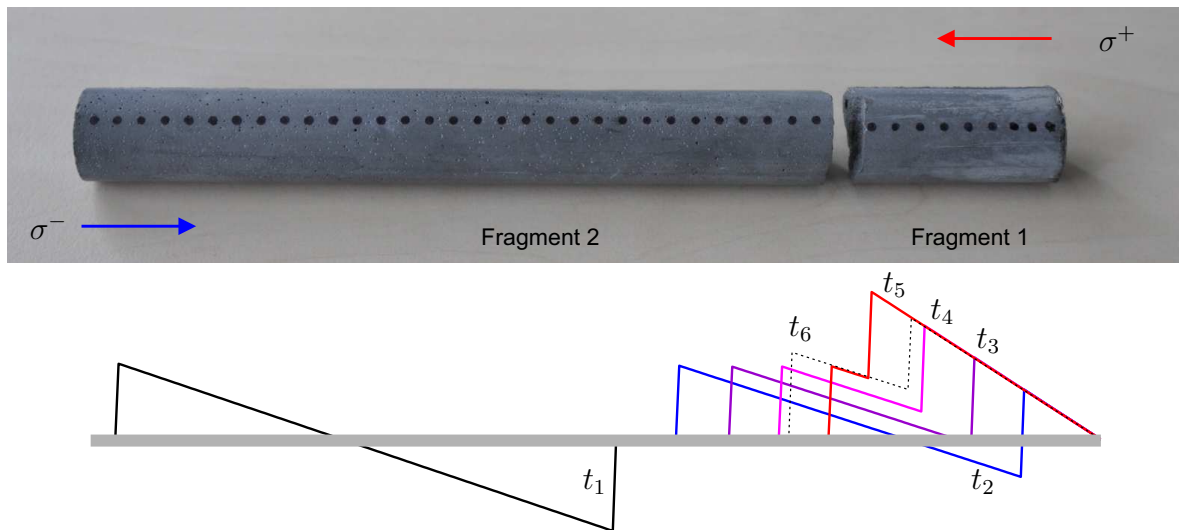
Figure 5.16.: A fractured UHPC specimen of group S_1 and schematic illustration of the superposition of incident and reflected stress wave for different times; t_1: incoming pressure wave pulse, t_2: first reflection at the free end, $t_3 - t_4$: superposition during reflection and t_5 is the peak stress which causes spallation. The dashed line describes further propagation which is never reached [3].

which induces a superposed wave front and a tensional stress state. Clearly, amplitude and position of the peak stress are defined by the shape of the wave and if, for example, the incoming wave is purely compressive, the maximum tension would simply follow from an inversion. This implies, that for a well defined wave superposition the specimen should be longer then the stress pulse.

Different approaches have been proposed to determine tensile resistance form spalling experiment. There are three methods which all are rely on d'Alembert's solution of the uniaxial wave equation in linear elasticity. In [296] these three methods are reviewed and the pros and cons of them are discussed. These spallation experiments refer to brittle materials with ideal cleavage, i.e., there is no plastic deformation or diffuse fragmentation in the crack zone.

A plain way to determine the tensile resistance is to measure the incident and reflected waves, 'shift' them to the position of fracture x_c and derive the superposed elastic stress state there. The dynamic tensile strength is then defined as the level of the tensile stress reached at the location of fracture. This approach has been used, e.g. in [297, 298], and we will follow it here using wave signals measured in the specimens.

$$R_m^{(A)} \equiv \sigma(x_c) \tag{5.15}$$

The stress shift requires a clear signal and assumes, e.g., that the initial compression does not damage the specimen. Also, at the time of failure the stress state in the specimen corresponds to a pure superposition of elastic waves without influence of the

failure process. In [299, 300] it is pointed out that the evolution of damage is bounded by the crack velocity and so the ultimate macroscopic stress in the crack zone might not correspond to the local microscopic stress. This effect, however, can be neglected under the prerequisite of clear cleavage.

Another way of evaluating the apparent tensile strength is to directly use a spallation experiment and define the stress at the instance of cracking as the tensile resistance, cf. [297]. This decohesion stress σ_c is approximated by the velocity difference of the fragments at the moment of spalling.

$$R_m^{(B)} \equiv \sigma_c = \rho\, c_L |\Delta v| = \rho\, c_L(v_{s,1} - v_{s,2}) \tag{5.16}$$

Here $v_{s,1}, v_{s,2}$ denote the axial velocities of the crack flanks. The accuracy of relation (5.16) strongly depends on the quality of the velocity measurement because at the instant of spalling the particle velocity has to be distinguished from a possible 'rigid' movement of the specimen. Precise successive picture capturing is needed for this method, otherwise some overestimation could happen. Again, the underlying theoretical considerations assume a superposition of elastic waves which leads to cleavage of the specimen.

The most common method to derive the dynamic apparent tensile strength exploits the fact, that the wave's particle velocity is reflected at the specimen's end and the superposition of incoming and reflected wave results in a velocity jump at the rear face. This pullback velocity $\Delta v_{\text{pullback}}$ can be measured to derive the corresponding stress.

$$R_m^{(C)} \equiv \sigma(l_s) = \frac{1}{2}\,\rho\, c_L\, \Delta v_{\text{pullback}} \tag{5.17}$$

The derivation of (5.17) bases on d'Alembert's solution where on a free end a stress wave is reflected with phase inversion whereas the particle velocity is simply reflected. Although the theoretical background for relation (5.17) may also be questioned, e.g., in [301] it is stated that "the rebound of the velocity is more pronounced in numerical solution than in experimental data", equation (5.17) has been used in several experimental investigations, cf. [302, 303, 304, 305]. These researchers used different devices such as acceleration gauges and laser extensiometers in order to determine the velocities [302, 306]. These methods have limits regarding the accuracy for small specimen. For large specimen the pullback velocity is the difference in velocity between the maximum value and the velocity at rebound. In our small samples, however, it rather difficult to clearly identify the velocity at rebound of the rear face. To measure the corresponding velocity difference our high speed photograph system is focused with maximal resolution on the specimen's end but we still face a high uncertainty here.

During the test, a high speed video camera (FASTCAM SA5) with capability of clear recording in low-light and with a maximum rate of 775000 fps is used as non-contact optical technique to record the spallation process. The light sensitive sensor of the camera provides a 12-bit analogue to digital converter with $17\mu m$ pixel size without interpolation. In order to record the velocities in the spalling experiment, points are

marked on each specimen and Photron FASTCAM Analysis (PFA) software [307] is employed with a recording rate of 262500 fps. Fig. 5.17 illustrates the recording of the velocity in our experiments. There are 40 points marked on the specimen (and 4 more on the incident bar) which are recorded during the experiment with the mentioned fps. In order to obtain the initial velocity and the velocities of the fragments with sufficient accuracy, the points are tracked with PFA software and the time of cracking is estimated. The initial velocity is calculated by averaging over the velocities of the marked points on the specimen. All the tests are conducted under normal conditions. Like other measuring devices, the SHPB was calibrated before a new test.
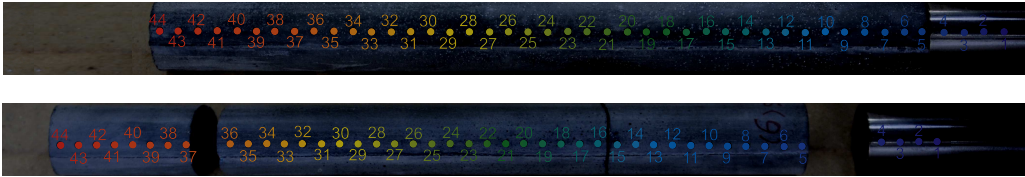
Figure 5.17.: Specimen in the spalling experiment. The upper and lower snapshot shows the specimen at the initial state and after fragmentation, respectively. In both images, the first four points are located on the incident bar and the $5^{\text{th}} - 44^{\text{th}}$ points are on the specimen.

Several fractured UHPC specimens are shown in Fig. 5.18. We see at the first glance that the spallation experiment gives reproducible results, i.e., the cracks are at the same position in every specimen. It should be noted, that the 'crack of interest' for us is the backside crack which occurs at a distance of about 44 mm from the rear end. After fragmentation both fragments move with different velocities and about $40\,\mu$s later, after another reflection, the second crack appears. We use the first spallation, because its position is crack is easier to focus with the fast cam, but selected measurements with the second crack confirmed the obtained values.

Figure 5.18.: UHPC specimens fractured in the spalling tests (left) and a typical fracture surface (right).

In this research, a full set of 23 specimens has been tested. Eight experiments failed because of flawed specimen (air bubbles) which lead to damage at the front end or to slanted cracks. The average tensile strength values obtained in our experiments at a strain rate of 30 s^{-1} are presented in Table 5.2. Regarding to the described methods, we denote the material's tensile resistance derived from Eqs. (5.15), (5.16) and (5.17).

Table 5.2.: Experimental results for the tensile strength using different methods of evaluation. We denote with $R_m^{(A)}$, $R_m^{(B)}$ and $R_m^{(C)}$ the strength obtained from the eqs. (5.15), (5.16) and (5.17), respectively.

Material	$R_m^{(A)}$ (MPa)	$R_m^{(B)}$ (MPa)	$R_m^{(C)}$ (MPa)
Cement S_0	-	10.6 ±1.01	12.2 ±0.82
UHPC S_1	14.9	12.1 ±1.84	16.9 ±0.51
UHPC S_2	19.8	17.8 ±1.61	19.5 ±0.93

These findings are in agreement with the typical mechanical properties of concrete and concrete-like materials. The apparent tensile strength of UHPC is in the expected range of about one-tenth of its compressive resistance. The mechanical properties of the low silica UHPC mixture seems be very similar to established recipes where values of $R_m^t = 8$ to $40\,\mathrm{MPa}$ are reported in [308, 309, 310, 311]. The obtained values for UHPC differ, but they show the same tendency of a higher resistance in the improved UHPC mixture S_2.

Theoretically, for cleavage fracture all three methods should give a reasonable approximation. For the cement specimen, however, we observe additional inclined fragments and so method A was not applicable here. The fractured surfaces of cement and UHPC specimens are illustrated in Fig. 5.19.
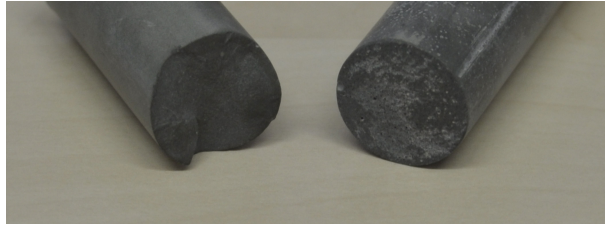
Figure 5.19.: Fracture surfaces of a cement specimen of group S_0 (left) and a UHPC specimen of group S_2 (right).

Since applications of UHPC and its variants are dramatically increased, understanding of their failure is vital for the designing the structures and also developing new cementitious composite material. In this respect, several experimental phenomena related to the UHPC failure such as size effect on strength and brittleness can be interpreted by fracture mechanics. In the following part, dynamic fracture energy of the studied UHPC is determined.

Calculation of dynamic fracture energy

Typically, brittle materials which break by cleavage have a low fracture energy. The speed of crack propagation is empirically known to be around $^1/_4$ of sound speed. It may roughly be estimated from energy considerations. Assume the kinetic energy density at the material element with volume $V_0 = A_c r_0$ to be completely dissipated by new a fractured surfaces A_c, it holds:

$$\frac{1}{2}\rho v_c^2 A_c r = 2\gamma_0 A_c \quad \Leftrightarrow \quad v_c = 2\sqrt{\frac{\gamma_0}{r_0\rho}} \tag{5.18}$$

The distance r_0 is an interatomic distance, here we use the lattice constant of silicon, $r_0 = 5.4\,\mathring{A}$. With a UHPC density $\rho = 2.37$ g/cm^3 and a typical surface energy of concrete, $\gamma_0 = 0.5$, (see [312], it strongly decreases with humidity), we obtain an estimate for the crack propagation speed v_c of 1265 m/s. This value correlates with our high-speed measurements, where a visible crack through the specimen appears within a time interval of less than 20 μs, i.e., $v_c > 20$ mm/20 μs $= 1000$ m/s.

After impact of the incident bar the specimen with mass m has a kinetic energy of

$$\mathcal{K}(x,t) = m \int_{t_{\text{imp}}} v(x,t)(\dot{x},t)dt \tag{5.19}$$

where the velocity function $v(x,t)$ accounts for both, the particle velocity of the incoming wave and the specimen's movement. The latter dominates in an accelerated specimen as explained in previous part. The initial velocity v_i in the specimen is nearly uniform and so the energy (5.19) simplifies to $\frac{1}{2}mv_i^2$.

The fracture energy $\mathcal{W}_c$ determines the amount of work necessary to form cracks and new surfaces within a specimen. In order to determine this work we balance the energy immediately before and after crack initiation, i.e., at the initial $(\cdot)_i$ and at the spalled $(\cdot)_s$ state. The difference of kinetic energy follows for the simple case of two fragments, see Fig. 5.16, as

$$\Delta\mathcal{K} = \frac{1}{2}\left(mv_i^2 - m_1 v_{s,1}^2 - m_2 v_{s,2}^2\right), \tag{5.20}$$

where m_1, m_2 and $v_{s,1}, v_{s,2}$ refer to the masses of the fragments and the velocities measured at the crack flanks of the fragments 1 and 2, respectively. We presume the UHPC materials to behave linear elastically, thus, the loss of kinetic energy between initial and spalled state may completely be attributed to the fracturing process. Consequently, we state $\Delta\mathcal{K} = \mathcal{W}_c$ to be the fracture energy of the specimen.

Experimentally the masses of the fragments are determined by weighting. Since the velocity plays a dominant role in the calculation of the energy difference (5.20), a very accurate measurement is needed here. We refer again to high-speed photography and digital image correlation as outlined in calculation of dynamic tensile strength.

The proposed method to determine the fracture energy is physically consistent and correct, as long as the underlying theory of brittle linear-elastic fracture matches reality. During the the failure process, some elastic and kinetic energy of the surrounding material is released into the fracture zone. The very homogenous material results in cleavage planes and little local fragmentation. Some energy of the elastic wave propagation is still trapped in the fragments and depending on its amount it will either result in subsequent spallation with new cleavage planes or it will be dissipated by microscopic damping. In other words, if the amplitude and length of the incoming stress pulse are 'large', multiple cleavage planes occur. Locally this means, that after the first crack the energy is still higher than the material's critical fracture energy and the same mechanism as before now proceeds within the fragments. For example, for a long stress pulse with an amplitude of 40 MPa and 78 μs length (measured at the incident bar) the first crack was observed at a distance of 44 mm from the free end, and a second crack in the large remaining fragment follows at a distance of 56 mm from the other side. Here we use a shorter incident stress pulses with length of 58 μs and an amplitude of about 30 MPa.

Please note that it is not meaningful to average the fracture energy over different cracks, as suggested e.g. in [313]. Instead, both cracks could be used separately to deduce $\mathcal{W}_c$ with Eq. (5.20). Of course, when the second crack is evaluated the masses m_1 and m_2 refer to the newly fragmented first fragment.

As mentioned earlier, in [313, 302, 305] similar spallation experiments have been conducted. The method to deduce $\mathcal{G}_c$ in these experiments differs from ours. In particular, the difference in linear momentum as a consequence of cracking is approximated by

$$\Delta p = m_2 \left(v_{i,2} - v_{s,2} \right) + m_1 \left(v_{i,1} - v_{s,1} \right) \tag{5.21}$$

where $v_{i,1}, v_{i,2}$ refer to the initial velocities of the (later) fragments. These velocity values are derived from measurements with strain gauges, so they basically account for the particle velocity of the incoming wave only. The fracture energy then is attributed to the difference in linear momentum multiplied with an axial crack opening velocity $\dot{\delta}_x$.

$$\mathcal{W}_c = \Delta p \, \dot{\delta}_x \tag{5.22}$$

The velocity $\dot{\delta}_x$ is not a well defined physical quantity. In particular, it is not related to the crack propagation speed. In [313] the mean difference in the fragments' velocity is used, $\dot{\delta}_x = \frac{1}{2} \left(v_{s,2} + v_{i,2} \right) - \frac{1}{2} \left(v_{s,1} + v_{i,1} \right)$, whereas in [314] half of the fragment's velocity differences are attributed to each crack flank, $\dot{\delta}_x = \frac{1}{2} \left(v_{s,2} - v_{i,2} \right) - \frac{1}{2} \left(v_{s,1} - v_{i,1} \right)$. Both choices are somewhat arbitrarily and the resulting fracture energy values differ. The fracture energy values obtained in this way seems realistic, the underlying values, however, contradict energy conservation. Generally, this method bases on exact measurements of the particle velocity in the specimen and therefore it requires a relatively large and heavy specimen with negligible motion, but with a rapid axial crack opening. A corresponding experimental setup is hardly realizable and so we chose a different approach here.

Following the classical Griffith theory of linear-elastic fracture, the fracture energy correlates the free-surface energy of a propagating crack to the elastic energy stored in the bulk of the material. The released bulk energy corresponds to the fracture energy. Referred to the crack surface A_c this gives the critical energy release rate of crack propagation (specific fracture energy).

$$\mathcal{G}_c = \frac{d\mathcal{W}_c}{dA_c} \tag{5.23}$$

Thus, the fracture energy $\mathcal{W}_c$ determined in our experiments needs to be referred to the actual fractured surface A_c of the specimen. Ideally, the crack is perpendicular to the specimen's axis and $A_c = \pi r_s^2$; here with a specimen radius of $r_s = 10$ mm. Then, the specific fracture energy simply follows as: $\mathcal{G}_c = \mathcal{W}_c / A_c$.

In practice, there may be uneven planes, slanted areas and different degree of roughness in the fractured surface. The determination of the critical energy release rate requires the knowledge of the fracture energy per unit of actual fracture surface, instead of projected area, see also [315]. To investigate this in detail, fracture surface inspections performed with a 3D laser microscope. This investigation showed that the fracture surfaces of cement specimens are quite smooth compared with two groups of UHPCs. This detail is presented later, in 5.2.3. The specific fracture energy is now determined as:

$$\mathcal{G}_c = \frac{\mathcal{W}_c}{\text{actual fractured surface}} \tag{5.24}$$

This corrected area basically accounts for the deviation from one-dimensional linear-elastic wave theory and may depend on the specimen size and the homogeneity of the material. Averaging the fracture area of all broken specimen (at one instance), here a corrected fracture surface of $A_c^{\text{actual}} = 1.96 A_c$ for cement and $A_c^{\text{actual}} = 2.59 A_c$ for both UHPC specimens were found. Please note that although the UHPC mixtures show different microscopic roughness, weighted with the unevenness of the surface they lead to very similar results. A circumferential contour of the fractured surface is shown in Fig. 5.20. This photo is composed of 33 single photographs of the boundary of the specimen.

Figure 5.20.: Full circumferential contour of a cracked S_1 specimen composed of 33 single photographs.

In Table 5.3 the results of the spalling experiments are summarized. As expected, the specific fracture energy of the improved UHPC recipe S_2 is higher than the S_1 values. The $\mathcal{G}_c$ value of pure cement is much lower. It should be pointed out here we are aware that the obtained dynamic fracture parameters are sensitive to the accuracy of the velocity measurements and, additionally, such value are known to show a certain dependence on specimen size. The general method to determine $\mathcal{G}_c$, however, is confirmed by numerical calculations.

Table 5.3.: Experimental results for the fracture energy $\mathcal{W}_c$ and the critical energy release rate $\mathcal{G}_c$; all parameters are given as averaged values over the full sets of specimen with standard deviation.

Material	$\mathcal{W}_c$ (mJ)	$\mathcal{G}_c$ (N/m)
Cement S_0	25.2 ± 11.4	40.9 ± 18.5
UHPC S_1	74.5 ± 38.1	91.7 ± 46.9
UHPC S_2	92.3 ± 29.5	113.6 ± 36.3

The stress-strain response obtained for the two UHPC mixtures S_1 and S_2 is displayed in Fig. 5.21. This curve is computed out of our data measured in a conventional SHPB experiment, [316]. The stress maximum and subsequent decay follow from the temporal evolution of the pulse and do not describe damage in the specimen.
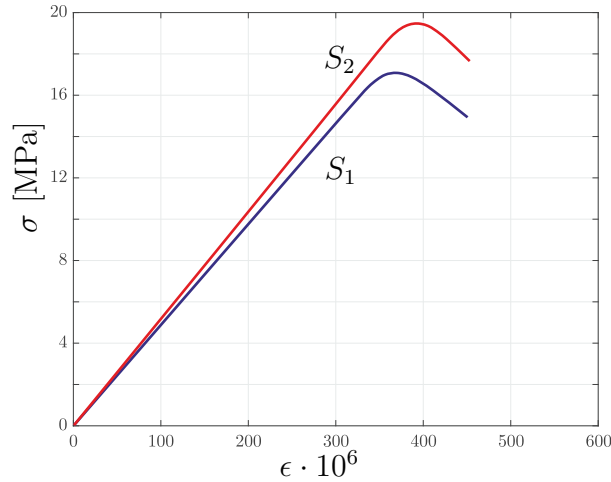
Figure 5.21.: Elastic stress-strain response for mixture S_1 (blue) and of mixture S_2 (red) obtained in the conventional SHPB setup under a strain rate of $30\,\mathrm{s}^{-1}$.

5.2.2. Fracture studies of UHPC by dynamic Brazilian tests

Let's remind ourselves that UHPC with unique properties, offers a variety of interesting applications and is used in buildings like bridges, bunkers or nuclear power stations. These types of structures can experience dynamic loading such as impact, earthquakes or industrial accidents and, therefore, knowledge and reliable data about the dynamic behavior of UHPC material are essential. For the design of engineering structures the constitutive equations in general states of loading as well as failure criteria are important. In this respect, the Brazilian splitting test is a common method to obtain the tensile strength in both quasi-static and dynamic conditions. The splitting experiment presupposes a tension-compression asymmetry of the material which is clearly given in concrete, UHPC and also in common ceramics. The standardized Brazilian test with quasi-static loading is documented in the ASTM C496 and DIN EN 12390-6 [102, 317] and dynamic Brazilian test by SHPB is recommended and conducted in [318] for the first time. In the Brazilian test, two opposing loads are applied to the cross section of the cylindrical concrete specimen and the tensile splitting strength perpendicular to the loaded diameter at the center of the specimen is identified with stress at failure,

$$\sigma_{\mathrm{f}} = \frac{2F_{\max}}{\pi LD} \tag{5.25}$$

where $F_{\max}$ is the maximum applied load, L and D are length and diameter of the specimen, respectively. The pros and cons of Brazilian tests in quasi-static and dynamic loading regimes have been discussed since the method has been introduced, but despite its limits it is still a popular experiment. In the current study, dynamic Brazilian tests conducted on two groups of UHPC specimens in order to investigate their fracture behavior.

Here we used two groups of UHPC specimens that all are cast from one homogenous mixture. Details of the specimens preparation is already described in 3.2.1. The first group is circular disc with diameter of 50 mm and thickness of 15 mm and the second group is the disc with same diameter and thickness, but with two flat ends. In [102] it is recommended that the thickness to the diameter ratio should be between 0.2 and 0.75 for concrete specimen. In the present work, for the UHPC specimens a thickness to diameter ratio of 0.3 is chosen. The SHPB which is used in this study has an air gun, aluminum incident and transmission bars with length of 1800 mm and a diameter of 20 mm, and a steel striker with a diameter of 20 mm and a length of 100 mm. The impact velocity of the striker determines the amplitude of the incident wave. There is a momentum trap at the end of the transmission bar. Fig. 5.22 show schematic of the SHPB used for the dynamic Brazilian test. The stress, strain and strain rate of the specimens are calculated from strain histories recorded by the strain gauges and using Eqs. (5.2) to (5.4).

By the SHPB impact, the stress increased in some points and reached a critical value leading to fracture of the UHPC disc specimen. In fact, corresponding to the lineare-
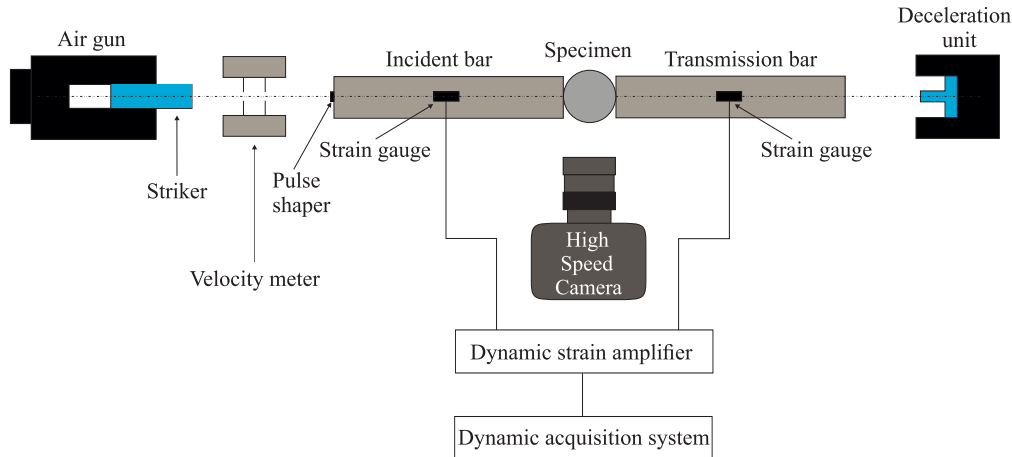
Figure 5.22.: SHPB arragement used for the Brazilian tests.

lastic theory, the crack is initiated from center of the UHPC Brazilian disc specimen, propagates along the diameter and continues till the specimen breaks into two halves.

In order to measure incoming, reflected and transmission pulses during the tests, we put the strain gauges in the middle of the incident and transmission bars also on the specimen. The strain gauges have a resistance of $120.0 \pm 0.1\,\Omega$ and a sensitivity coefficient of 2.14 with tolerance of $\pm1\%$ within $\pm100°$C. All the data and the strain histories obtained from strain gauges are acquired by the HBM GEN7t system with the maximum sampling rate of one mega samples per second. Using a dual rate recording principle, long term observations can be continuously recorded while rapidly occurring events can be captured concurrently. Moreover, a high speed camera system is used which is described later.

In order to check the dynamic stress equilibrium condition during the experiments, the forces (5.7) and (5.8) at both ends of the specimen are compared. To this end, the factor $R(t)$, which relates the difference of forces at both ends of the specimen to the average value within the specimen, is calculated from Eq. (5.9) and specimen is considered to be in equilibrium when $R(t)$ approaches zero. For our Brazilian test we obtained values of about $R = 0.055$, i.e. the assumption of dynamic stress equilibrium is confirmed.

In the test by SHPB, the bar interfaces should be perpendicular to the stress wave propagation direction. In this respect, a precise alignment between the bars and the specimen is necessary. In the current study, careful alignment is performed for each test and calibration of the device is conducted before test to reduce the errors. The calibration is carried out by comparison of the wave speed and delay for a wave to travel in the bar. This calibration shows alignment of the bars, sensitivity of the strain gauges and accuracy of the experimental set up. Th bars geometry and material plays important role on validity of the test and the results. Indeed, the length/diameter ratio (l/D) of the bar greater than 20 and input stresses below the elastic limit of the bars

can further ensure one-dimensional wave propagation. In our research, aluminum bars with $(l/D)= 90$ are used.

More over, the amount of the reflected pulse is not only depend on the contact configuration between the specimen and the bars, but also the bar materials play an important role. In fact, acoustic impedance of bars and tested materials should be near to each other, and for this reason, aluminum bars have been chosen. Fig. 5.23 shows the Brazilian disc specimen under SHPB test condition before the impact.
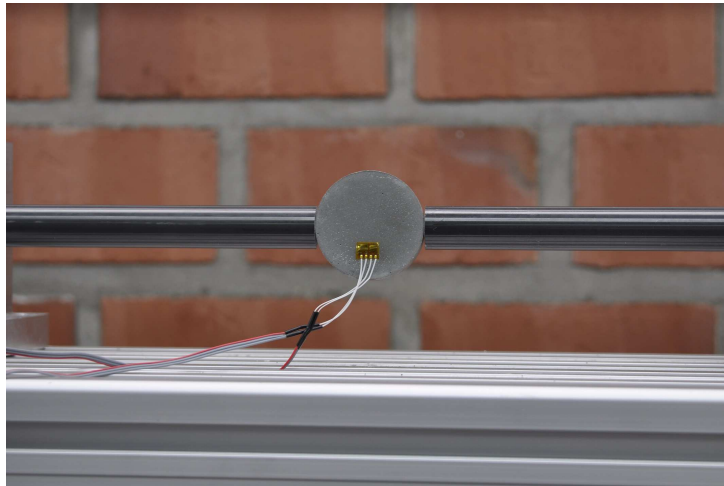
Figure 5.23.: UHPC Brazilian disc specimen positioned in the SHPB.

It should be noted that in a SHPB Brazilian test in some cases the primary crack occurred as loading continued and a higher load is carried by cracked specimen before final fracture. In this case, the failure load is lower than the recorded peak load. This overload effect might lead to an overestimate of the tensile strength. To avoid this overload error we proceeded as follows: by Eqs. (5.7) and (5.8) the loading history is calculated. To determine failure onset, a strain gauge is placed on the UHPC Brazilian disc specimen with a special distance from the center line of the disc, see Fig. 5.23. The specimen gives an elastic release wave at cracking and this wave provides the turning point in the signal which is recorded by the strain gauge. The initiation of cracking is determined by this turning point, because a sudden decrease of the strain as function of time corresponds to the crack initiation point. Furthermore, the elastic wave produced by cracking travels at the sound speed of UHPC and the bar material. The distance between the failure point and the strain gauge is known, so the time of the wave propagation from specimen center line to the strain gauge location can precisely be calculated. The recorded signals of the strain gauges are synchronized, to determine the strain magnitude at failure onset. Specifically, the elastic wave velocity of the studied UHPC is 4000 m/s and the strain gauge is placed at a distance of 4 mm from the specimen center line. Thus, the time shift for the strain gauge signal is $1\mu s$. By this method, a strain value

116

is calculated for failure onset and the overload is avoided by adapting the loading pulse accordingly. Compared with the size of the UHPC specimens, the placed strain gauge on the surface of the specimen is very small and thin, thus the effect to crack bridging to the splitting crack by the adhesive and the gauges can be neglected.

As already mentioned, the SHPB experiments require a careful shaping of the loading strain pulse. Suggestions for pulse shaping techniques, especially for brittle material including concrete and concrete-like materials, have been made in several works, [319, 320, 321]. Emphasis is usually put on a reproducible and well defined strain rate. For brittle materials the additional problem arises, that a sharp increasing stress pulse may generate premature failure of the specimen. Here, we shaped the incident pulse to obtain a constant strain-rate loading. In fact, by trial and error the circular paper sheets and aluminum paper with a thickness of 0.8 mm and a diameter of 10 mm were found to shape the pressure pulse at best. Velocity measurements of the striker confirmed reproducible loading conditions. Fig. 5.24 shows the recorded strain and the strain-rate over time. Both are measured in the middle of the incident bar, which is impacted by the striker. A well defined pulse can be seen. The strain rate-time curve clearly shows that the strain-rate is constant after 50 μs which is the situation of interest when the specimen is in the dynamic equilibrium.
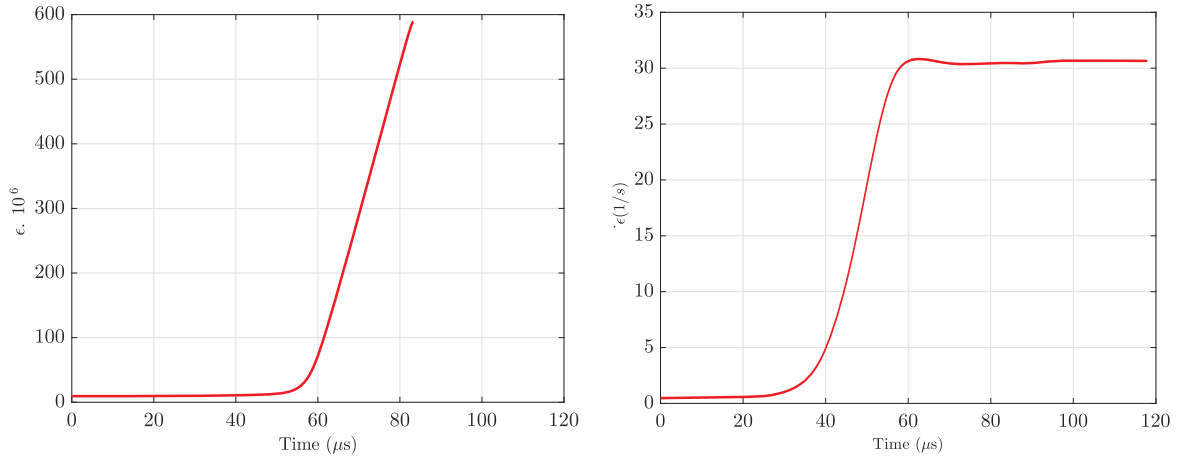
Figure 5.24.: Recorded loading impulse: (a) strain vs. time and (b) strain-rate vs time.

Once loaded, the UHPC specimen remains in equilibrium till the fracture occurs. The stress on specimen-incident bar interface (σ_1) and also specimen-transmission bar interface (σ_2) are determined by:

$$\sigma_1 = \frac{A_b}{A_s} E(\varepsilon_I + \varepsilon_R) \tag{5.26}$$

$$\sigma_2 = \frac{A_b}{A_s} E \varepsilon_T \tag{5.27}$$

From these stresses or the corresponding forces (5.7) and (5.8) the stress at the center of the UHPC Brazilian disc specimen is calculated as the splitting stress (5.25), i.e.,

$$\sigma(t) = \frac{F_1(t) + F_2(t)}{\pi LD} = \frac{AE(\varepsilon_I(t) + \varepsilon_R(t) + \varepsilon_T(t))}{\pi LD} \tag{5.28}$$

The dynamic tensile strength of the UHPC specimen is the value of $\sigma(t)$ when the Brazilian test specimen fails, ie., when the forces reach its maximum.

$$\sigma^{\circ}_{\text{fdyn}} = \frac{2F_{max}}{\pi LD} \tag{5.29}$$

In current research project, 20 circular Brazilian specimens are tested and all the experiments are performed at a strain rate of $30\,s^{-1}$. The measured data are listed in Table 5.4. The results of the measurements give a dynamic tensile strength of $\sigma^{\circ}_{\text{fdyn}} = 19.53 \pm 0.41\,\text{MPa}$.

Table 5.4.: Experimental results for the circular Brazilian test specimens.

Specimen No.	$F_{\max}$ (kN)	$\sigma^{\circ}_{\text{fdyn}}$ (MPa)
1	23.1	19.61
2	23.8	20.21
3	23.2	19.71
4	22.7	19.27
5	23.1	19.61
6	22.8	19.63
7	22.6	19.19
8	23.2	19.71
9	23.8	20.21
10	22.6	19.19
11	23.8	20.21
12	22.7	19.27
13	23.1	19.61
14	22.9	19.44
15	23.1	19.61
16	23.8	20.21
17	22.1	18.76
18	22.3	18.93
19	22.8	19.36
20	22.5	19.11
Avg.		19.53±0.41

Additionally to the circular specimens we also tested flat end Brazilian disc specimens. The geometry is illustrated in Fig. 5.25. The series of the experiments, on flat end
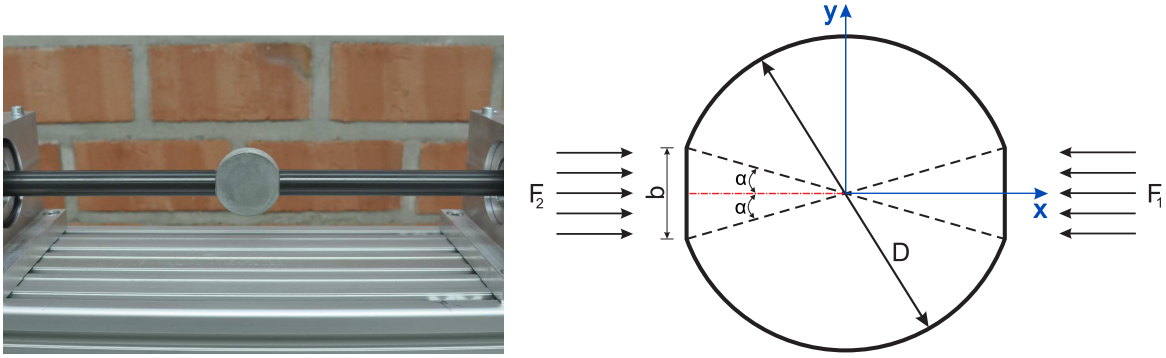
Figure 5.25.: Flat end UHPC Brazilian disc specimen positioned in the SHPB and specimen geometry.

specimens are also carried out at the strain rate of $30\ s^{-1}$. The flat ends provide a perfect and complete contact between the specimen and the bars and avoid stress concentrations. The angle $\alpha = \arcsin(b/D)$ varies from 21.7° to 22.6° for the specimens studied here, where b is the width of the flat end specimen. In the SHPB experiment the line loading is now replaced by surface pressure along the flat end. Compared to the circular Brazilian disc the specimen's adjustment in the experiment is more convenient and there is no need for a special device in order to center it.

The details of the flat end specimens are regards to the recommendations in the literature, where the angle 2α should be in the range of 20°-30° to keep the character of the experiment, [322]. Several experimental and numerical investigations are performed with static and dynamic Brazilian flat end specimen in a variety of materials [323, 324, 325]. In [326] it is concluded that simply the crack initiation in the center of the disc confirms the validity of flat end Brazilian disc tests. Analytical calculations, however, restrict $\alpha \leq 10°$ in order to linearize the trigonometric functions. A comprehensive study on the shape effect and other experimental influence in static Brazilian experiments can be found in [327].

When a pair of loads is applied in the circular Brazilian disc specimen, the tensile stress in the center of the disc is given by Eq. (5.25). This solution is deduced from the theory of linear elasticity and corresponds to one principal stress component in the plane model. For clarity we name this stress σ_{y} and refer it to a cartesian coordinate system with origin in the disc center. The second principal stress component is the compressive stress in axial direction, σ_{x}, which has three times the magnitude but the opposite sign.

Especially we know from the analytical solution of Frocht [328] that along the loading axis the stress components decline with some geometry factor C,

$$\sigma_{\mathrm{x}} = \frac{2F}{\pi LD} C_{\mathrm{x}}(x) \qquad \text{and} \qquad \sigma_{\mathrm{y}} = \frac{2F}{\pi LD} C_{\mathrm{y}}(x) \,. \tag{5.30}$$

and these factors are now

$$C_{\text{x}} = \left[1 - \frac{16D^2x^2}{(D^2 + 4x^2)^2}\right] \qquad \text{and} \qquad C_{\text{y}} = \left[1 - \frac{4D^4}{(D^2 + 4x^2)^2}\right]^2 . \qquad (5.31)$$

This analytical solution had been modified by Awaji & Sato [329] to account for two flat ends of the width b. The disc is now subjected to a line load $pb = F$. The tensile stresses in the center of the specimen are

$$\sigma_{\text{x}} = \frac{2F}{\pi LD}\left[1 - 1.15\left(\frac{b}{D}\right)^2 + 0.22\left(\frac{b}{D}\right)^3\right] . \qquad (5.32)$$

In our case we have $b/D \approx {}^3\!/\!_8$ which gives for the correction term $[1 - 0.162 + 0.012] = 0.85$ and thus a significantly reduced tensile stress. With this calculation at hand, and with expression (5.29) for the maximal tensile stress in the circular specimen, the splitting stress of the flat end Brazilian specimen is

$$\sigma_{\text{fdyn}}^{\shortparallel} = c_\alpha \sigma_{\text{fdyn}}^{\circ} \qquad (5.33)$$

where c_α is the bracketed term in (5.32). Please note, that in the trivial case of $\alpha = 0°$ it holds $c_\alpha = 1$ because this case corresponds to the circular disc.

Experimental results of the flat end specimens are presented in Table 5.5. In total 25 flat end UHPC specimens have been tested and the mean value of the dynamic tensile strength is $\sigma_{\text{fdyn}}^{\shortparallel} = 18.85 \pm 0.43\,\text{MPa}$.

The splitting stress of the flat end specimen is only about 96% of the value obtained with circular specimen. This, however, is more than we would expect from the corrected analytical solution (5.33) which gives 85% for our geometry. Thus, the theoretically expected stress reduction of the analytical solution may be questioned in the dynamic loading regime, because also in the circular disc there will be some flattening at the ends of the specimen during impact.

Considering the general technique of Brazilian tests the question arises, how the obtained splitting stress of the Brazilian test can be related to the uniaxial tensile strength of the material. Malárics [327] investigated this issue in the static regime and found, that for normal concrete the tensile strength is about $1.2 - 1.3$ times the splitting stress. The factor reduces to 1 for high-performance concrete; UHPC was not studied. The likely reason for this relation is, that the in high-performance concrete the stress state is very close to the ideal solution, i.e, the specimen does neither crack at the load zone nor show distributed damage or spall. Therefore we extrapolate, that also in our case the measured values of about $19\,\text{MPa}$ correspond to the tensile strength of the material.

The impact by the SHPB leads to crack propagation along the diameter and towards the two flat ends. Like the circular Brazilian disc specimens, the flat end Brazilian specimens broke into two halves. When the broken halves were put together they match

Table 5.5.: Experimental results for the flat end Brazilian test specimens.

Specimen No.	$F_{\max}$ (kN)	$\sigma_{\mathrm{f\,dyn}}^{\|}$ (MPa)
1	22.7	19.27
2	22.3	18.93
3	22.6	19.19
4	21.7	18.42
5	22.4	19.02
6	22.6	19.19
7	21.9	18.59
8	21.1	17.91
9	22.5	19.11
10	22.3	18.93
11	21.5	18.25
12	22.4	19.02
13	22.6	19.19
14	22.7	19.27
15	22.1	18.76
16	22.8	19.36
17	22.5	19.11
18	22.4	19.02
19	22.5	19.11
20	21.4	18.17
21	21.6	18.34
22	21.3	18.08
23	22.7	19.27
24	22.4	19.02
25	22.9	19.44
Avg.		18.85±0.43

each other very well, i.e., there is hardly any further fragmentation. Some broken UHPC specimens of each mentioned group are shown in Fig. 5.26

Although, in both circular and flat end Brazilian specimens crack initiation is supposed to be at the center of the specimen, due to the infinite compressive stresses under line loads on the circular specimen, the crack initiation might be started around the loading ends which can lead to not reliable data. In the current study, the photographic records shows that in all the tests, the crack emerged on the center of the specimen and it's propagates along the diameter and toward the two flat ends. We tested all the circular and flat end specimens with striker velocity of 6 m/s. Later, some flat end especimens are tested with the striker velocity of 8.5 m/s. Fractured surfaces of the specimens which are impacted by two different striker velocities are investigated and the surface morphology

Figure 5.26.: Broken circular and flat end UHPC specimens.

is presented later, in 5.2.3. Increase in the applied load in the flat end specimens led to multiple cracks along the fracture. Fractured specimens which experienced higher striker velocity are shown in Fig. 5.27. As it can be seen, the triangular breakage zone is occurred in the fractured specimens by higher impact velocity. This phenomenon is stated by the researchers on the dynamic Brazilian tests on marble and concrete [323, 92]. This local failure zone is near to the contact area of the bar and the specimen. It can be occurred due to high compressive stress concentration at this contact area.

Figure 5.27.: Fractured Brazilian specimens with higher impact velocity.

During the dynamic Brazilian tests, a high speed video camera (Fastcam SA5) with capability of clear recording in low-light and with a maximum rate of 775000 frames per second is employed as non-contact optical technique to record the process from initial impact till disc specimen failure. The light sensitive sensor of the camera provides analogue to digital converter without interpolation. This accuracy is a serious requirement

for a precise motion analysis. In Fig. 5.28 the evolution of the crack on the sample surface is illustrated. The relative delay on occurrence of the micro-cracks is a result of the strain rate increase which leads to rise of the strength of concrete and cementitious composite materials.
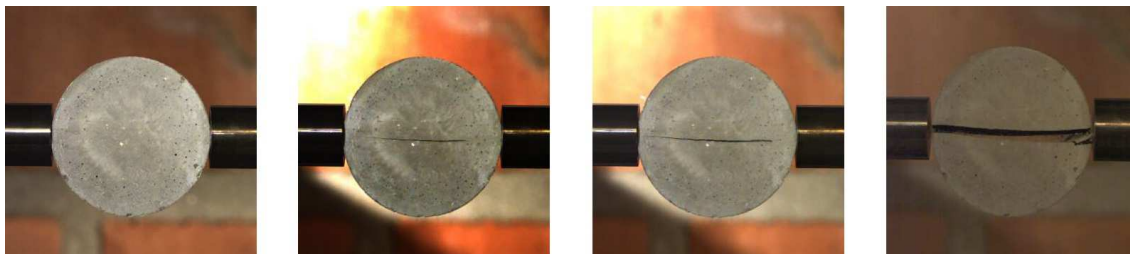
Figure 5.28.: Crack propagation on the Brazilian test; from left to right: (i) bars contact the specimen, (ii) initial fracture, (iii) crack propagation, (iv) final fracture.

Analysis of the recorded movies proved that the crack initiated from the center of the UHPC specimen, propagates along the diameter and continuous till specimen breaks into two halves. Furthermore, it is concluded that when the impact velocity is increased the period of stresses equilibrium at the bars-specimen interfaces becomes shorter and the studied UHPC specimens are failed earlier.

5.2.3. Microscopic inspections

Fracture processes are based on different individual aspects and leads to various type of failures. Optical investigations on the fracture surfaces can provide some essential details about the behavior of the material and process of fracture. Fracture behavior influenced by type of loading, environmental conditions and multiaxiality of the loading. However, in order to model the crack propagation process, it is necessary to understand the mechanism of the fracture and it can be accomplished microscopic inspection.

In order to investigate this in detail, fracture surface inspections were carried out with a 3D laser microscope (KEYENCE VK9700K). This microscope employs a laser confocal technology with a short wave laser light source and a white light source, which provides focussed images for all depths of the surface. We utilized the 3D laser microscope determined the actual fractured area of one of the cracked halves on each specimen. This microscope is used for investigations on UHPC specimens of spallaing and dynamic Brazilian experiments.

UHPC specimens of spalling tests

This microscopic study indicated that the fracture surfaces of cement specimens are quite smooth compared with the other two groups of studied UHPC specimens. Typical

details of the fractured surfaces are displayed exemplary in Fig. 5.29 for both UHPCs. The variations in height is up to about 440 μm for S_1 and up to about 240 μm for S_2, indicating that the fractured surface of the UHPC made by second recipe shows a smoother appearance than that of the first group. This tendency has been confirmed by other surface inspections and also by simple visual impressions. The results, in turn, justify to treat UHPC as a homogenous and brittle material.
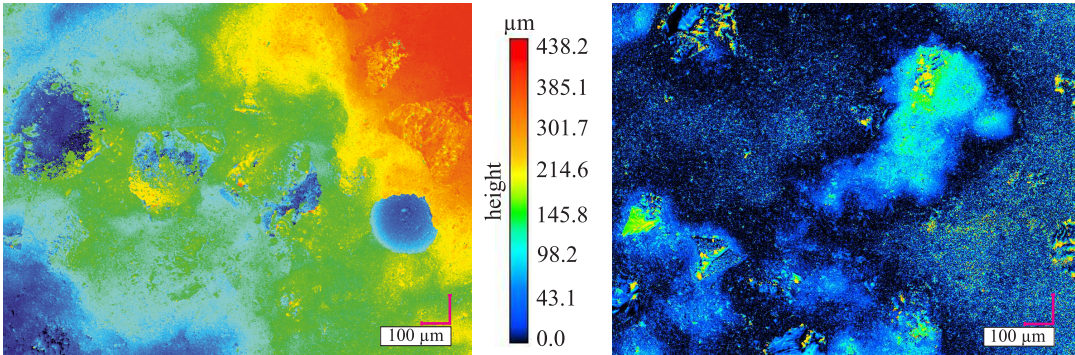
Figure 5.29.: Laser-scanning images: snapshot in left shows the fracture surface of a group S_1 specimen, and in the right shows the fracture surface of a group S_2 specimen. By comparison it's proved that the roughness of the fracture surface in group S_1 is higher then the group S_2.

UHPC specimens of dynamic Brazilian tests

Optical investigations on the fracture surfaces may give some essential details about the process of fracture. Beside of the above-mentioned microscope, a free-angle observation system is also employed for optical study of fracture surfaces. Fig. 5.30 shows the fractured surfaces of two UHPC disc specimens which are tested by two different impact velocities on the Brazilian tests.
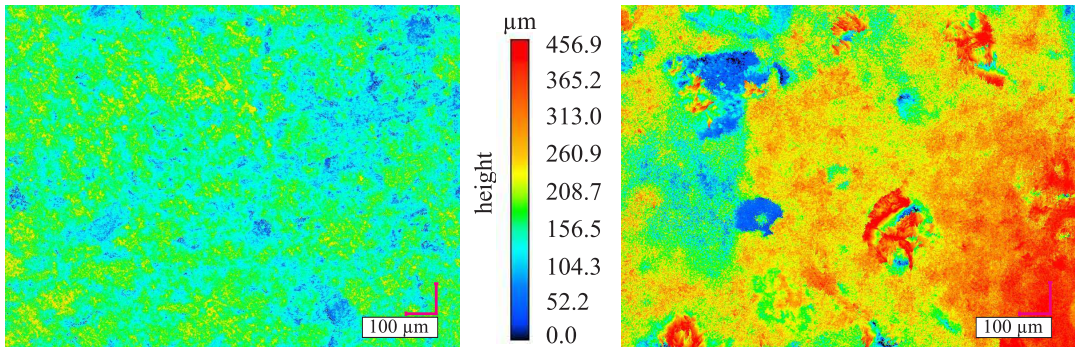
Figure 5.30.: Fracture surfaces of Brazilian specimens.

124

Pressures of 5.5 bar and 8.5 bar are applied for an impact of the striker with velocities of 6 m/s and 8.5 m/s, respectively. On the fracture surfaces of both specimens, the heights are measured from the deepest point after fracture. As it can be seen in Fig. 5.30, a higher impact velocity shows a smoother failure surface.

On the specimen that is tested by a higher impact velocity, the variations in height are up to 300 μm, see Fig. 5.30 (left). This variation in height is larger and up to 456.9 μm for the other specimen which is loaded by a smaller impact velocity Fig. 5.30 (right). This indicates that the fractured surface of the UHPC of a higher impact velocity shows a smoother appearance than the fractured surface of lower impact velocity.

6. Numerical simulations and analysis

In this chapter numerical analysis which are performed for the studied composites, are presented. The first part of this chapter is related to the FEM of the sandwich T-joints, and in the second part numerical analysis of spalling tests and dynamic Brazilian experiments are explained. These finite element models can be used to predict performance and behavior of the materials, and also can be employed to identify weakness of the design. To provide an overview, existing numerical studies of concrete and UHPC under spalling and Brazilian tests by SHB are summarized and presented in Appendix B. It should be noted that, we already published most of this chapter in [243, 245].

6.1. Finite element modeling of the sandwich T-joints

In parallel to the experimental tests, finite element models of the T-joint have been built where the honeycomb core and the face sheets are explicitly modeled with their specific details. The corresponding material properties of the core and the skins are listed in Table 6.1.

Table 6.1.: Properties of core and face sheets.

Materials	E-Modulus (MPa)	Poisson's ratio	Shear Modulus (MPa)
first GFRP layer	$E_1 = 20100$ $E_2 = 19500$ $E_3 = 5000$	$\nu_{xy} = 0.04$ $\nu_{yz} = 0.25$ $\nu_{yz} = 0.25$	$G_{xy} = 7000$ $G_{yz} = 3610$ $G_{yz} = 2850$
second GFRP layer	$E_1 = 24600$ $E_2 = 23100$ $E_3 = 5000$	$\nu_{xy} = 0.04$ $\nu_{yz} = 0.25$ $\nu_{yz} = 0.25$	$G_{xy} = 7500$ $G_{yz} = 3775$ $G_{yz} = 2935$
honeycomb core	$E = 1550$	$\nu_{yz} = 0.2$	—

The aim of these finite element analyzes is twofold. On the one hand, we want to reproduce the experiments as accurate as possible in order to validate the provided limit loads. To this end, a model of the T-joint sample with all its specific details is set up. This model is computationally expensive but reproduces the deformation of the specimen nicely. On the other hand, a simplified model is provided which captures the essential

mechanical behavior in a homogenized way. As before, the failure of the connection by crack propagation is modeled explicitly. The homogenized material properties are adapted to experiment and the detailed numerical simulation. The simplified model allows for large scale computations of joint sandwich structures as required in the design process.

At first a detailed finite element model of the T-joint has been built where the honeycomb core and the face sheets are explicitly modeled. All detailed structures are modeled with solid shell elements. In order to replicate the real test, the loading and boundary conditions are applied as similar to the actual tensile experiment as possible. In total, a mesh of 52252 elements is used for the analyses. The aging is captured by a reduction of the three elastic moduli according to relation (5.1), cf. Fig. 5.5. The finite element analyses are computed with the software ABAQUS; the resulting deformed structure before and after fracture is shown in Fig. 6.1.
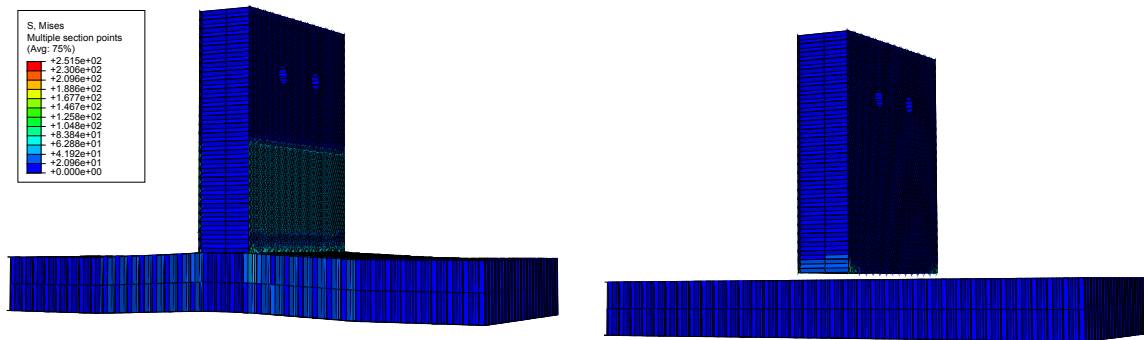
Figure 6.1.: Finite element analysis of the sandwich T-joint under tensile loading: von Mises stress in the deformed model before and after fracture.

The detailed model requires a rather long computational time and it's computationally expensive, but with the proper cohesive properties of the connection it reproduces the deformation of the specimen nicely, provides up to 90 % of the peak loading. This corresponds to the linear-elastic zone of the stress-strain curve in Fig. 5.4. In Fig. 6.2 the corresponding load-displacement curves with material degradation are shown according to the continuum damage theory of Fig. 5.5. Please not that not only the material properties, but also the core wall thickness have a significant influence on the sandwich T-joint behavior in tensile testing. The latter had been discussed, e.g., in [330] where five honeycomb configuration with various wall thicknesses (0.1 to 2.2 mm) are tested. The effective stiffness of the sandwich panel rises significantly with the honeycomb wall thickness. Later, in [67] Nomex honeycomb cores are characterized by means of tensile experiments. The researchers mentioned that thin and long cell walls tend to buckling, whereas thick and short cell wall can reach the critical stress before buckling. Similar results have been found in [331]. Here the thickness of a single honeycomb cell wall is 0.054 mm.
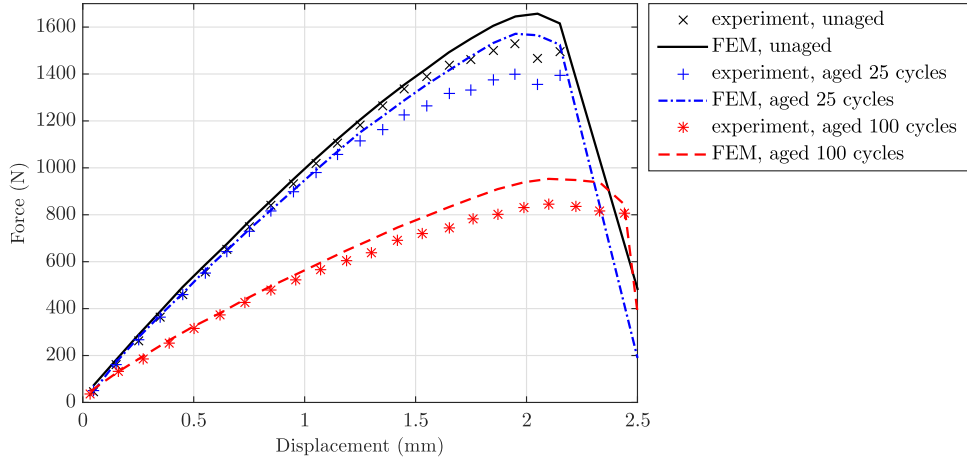
Figure 6.2.: Load-displacement curves computed for the detailed honeycomb core model vs. mean values of the experiments.

An additional homogenized model has been deduced for parametric studies of the fracture process. For this simplified approach we employ the same dimensions, a fine mesh of hexagonal elements, the same boundary conditions but a homogenized material. In particular, a bilinear material model has been chosen, with an elastic modulus of $E = 265\,\text{MPa}$ and a poisson number of $\nu = 0.2$ for the unaged model. If locally a maximum stress σ_0 is reached, the modulus reduces to the half; the poisson number remains unchanged. This bilinear model is only a minor deviation from linear elasticity typically presumed in brittle fracture but it 'rounds' the stress-strain curve. In some sense it levels out the stress concentrations at the clamped boundaries. To account for aging, we set for the 25 cycles aged specimen a reduced elastic modulus of $E = 260\,\text{MPa}$, which corresponds to $d = 0.011$ in equation (5.1). For the 100 cycles aged specimen the elastic modulus is $E = 160\,\text{MPa}$. The local maximum stress value is set $\sigma_0 = 2\,\text{MPa}$, $\sigma_0 = 2\,\text{MPa}$, $\sigma_0 = 1.2\,\text{MPa}$ for the corresponding groups of specimen. These values reflect nicely the loss of stiffness of the specimens in the course of aging, cf. Fig. 5.5 and equation (5.1).

Cohesive zone model

In order to model the fracture of the adhesive joint a cohesive element technique is employed. In this respect, the cohesive elements can be applied in two ways. First, the cohesive element represents the entire adhesive layer [332, 333, 334] or, second, in the FPZ the cohesive element is used while both adjacent structures and the adhesive layer itself are modeled as a continuum [335, 336]. We follow the first approach here.

In a cohesive zone model fracture is assumed to happen along an extended crack tip

triggered by tractions. The relation between the (effective or normal) crack opening displacement δ and the effective tractions on the crack flanks $\sigma \equiv |\mathbf{t}|$ is defined by a cohesive law $\sigma(\delta)$. Most common is an energy-based bilinear binding law where the critical fracture stress is the limit load. Its value σ_c determines the onset of cracking. The specific fracture energy (Griffith energy release rate) controls the rate of crack opening. From its critical value G_c follows the critical crack opening displacement δ_c, see Fig. 6.3.
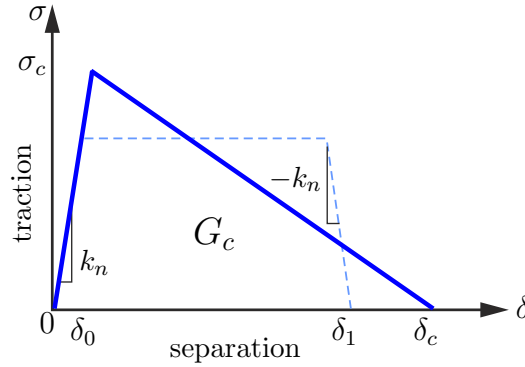
Figure 6.3.: Bilinear cohesive law expressed in terms of an effective opening displacement δ and the effective cohesive traction σ. The dashed lines show the trilinear modification [3].

With given G_c and initial stiffness k_n the initial and the critical crack opening displacement are known,

$$\delta_0 = \frac{\sigma_c}{k_n} \qquad \delta_c = \frac{2G_c}{\sigma_c} \, ,$$

and $\sigma = k_n \delta$ for $\delta < \delta_0$. The traction-separation law for $\delta \geq \delta_0$ is then

$$\sigma = \sigma_c \left(1 - \frac{\delta - \delta_0}{\delta_c - \delta_0} \right) . \tag{6.1}$$

The corresponding fracture energy potential follows from the integration of the traction separation law (6.1) as

$$G(\delta) = \sigma_c \delta \left(1 - \frac{\delta - 2\delta_0}{2(\delta_c - \delta_0)} \right) \tag{6.2}$$

Unloading with $\sigma(\delta) < \sigma_{\max}$ is prescribed by a linear relation to the origin.

From (6.2) we can find the critical fracture energy

$$G_c = \frac{1}{2} \sigma_c \delta_c \, . \tag{6.3}$$

Equation (6.1) states the simplest version of a cohesive law. It can be replaced by more elaborated relations, e.g. the universal exponential binding law [337, 338]. However,

several investigations showed that the critical fracture stress σ_c and the specific fracture energy G_c are the essential parameters, while the shape of the traction-separation curve can considered to be of minor importance in fracture of brittle adhesives [339, 340, 341, 342]. This changes, however, if the adhesive softens and shows plastic deformation. Such a transition to more ductile fracture can be captured by a modification of the traction-separation law 6.1 to a trilinear law. Therefore, we assume a loading with initial stiffness k_n like in Fig. 6.3, then a (nearly) constant zone with $\sigma = \sigma_c$ till δ_1 and then follows the decay with the slope $-k_n$.

$$
\sigma = \begin{cases} \sigma_c \frac{\delta}{\delta_0} & \text{if} \quad 0 \leq \delta \leq \delta_0 \\ \sigma_c & \text{if} \quad \delta_0 < \delta \leq \delta_1 \\ \sigma_c \left(1 - \frac{\delta - \delta_1}{\delta_0}\right) & \text{if} \quad \delta_1 < \delta \leq \delta_c \end{cases} \tag{6.4}
$$

The corresponding opening displacement values are again given by the critical fracture energy which now is

$$
G_c = \frac{1}{2} \sigma_c \left(\delta_1 + \delta_c - \delta_0 \right) . \tag{6.5}
$$

Typical values for G_c are $1\,\mathrm{N/mm}$ for brittle polymers which compare to $100\text{-}1000\,\mathrm{N/mm}$ for brittle metals and $0.001 - 0.1\,\mathrm{N/mm}$ for ceramics [343].

Results

Assuming a uniform stress state in the glued connection of web and flange of the honeycomb core T-joint, our experimental results indicate a critical fracture stress of $1.15\,\mathrm{MPa}$ for the unaged specimen. A critical energy release rate, G_c of $0.92\,\mathrm{N/mm}$ reflects the almost immediate fracture after a short period of softening. The critical fracture stress $\sigma_{c,0}$ is reduced by 10% for the 25 cycles aged specimen to $\sigma_{c,25} = 1.03\,\mathrm{MPa}$ and by 40% for the 100 cycles aged specimen, $\sigma_{c,100} = 0.62\,\mathrm{MPa}$. These values have been confirmed by numerical simulations of the fracture process. For the critical energy release rate a variation of about 1/3 hardly affects the computational results and therefore this value is difficult to specify. We set here $G_c = 1\,\mathrm{N/mm}$ for all specimen groups and model the unaged glue by a bilinear and the aged glue by an trilinear cohesive law. This approach reflects the softening observed in the experiment and indicates, that the material degradation of the adhesive during aging leads to an elasto-plastic fracture. This also explains the different failure mode of the T-joint where parts of the fiber sheets rupture (adhesive mode). In total, the numerical simulations show a reasonable agreement with results which are obtained from the experiments.

The results for the detailed honeycomb core model are shown in Fig. 6.1 and Fig. 6.2. The load-displacement curves nicely reflect the effect of material degradation. In Fig. 6.4 the load-displacement curves computed with the homogenized model and the trilinear
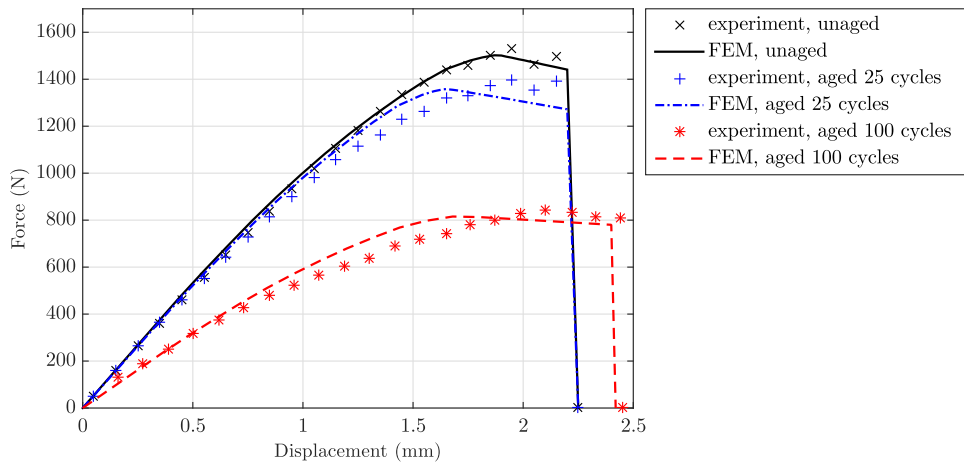
Figure 6.4.: Load-displacement curves vs. mean values of the experiments for the homogenized model.

cohesive law are displayed. Again, the deduced set of parameters is confirmed by comparison with the (averaged) experimental values.

Finally we want to mention, that the chosen combination of aramid paper honeycomb sandwich joints and Ureol 1356 adhesive is close to optimal for a rectangular edge joints. This shows, if we numerically rise the bonding of the adhesive, i.e., the critical fracture stress σ_c, see Figure 6.5. Then the the T-joint will fail by shear failure of the the honeycomb core at a load which is very close to the failure-by-fracture load. The situation would then correspond to mode (c) of our classification of fractures modes in sandwich T-joint connections, Fig. 5.1.
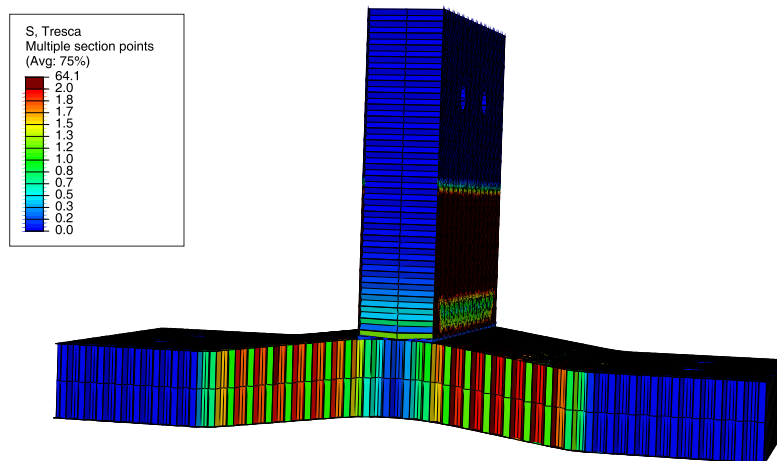
Figure 6.5.: Shear stress in the sandwich T-joint under tensile loading without decohesion.

6.2. Numerical analysis of UHPC specimens under dynamic loadings

UHPC specimens which are utilized in spalling and dynamic Brazilian tests, are also numerically studied. Here, the details of these investigations are presented below.

Numerical verification of UHPC specimens on spalling tests

With the aim to verify the experimentally collected data numerical simulations by means of a finite element method (FEM) which allows for arbitrary crack motion is employed. The crack is modeled as a cohesive zone in which separation is driven by cohesive tractions. We use here the technique of adaptively inserted cohesive elements, but the fracture mechanical background of, e.g., the eXtended Finite Element Method is the same. In the cohesive element approach layer elements are inserted along the edges or faces of the 2D or 3D mesh, see Fig. 6.6.

(a) geometry

(b) 2d and 3d cohesive element
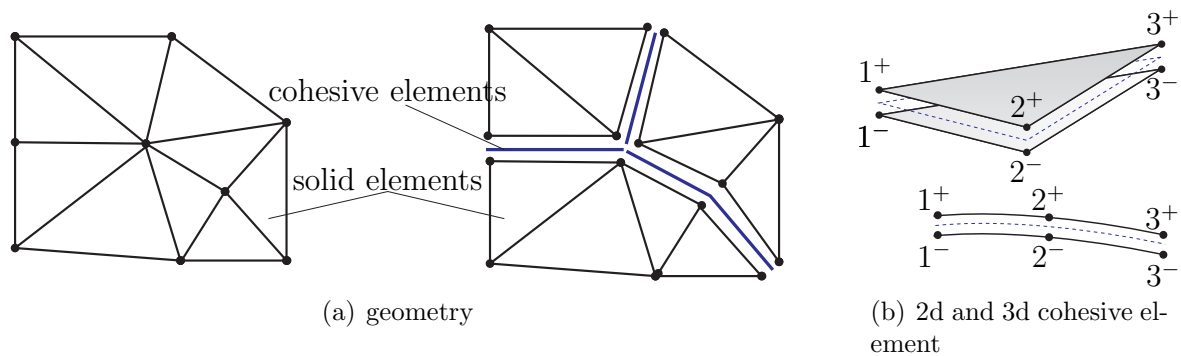
Figure 6.6.: Discretization of a solid with the cohesive element technique (a) and geometry of a cohesive element (b). The upper and lower surfaces + and − coincide if the element is closed.

In the cohesive element approach layer elements are inserted along the edges or faces of the 2D or 3D mesh, see Fig. 6.6. Within these cohesive elements a crack-opening constitutive law models the dissipation of the fracturing process. Cohesive elements are only inserted in the meshed structure when the local stresses exceed a critical traction which allows an adaptive meshing of arbitrary crack paths, cf. [344]. Here we use an axisymmetric model of the specimen with material parameters $E = 50\,\text{GPa}$, $\nu = 0.2$ and $\rho = 2378\text{kg/m}^3$ and assume a value close to the tensile resistance as an insertion criterium (18 MPa). The incoming stress impulse is modeled with a trapezoidal approximation; more details on the method can be found in [338]. Fig. 6.7 illustrates, that the location of the inserted cohesive elements corresponds well to the experimentally observed crack position.

Once the cohesive elements are activated, the local traction σ follows a modified Rose-

Ferrante-Smith cohesive law for the concrete material, [345],

$$\sigma(\delta) = e\sigma_c \frac{\delta}{\delta_c} \exp\left(-\frac{\delta}{\delta_c}\right) \tag{6.6}$$

where δ is the crack-opening displacement, $e = 2.718\ldots$ is the Euler-Number; σ_c is the stress at decohesion and δ_c the corresponding critical crack opening for which the maximum stress σ_c is achieved. In general, the cohesive traction σ as well as the crack opening displacement δ are vectorial quantities but we will simplify the equations here with respect to our specific experiment. The critical energy release rate $\mathcal{G}_c$ is deduced from Eq. 6.6 as the area under the graph in Fig. 6.7.

$$\mathcal{G}_c = \int_0^{\delta_\infty} \sigma(\delta)d\delta = e\sigma_c\delta_c\left(1 - \left(1 + \frac{\delta_\infty}{\delta_c}\right)\exp\left(-\frac{\delta_\infty}{\delta_c}\right)\right) \tag{6.7}$$

The irreversibility of fracture manifests itself upon unloading. With law 6.6 unloading to the origin is described by $\sigma \propto \delta$ for $\delta < \max(\delta)$ or $\dot\delta < 0$ and consequently,

$$\dot\delta = \begin{cases} \dot\delta & \text{if } \delta = \max(\delta) \text{ and } \dot\delta \geq 0 \\ 0 & \text{otherwise} \end{cases} \tag{6.8}$$

defines the kinetic equations for the evolution of the internal variable in the present model. In case of our spallation experiment this translates into an effective crack opening once the critical fracture energy is reached and a into reduced tensile resistance, if the energy of the tensile wave is not sufficient. The latter corresponds to experimental observations when the striker hits the specimen with low pressure. In this case a first strike does not break the specimen but after several repeated low pressure strikes the material fails.

From Eq. (6.6) it also follows, that if the insertion criterium for the cohesive elements is set to low, elements will be inserted in (many) other positions then the final crack location. These cohesive elements will not open to form a crack. This is correct, However, it yields to wave scattering and numerical dissipation, and the numerical simulation of the fracture process suffers. In our simulations we mesh the specimen uniformly with 2560 elements and set the traction for insertion of cohesive elements to 15 MPa.

In [4] an inverse analysis has been performed, where the data obtained in our experiments are used to define a range of input data for the specific fracture energy $\mathcal{G}_c^{\text{inp}}$. With this value the spallation experiment is simulated and from the computed velocities and masses, the 'measured' value $\mathcal{G}_c^{\text{sim}}$ deduced via Eqs. (5.20) and (5.24). To this end, the velocities of the fragments are determined by

$$v_{\text{spec}} = \sqrt{\frac{2\sum_e \mathcal{K}_e}{m_{\text{spec}}}}, \qquad v_{\text{fra,1}} = \sqrt{\frac{2\sum_{e(\text{fra,1})} \mathcal{K}_e}{m_{\text{fra,1}}}}, \qquad v_{\text{fra,2}} = \sqrt{\frac{2\sum_{e(\text{fra,2})} \mathcal{K}_e}{m_{\text{fra,2}}}}, \tag{6.9}$$

where e denotes one finite element with a kinetic energy of $\mathcal{K}_e = \frac{1}{2}m_e|\boldsymbol{v}_e|^2$.
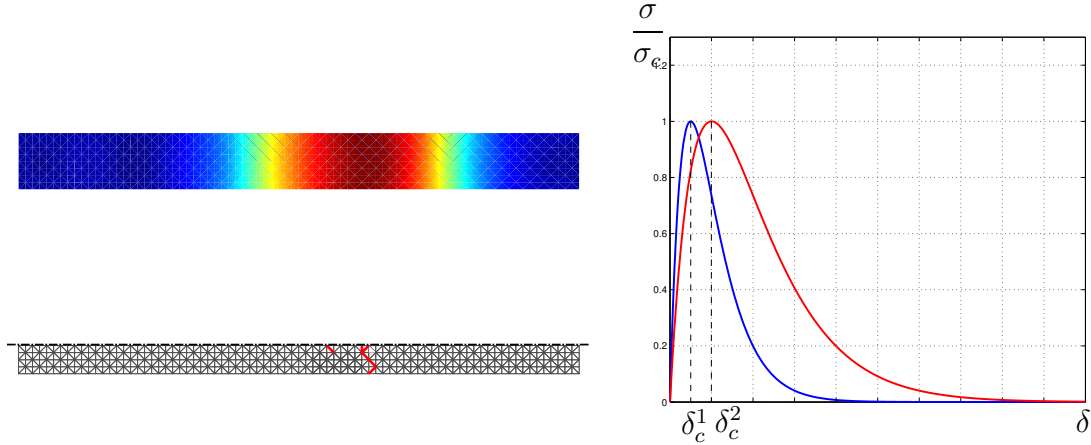
Figure 6.7.: Illustration of the cohesive technique. Left: stress in the specimen immediately before crack initiation and location of the open cohesive elements (red) in the finite element mesh for $\sigma_c = 18\,\text{MPa}$ and $\mathcal{G}_c = 100\,\text{N/m}$. Right: cohesive law given by Eq. (6.6). The normalized nominal tension σ/σ_c is plotted vs. the crack opening displacement δ for two parameters $\delta_c = \delta_c^1$ and $\delta_c = \delta_c^2$. The areas below the graphs mark the specific fracture energy $\mathcal{G}_c$. The figures are taken from [4].

In Fig. 6.8 the computed specific fracture energy $\mathcal{G}_c^{\text{sim}}$ is shown. In the optimal case is $\mathcal{G}_c^{\text{inp}} = \mathcal{G}_c^{\text{sim}}$, this is marked with a dotted line. The computed values show a clear proportionality between $\mathcal{G}_c^{\text{inp}}$ and its simulated counterpart $\mathcal{G}_c^{\text{sim}}$. This generally validates the chosen method of energy balance. However, the value of $\mathcal{G}_c$ deduced from the simulation is higher the real one. This corresponds to a higher difference in the kinetic energy, i.e., for the given initial velocity the velocity of the fragments is underestimated, i.e. there is too much energy dissipated. This results from the fact that some of the adaptively inserted cohesive elements are 'useless', they are inserted in a wrong place and do not fully open. This partial opening costs energy which is dissipated but does not contribute to spallation. Therefore we observe $\mathcal{G}_c^{\text{inp}} < \mathcal{G}_c^{\text{sim}}$ with discrepancies between 30% and 50%, see Fig. 6.8.

It should be mentioned that an evaluation of the conservation of momentum (5.21) is also possible, all required values can easily be deduced from the simulation. Here an inverse analysis also results in clear correlation between input and simulated data with $\mathcal{G}_c^{\text{inp}} < \mathcal{G}_c^{\text{sim}}$, however, the error is larger. Reason for this is that the numerical approximation of $\dot{\delta}$ is rather inaccurate.

Numerical simulations of UHPC specimens under dynamic Brazilian tests

In order to evaluate the effect of the flat end in dynamic Brazilian tests we simulate our experiments by means of a finite element analysis. To compute crack initiation and propagation, the eXtended Finite Element Method (XFEM) was chosen. Specifically, the commercial program Abaqus [346] is employed where a two-dimensional XFEM version
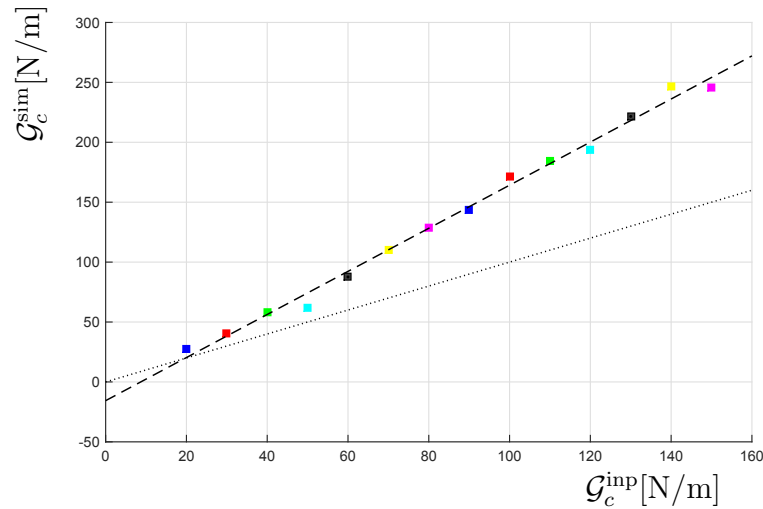
Figure 6.8.: Determination of the specific fracture energy with the cohesive element technique: displayed are the values $\mathcal{G}_c^{\mathrm{sim}}$ derived from the velocity and mass data obtained in the simulation vs. the input parameter $\mathcal{G}_c^{\mathrm{inp}}$ of the experiment. The dotted line marks the identity $\mathcal{G}_c^{\mathrm{sim}} = \mathcal{G}_c^{\mathrm{inp}}$; the dashed line is approximated with $R^2 \approx 0.9928$. The figure is taken from [4].

is implemented.

The specimens' geometries are created according to the experimental section, i.e., the first model is a complete circular disc of diameter 50 mm and the second one has two flat ends with b = 17mm, see Fig. 5.25. Two dimensional continuum plain strain elements (CPE4) were used for discretization. Because the aim of our computations is a comparison of the two shapes, such a simplification is justified. The meshes of the circular and the flat end Brazilian specimen are shown in Fig. 6.9. Two flat rigid parts were used to model the adjacent bars.
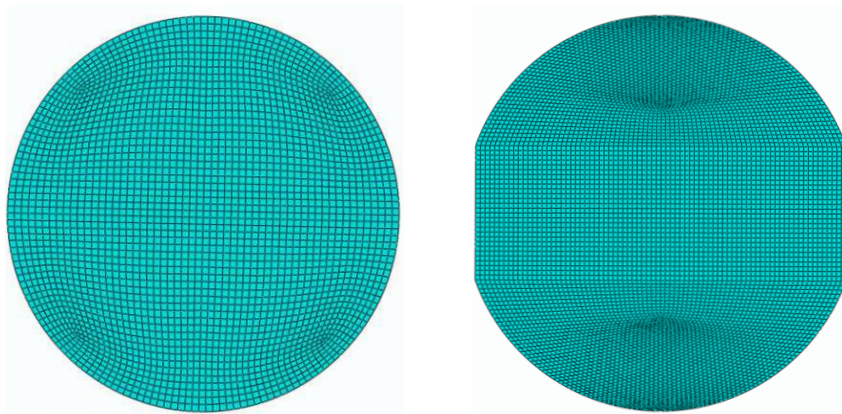
Figure 6.9.: FEM mesh of the Brazilian specimens, circular specimen (left) and flat end specimen (right).

The XFEM is an extension of the finite element method which allows discontinuous (cracked) interfaces independent of the finite element mesh. Specifically, Abaqus uses an XFEM approach which is based on a traction-separation cohesive behavior, cf. [347], similar to classical cohesive zone models. Before crack initiation the material has a linear elastic behavior. The elastic modulus and Poisson's ratio for UHPC are $E = 55$ GPa and $\nu = 0.18$, respectively. If a crack initiation criterion is reached, the elastic behavior is followed by crack evolution which degrades the material stiffness.

For crack initiation, the maximum principal stress criterion was used. This model can be represented with a parameter

$$f = \max \left(\frac{\langle \sigma_{\max} \rangle}{\sigma_{\mathrm{f}}} \right) \tag{6.10}$$

where σ_{f} is the tensile strength and the Macaulay bracket $\langle \cdot \rangle$ denotes the positive part. The crack is assumed to initiate when the parameter f reaches the value of one within a given tolerance, $1.0 \leq f \leq 1.0 + f_{\mathrm{tol}}$. We used $\sigma_{\mathrm{f}} = 19.6$ MPa for the circular disc and $\sigma_{\mathrm{f}} = 16.6$ MPa for the flat end sample with a tolerance of 0.1 for the fracture criterion.

Once the initiation criterion is reached, the stiffness K of the cohesive zone degrades. Here, a scalar damage variable D, which initially has a value of 0, is used to degrade the cracked element to $(1 - D)K$. The evolution of D is governed by an energy based exponential softening traction-separation law. Crack opening is controlled by the difference of the specific elastic energy (which is the area under traction-separation curve after the crack initiation criterion is met) and the critical fracture energy G_c. In our study, the critical value was set to $G_c = 100$ N/m which corresponds to our experimental results in [348].

Fig.6.10 shows the crack initiation and crack propagation path for the circular and the flat end specimen, respectively. Displayed are the maximum principle stresses uniformly scaled. In both cases, the crack starts from the middle of the specimen and propagates parallel to the bar direction until the specimen is split. The effect of the flat end on the crack path seems to be negligible.

The tensile stress difference between the circular and the flat end specimen and its effect on crack initiation are compared in Fig. 6.11. Here the maximum principal stress contours of both specimens are displayed shortly before and right after crack initiation. We see that the principal stress is somewhat lower in the flat end specimen which roughly corresponds a reduced tensile strength like in Eq. (5.32). The crack initiates as soon as the principal stress reaches the critical value of 19.6 MPa and 16.6 MPa in the circular and the flat end specimen, respectively.

Finally, for both Brazilian specimens the propagated cracks, which lead to final fracture, are compared in experiments and simulations. We refer to Fig. 5.28 for the experiments and to the last line of Fig. 6.10 for the XFEM analyzes. For both types of specimens the crack is straight and the cracking zone is placed near or at the horizontal diameter of the specimen which is, regarding inevitable imperfection of experimental setting and material, a good agreement.
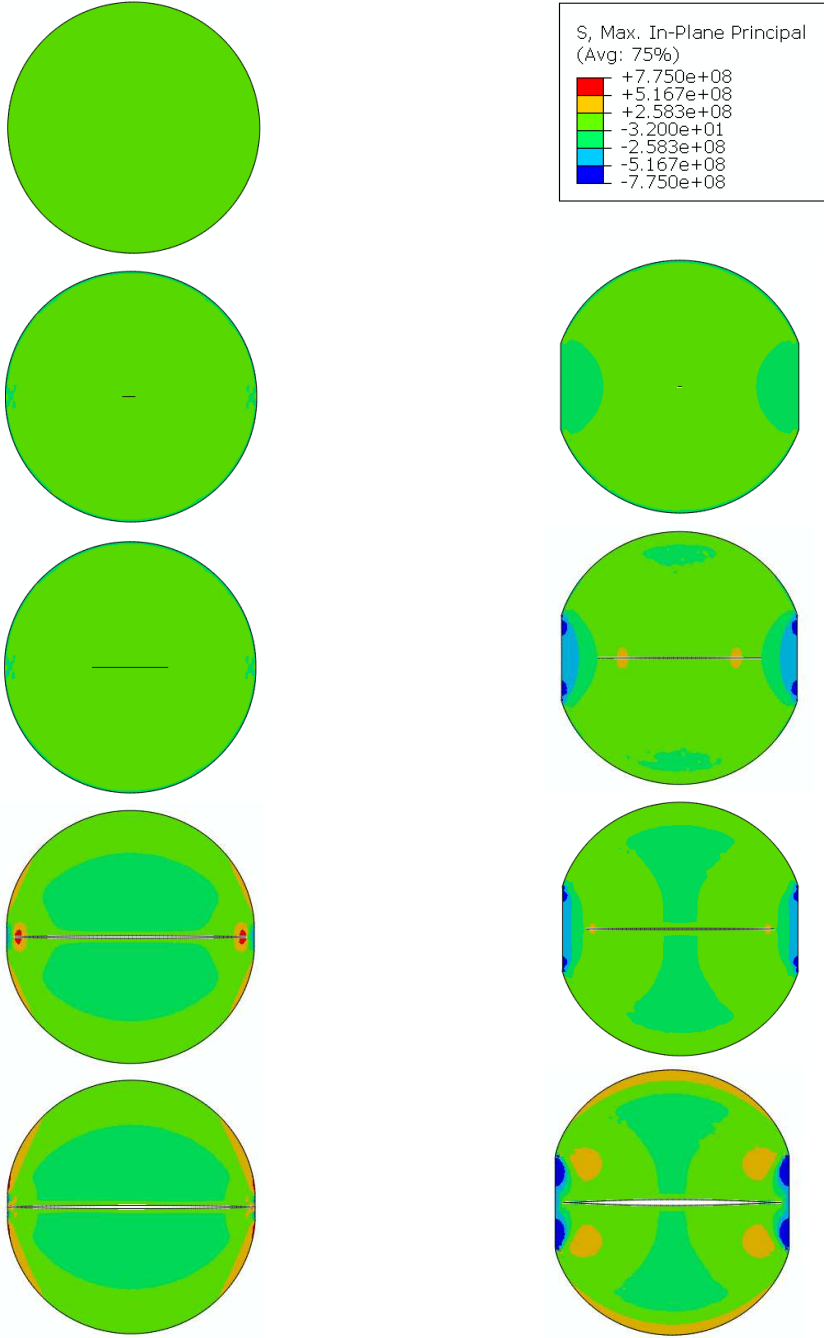
Figure 6.10.: FEM computation with circular (left) and flat end specimens (right) at five instances. The initial state of the flat disc is replaced by the legend of the displayed stresses (Pa).
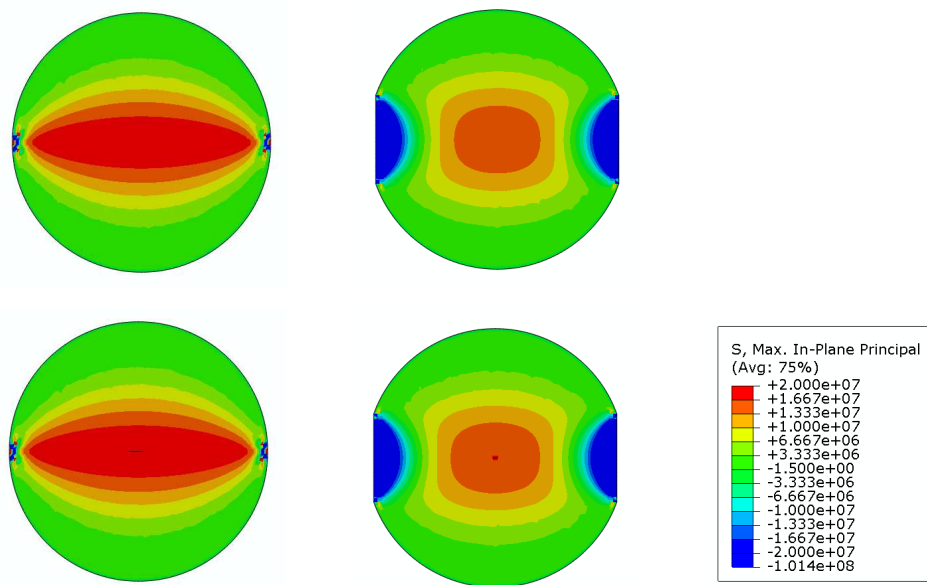
Figure 6.11.: Maximum principal stress contours for the circular and the flat end specimen before (up) and right after (down) crack initiation.

7. Conclusions and future works

In this dissertation, our attention has been focused on experimental investigations on two different composites. For this purpose, series of the tests are performed on the studied materials. In this chapter, major findings and conclusions about studied composites are presented, followed by scope of future research work in this topic.

7.1. Conclusions

Since various composites shows superior performance, applications of them dramatically increased in lots of domains. Several years working experience of the composites, help designers and manufacturers to develop these applications. In fact, compared with traditional metals unique properties of composites such as higher strength to weight ratio, reduced maintenance requirements, long-term durability, corrosion or weather resistance and low thermal conductivity converted them to favorable material in variety of domains. In the recent years, development and new applications of sandwich-structured composites and cementitious composites are highly extended. For future material developments, new applications and also future computational models, response of these materials to the various loadings and environmental conditions should be determined precisely.

The sandwich-structured composites are constructions which uses strong facing materials bonded to lightweight core. This provides the most efficient strength to weight and also stiffness to weight structure. Although almost any type of material can be utilized as face sheet in sandwich structures, currently various part of aircraft interior are fabricated by GFRP and CFRP. Installation of new in-flight entertainments leads to significant increase of these composites. Since, adhesively-bonded sandwich composites are currently widely used in aircraft interior, we tested the sandwich T-joints in order to investigate their behavior on different loadings and environmental conditions, and identify the damage procedure.

UHPC material and its variants as new generation of concrete shows improved performance and higher strength than traditional concrete. cementitious materials are highly sensitive to the strain rate under tension, compression or flexure. Thus, the mechanical properties which are obtained under quasi-static loading condition cannot be used for design of the structures under dynamic loading regime. In order to study behavior

of this material and determine their mechanical properties under high strain rate, we performed various experiments.

In specifying the composites, obtain the accurate material properties is count as a critical task. In this respect, reliable data can be obtained from actual testing and analysis of response of the material and the structure. This result can be used to describe the strength and response of the material to the various conditions, which are benefial for material development and for future finite element analysis. In this thesis, two type of composite material experimentally investigated. The first group of the studied specimens are sandwich T-joints made by sandwich composite. The second group is UHPC specimens which are experienced different experiments.

Various composites are used in aerospace industry. One of the most employed composite in aircraft interior, is sandwich-structured composite made by honeycomb core with GFRP face sheet. In this research, sandwich T-joints which are scaled joint of the aircraft galley are used as first group of the studied specimens. The studied T-joints are employed for almost all types of the galley that are fabricated by honeycomb sandwich composite in passenger aircraft. The detail of the studied T-joints specimens are presented in chapter 3. In the real application of this part in aircraft galley, they experienced various environmental conditions. In order to investigate mechanical behavior and fracture of this sandwich-structured composite, ageing issue is considered and this mechanical event is simulated in the laboratory. In this regard, two groups of the T-joints are experienced ageing temperature in the range of $-35°$C and $70°$C each temperature kept for 12 hours. For the first and second groups of aged specimens, 25 cycles and 100 cycles are conducted, respectively. As it was aim of this research, experiment conditions for both static and dynamic loading regiems are determined and series of the tensile tests are carried. In this respect, quasi-static tensile tests with strain rate of $1 \times 10^{-2}\, s^{-1}$ are performed on the room condition for both aged and unaged specimens. On the tests, a rigid fixture was fabricated and used not only to fix each specimen on the test position, but also to minimize non-symmetric effect. Experimental procedure and the stress-strain curves of the aged and unaged specimens after quasi-static tensile tests are presented in chapter 5. From the experimental data we concluded an effective elasticity of the unaged studied specimens is $E = 43.42$ MPa and it is reduced to $E = 42.95$ MPa and $E = 17.05$ MPa for the first and the second groups of the aged specimens. This reduced elasticity is showed also in our finite element analysis in chapter 6. Furthermore, series of the dynamic tensile tests are conducted by a servo-hydraulic high-speed testing machine at strain rate of $5000\, s^{-1}$. Since the sandwich composites meet high rate of loading in their service time, study effect of this loading is necessary. The obtained results shows that the fracture load in the dynamic loading condition is higher than quasi-static loading. Also, in compare with the ageing, the strain rate effect considered minor. in other word, tensile failure strain is changed significantly with the environmental conditions. On the tests, two high speed video cameras are employed and full-field strain measurement on the desired area of the composite Tjoint under load is provided by the DIC technique. For quasi-static and dynamic tensile tests and also aged and unaged specimens, fracto-

graphic analysis are performed which are presented in chapter 5. The obtained results from both static and dynamic loading conditions, prepared reliable data about fracture behavior of sandwich T-joints. This experimental results can be used by designers and there is possibility to predict the remaining service life. Moreover, the achieved results are beneficial for future computational models of sandwich-structured T-joints.

In the second phase of the current research, UHPC specimens as cementitious composite are studied. Due to the demands of engineering structures with high-impact resistance, applications of this material increased very fast. In order to further material developments and improve the load-carrying capabilities of UHPC, accurate data extracted from the experiments is needed. Toward this goal, series of the tests are performed on cylindrical and circular UHPC specimens which are fabricated with two different recipes, described in chapter 3. Regarding to the objective of this research, these specimens are used to determine mechanical properties at high strain rate by split Hopkinson bar. For this purpose, the 20 mm long cylindrical UHPC specimens with diameter of 20 mm are utilized and dynamic elastic moduli equal to $E = 48.6 \pm 0.5\,\mathrm{GPa}$ and $E = 51.3 \pm 0.5\,\mathrm{GPa}$ are determined for two different recipes. In order to calculate dynamic tensile strength, series of spalling tests are carried out on cyclindrical UHPC specimen with diameter of 20 mm and length of 200 mm. Various approaches have been proposed to determine tensile resistance form spalling experiment, which all are rely on d'Alembert's solution of the uniaxial wave equation in linear elasticity. We determined dynamic tensile strength of the studied cylindrical UHPC specimens based n three different approaches. The obtained results are presented in chapter 5. The achieved values are different in the range of $R_m = 12.1 \pm 1.84$ MPa to $R_m = 19.5 \pm 0.93$ MPa based on different approaches and UHPC with various recipes, but they show the same tendency of a higher resistance in the improved UHPC mixture. Moreover, according to the aim of the current research, these cylindrical UHPC specimens are used to determine dynamic fracture energy by the spalling tests. It is assumed the UHPC materials to behave linear elastically, therefore, the loss of kinetic energy between initial and spalled state can completely be attributed to the fracturing process. We stated that the difference of kinetic energy of two fragments is fracture energy of the specimen. Consequently, specific fracture energy is determined by dividing the determined fracture energy to the actual fractured surface. For the UHPC specimen which is prepared by the second recipe, the specific fracture energy is $\mathcal{G}_c = 113.6 \pm 36.3$ N/m. The complete results are presented in chapter 5 for cement specimens and also the UHPC with different recipes.

Furthermore, we performed dynamic Brazilian experiments as an alternative way to determine dynamic tensile strength of UHPC material. In this respect, we utilized two groups of circular UHPC specimens. In the first group, the circular UHPC specimens are constructed with diameter and thickness of 50 mm and 15 mm, respectively. The specimens on the second group are prepared with same diameter and thickness, with 18 mm flat ends on their boundary. Both groups are made by the same recipe. Detail of these specimens is mentioned in chapter 3. This flat end, provides loading angle varies from 21.7° to 22.6° for the specimens studied here. The obtained results indicated

that dynamic tensile strength of circular and flat end UHPC specimens are $\sigma_{\mathrm{f\,dyn}} = 19.53 \pm 0.41$ MPa and $\sigma_{\mathrm{f\,dyn}} = 18.85 \pm 0.43$ MPa, respectively. The value of flat end specimens show 96% of the strength of the circular specimen. The theoretical solution gives 85% which is stronger reduction of tensile strength. In the dynamic regime the shape correction factor seems to overcompensate the geometrical effect. The details of the dynamic Brazilian tests and its results are comprehensively described in chapter 5. The obtained results have been confirmed by a simulation of our experiments. During the dynamic Brazilian tests, high speed video camera is utilized and the evolution of the crack on the sample surface is recorded. After both spalling and dynamic Brazilian experiments, microscopic inspections on the fractured specimens are conducted. This investigation is described in chapter 5.

The conducted experiments on the both groups of the studied composites are numerically simulated and analyzed which are explained in chapter 6. The sandwich T-joints are modeled within the commercial finite element software Abaqus. In this regard, cohesive element technique is used for study fracture of adhesively bonded T-joint. Force-displacement curves of agend and unaged specimens are obtained and presented. In total, the numerical simulations show a reasonable agreement with results which are obtained from the experiments. Numerical analysis of UHPC under spalling tests also performed. in detail, we employed an adaptive cohesive element technique in order to locate the prior unknown crack. This technique bases on the crack tip opening displacement where fracture is assumed to happen along a crack zone controlled by the traction on the crack flanks. This numerical fracture simulations validated the measurements in the sense, that the finite element analysis can reproduce the experiments. With the aim of verify the experiments, the dynamic Brazilian experiment is also numerically simulated in Abaqus. In this regard, XFEM is employed to compute crack initiation and propagation on the studied UHPC specimens. The numerical results indicated that the critical stress for crack growth is reached at about the same loading state which is obtained experimentally for both, circular and flat end specimens.

Beside of the experimental investigations about behavior of studied composites, applications of AI in mechanical engineering and particularly in the area of fracture mechanics are reviewed. In this respect, fracture mechanics is divided to four sub-domains, and applications of five AI approaches on these sub-domains are reviewed. The considered sub-domains of fracture mechanics are: (a) failure mode and failure mechanism identification, (b) damage and failure detection and diagnosis, (c) fault and error detection, diagnosis and (d) mechanical fracture and fracture parameters. This review is performed from the technical point of view on particular applications of artificial neural networks, Bayesian networks, genetic algorithms, fuzzy logic and case-based reasoning. Details of this review is presented in chapter 4.

As a consequence of the objective and scope of this thesis, number of key areas for further research have been identified and it would be more fruitful if the following points are considered in the future research works.

7.2. Future works

New applications of composites in aircraft interior is an ongoing topic of research. It is predicted that in the next ten years, number of single-aisle aircraft that fly longer routes will be increased significantly, which represent about half of the all operating commercial aircraft. Because of the longer traveling distance, fuel consumption is more crucial issue in this aircrafts. In this case, composites and high-performance composites play important role in order to optimum the aircraft weight and eventually fuel reduction. In this respect, research works with focuses on performance of composites looks necessary to reach new materials. To achieve this goal, researches with application of AI approaches to predict failure and behavior of composite are beneficial. Particularly, CBR can be applied in order to estimate mechanical response of sandwich-structured composite and predict fracture behavior. We implemented a CBR system to predict fracture in the sandwich composite joints, and as future work it can be developed to cover other types of composite joints. This can be a successful method for the accurate fault detection and also prediction of damage location. Analysis by this technique can provide clear understanding of the structure performance and eventually leads to material development.

Furthermore, high rate of loading experiments on adhesively-bonded sandwich composites can provide reliable data for characterization and new design. In this respect, split Hopkinson bar can be employed to perform dynamic tests on adhesively-bonded sandwich joints. This experiment should be well equipped with ultra-high speed photography system to obtain exact data about growth of the debonding and crack propagation. Since applications of sandwich composites is increased day to day, fundamental guideline can help to provide the required structure with optimum cost and minimum consumed material. For instance, using the largest cell size which can be employed or utilizing hexagonal cell configuration when is possible, the cost can be reduced. Beside of the future researches, providing a comprehensive documented data is recommended.

Due to the new demands on engineering structures, cementitious composites are center of worthy attention. Therefore, future research works are crucial in new developments and optimize the performance and construction. To this end, utilizing fiber made of different materials, with various diameter and length should be considered to reach the optimum mixture. Moreover, since structures made by UHPC experience different ambient during their service life, freeze-thaw stability testing can be applied on UHPC specimens to study encounter of this material to various environmental conditions. As performance and response under dynamic loading are affected by several parameters, accurate data about fracture behavior in the early design stage is essential. In term of optimization, it is expected to obtain precise results if AI approaches applied on fracture studies of UHPC materials. The performance and efficiency of UHPC and its variants can be largely improved by this optimization. We implemented an intelligent system to predict mechanical properties of UHPC material. In a future work, this system can be developed to predict mechanical properties of various cementitious composites.

Furthermore, since biomaterials experiences various loadings during their service life in human body, experimental investigations on the deformation behavior of these materials can be planned. To this aim, it is considered to utilize SHB in order to determine mechanical properties of the biomaterials. For instance, restorative dental materials are considered for the test to obtain strain rate dependent dynamic strength. This experimental set-up provides dynamic elastic property analysis, and also the dynamic fracture toughness can be measured. Since the dynamic loadings leads to angular distortion on the biomaterials inside the human body, it is expected these tests indicates more details of dynamic fracture on these materials and the results help material developments and future numerical simulations.

Bibliography

[1] Diehl Aerosystems: Service Modules - Cabin interior - Galleys for passenger aircraft, `http://www.diehl.com/en/diehl-aerosystems` (2017).

[2] F. Toulemonde, J. Resplendino, International symposium on UHPC, in: Proceedings of the 2nd international symposium on ultra high performance concrete, Marseille, French, 2013, pp. 1–832.

[3] K. Weinberg, Lecture notes on fracture mechanics, unpublished note (2017).

[4] T. Dally, Vergleich von Kohäsivelement-Methode und Phasenfeld-Methode anhand ausgewählter Probleme der Bruchmechanik, unpublished Ph.D. thesis (2017).

[5] S. Heimbs, P. Middendorf, M. Maier, Honeycomb sandwich material modeling for dynamic simulations of aircraft interior components, in: Proceedings of the 9th international LS-DYNA users conference, Dearborn, USA, 2006, pp. 1–13.

[6] The Institute for Buildings and Materials Chemistry, University of Siegen, `https://www.chemie-biologie.uni-siegen.de/bwc/home/home.html` (2017).

[7] R. Seymour, R. Deanin, History of polymeric composites, CRC Press, Taylor and Francis Group, 1987.

[8] M. Schwarts, Composite Materials Handbook, MacGraw Hill, 1983.

[9] B. Harris, Engineering Composite Materials, Woodhead, 1999.

[10] A. B. Strong, Fundamentals of Composites Manufacturing, Society of Manufacturing Engineers (SME), 1989.

[11] K. Reifsnider, Fatigue of Composite Materials, Elsevier Science, 1991.

[12] R. Talreja, Damage Mechanics of Composite Materials, Elsevier Science, 1994.

[13] S. Mileiko, Metal and Ceramic Based Composites, Elsevier Science, 1997.

[14] N. Hu, Composites and Their Properties, InTechOpen science, 2012.

[15] K. Chawla, Composite Materials, Springer, 2012.

[16] F. Campbell, Structural Composite Materials, ASM International, 2010.

[17] T. Bitzer, Honeycomb Technology, Springer Science and Business Media, 1997.

[18] Euro-Composites, A leading company in high-quality composite materials, `http://www.euro-composites.com/en/` (2017).

[19] Y. C. Lu, Composite Materials: Advanced Materials and Lightweighting, SAE International, 2015.

[20] U. S. D. of Transportation, Aviation Maintenance Technician Handbook, Federal Aviation Administration, 2012.

[21] P. Stickler, M. Ramulu, P. Johnson, Experimental and numerical analysis of transverse stitched T-joints in bending, Compos. Struct. 50 (2000) 17–27.

[22] B. Buitrago, C. Santiutes, S. Sanchez-Saez, E. Barbero, C. Navarro, Modelling of composite sandwich structure with honeycomb core subjected to high velocity impact, Compos. Struct. 92 (2010) 2090–2096.

[23] T. Koh, S. Feih, A. Mouritz, Experimental determination of the structural properties and strengthening mechanisms of z-pinned composite T-joints, Compos. Struct. 93 (2011) 2222–2230.

[24] F. Yang, Q. Lin, J. Jiang, Experimental study of fatigue failure and damage of sandwich structure with PMI foam core, Fatigue Fract. Eng. Mater. Struct. 38 (2015) 456–465.

[25] J. S. Yang, L. Ma, R. Schmidt, G. Qi, K. U. Schröder, J. Xiong, L.-Z. Wu, Hybrid lightweight composite pyramidal truss sandwich panels with high damping and stiffness efficiency, Compos. Struct. 148 (2016) 85–96.

[26] W. Shaoquan, D. Shangli, G. Yu, S. Yungang, Thermal ageing effects on mechanical properties and barely visible impact damage behavior of a carbon fiber reinforced bismaleimide composite, Mter. Des. 115 (2017) 213–223.

[27] A. Baker, S. Dutton, D. Kelly, Composite Materials for Aircraft Structures, American Institute of Aeronautics and Astronautics, Inc, 2004.

[28] CFC, Composite Market Outlook, `http://www.compositesforecasts.com/` (2017).

[29] C. Worlds, The Markets: Aerospace, `http://www.compositesworld.com/` (2015).

[30] Euro-Composites, `http://www.transparencymarketresearch.com/` (2017).

[31] M. V. Pollio, The Ten Books on Architecture, Harvard University Press, 1960.

[32] R. Palley, Concrete: A Seven-thousand-year History, Quantuck Lane Press, 2010.

[33] P. Jahren, T. Sui, History of Concrete: A Very Old and Modern Material, World Scientific, 2017.

[34] A. Skempton, John Smeaton, ICE Publishing, 1981.

[35] S. Macdonald, Concrete: Building Pathology, Blackwell Science Ltd, 2002.

[36] J. Loudon, An Encyclopaedia of Cottage, Farm, and Villa Architecture and Furniture, Longman, 1846.

[37] C. Stanley, Highlights in the history of concrete, ICE Publishing, 1979.

[38] P. Richard, M. Cheyrezy, Composition of reactive powder concrete, Cem. Conc. Res. 25 (1995) 1501–1511.

[39] X. Zhang, G. Ruiz, R. Yu, M. Tarifa, Fracture behavior of high-strength concrete at a wide range of loading rate, Int. J. Impact Eng. 36 (2009) 1204–1209.

[40] L. Huynh, S. Fostr, H. Valipour, R. Randall, High strength and reactive powder concrete columns subjected to impact: experimental investigation, Const. Build. Mater. 78 (2015) 153–171.

[41] J. Lu, K. Zhu, L. Tian, L. Guo, Dynamic compressive strength of concrete damaged by fatigue loading and freeze-thaw cycling, Const. Build. Mater. 152 (2017) 847–855.

[42] P. Richard, M. Cheyrezy, Reactive concrete with high ductility and 200-800 MPa compressive strength, Am. Concr. Inst 144 (1994) 507–518.

[43] F. D. Larrad, T. Sedran, Optimization of ultra-high performance concrete by the use of a packing model, Cem. Concr. Res. 24 (1994) 997–1009.

[44] R. Adeline, M. Cheyrezy, La passerelle de Sherbrooke: premier ouvrage d'art en BPR - The Sherbrooke footbridge, La technique franaise du Beton (1998) 343–348.

[45] M. Schmidt, E. Fehling, Ultra-high performance concrete: research, development and application in Europe, in: Proceedings of the 7th international symposium on the utilization of high-strength and high-performance concrete, Washington, USA, 2005, pp. 51–78.

[46] M. Rebentrost, G. Wight, Experience and applications of ultra-high performance concrete in Asia, in: Proceedings of the 2nd international symposium on ultra-high performance concrete, Kassel, Germany, 2008, pp. 19–30.

[47] M. Schmidt, E. Fehling, C. Geisenhansluke, Ultra-high performance concrete, in: Proceedings of the international symposium on ultra-high performance concrete. Kassel, Germany, 2004, pp. 1–844.

[48] M. Schmidt, E. Fehling, S. Stuerwald, Ultra-high performance concrete, in: Proceedings of the 2nd international symposium on ultra-high performance concrete, Kassel, Germany, 2008, pp. 1–920.

[49] M. Schmidt, E. Fehling, C. Glotzbach, S. Froehlich, S. Piotrowski, Ultra-high performance concrete, in: Proceedings of the 3rd international symposium on ultra-high performance concrete, Kassel, Germany, 2012, pp. 1–1058.

[50] G. Birelli, UHPFRC development: Review of a determining application, Designing and Building with UHPFRC (2013) 21–41.

[51] T. Leutbecher, E. Fehling, Tensile behavior of ultra-high-performance concrete reinforced with reinforcing bars and fibers: Minimizing fiber content, ACI Struct. J. 109 (2012) 253–263.

[52] L. Karen, R. Scrivener, K. James, Innovation in use and research on cementitious material, Cem. Concr. Res. 38 (2008) 128–136.

[53] S. Yang, S. Millard, M. Soutsos, Influence of aggregate and curing regime on the mechanical properties of ultra-high performance fiber reinforced concrete (UHPFRC), Const. Build. Mater. 23 (2009) 181–186.

[54] F. Toutlemonde, J. Resplendino, Designing and Building with UHPFRC, John Wiley & Sons Inc, New York, 2013.

[55] B. Graybel, M. Davis., Cylindrical or cube: strength testing of 80 to 200 MPa ultra-high performance fiber-reinforced concrete, ACI Mater. J. 105 (2008) 603–609.

[56] K. Wille, D. Kim, A. Naaman, Strain hardening UHPC-FRC with low fiber contents, Mater. Struct. 44 (2011) 583–598.

[57] D. Nguyen, G. Ryu, K. Koh, D. Kim, Size and geometry dependent tensile behavior of ultra-high performance fiber-reinforcement concrete, Composites Part B. 58 (2014) 279–292.

[58] Y. Aminanda, B. Castanie, J. Barrau, P. Thevenet, Experimental analysis and modeling of the crushing of honeycomb cores, Appl. Compos. Mater. 12 (2013) 213–227.

[59] L. Aktay, A. Johnson, B. Kroplin, Numerical modelling of honeycomb core crush behavior, Eng. Fract. Mech. 75 (2008) 2616–2630.

[60] M. Kaman, M. Solmaz, Experimental and numerical analysis of critical buckling load of honeycomb sandwich panels, J. Compos. Mater. 24 (2010) 2819–2831.

[61] M. Giglio, A. Manes, A. Gilioli, Investigations on sandwich core properties through an experimental-numerical approach, Composites Part B. 43 (2012) 361–374.

[62] G. Petrone, S. Rao, S. Dorsa, B. Mace, F. Franco, D. Bhattacharyya, Initial experimental investigations on natural fiber reinforced honeycomb core panels, Composites Part B. 55 (2013) 400–406.

[63] I. Ivanez, S. Sanchez-Saez, Numerical modelling of the low-velocity impact response of composite sandwich beams with honeycomb core, Compos. Struct. 106 (2013) 716–723.

[64] M. Lewin, J. Preston, Handbook of fiber science and technology V.3: High technology fibers, CRC Press, 1996.

[65] D. Kim, J. Lee, Compressive mechanical properties of the nomex/thermoset honeycomb cores, Polym. Adv. Technol. 8 (1997) 1–7.

[66] A. Karakoc, K. Santaoja, J. Freund, Simulation experiments on the effective inplane compliance of the honeycomb materials, Compos. Struct. 96 (2014) 312–320.

[67] R. Roy, S. Park, J. Kweon, J. Choi, Characterization of nomex honeycomb core constituent material mechanical properties, Compos. Struct. 117 (2014) 255–266.

[68] A. Gardziellla, L. Pilato, A. Knop, Phenolic Resins: Chemistry, Applications, Standardizations, Safety and Ecology, Springer, New York, 2000.

[69] L. Gibson, M. Ashby, Cellular solids: Structures and properties, Pergamon Press, New York, 1999.

[70] L. Liu, H. Wang, Z. Guan, Experimental and numerical study on the mechanical response of nomex honeycomb core under transverse loading, Compos. Struct. 121 (2015) 304–314.

[71] D. Roylance, Stress wave propagation in fibers: effect of crossovers, Fiber Sci. Technol. 13 (1980) 385–395.

[72] K. Loewenstein, The manufacturing technology of continues glass fibers, Elsevier, 1993.

[73] Gurit, Composite supplier, `http://www.gurit.com/Our-Business/` (2017).

[74] E. M. Petrie, Handbook of adhesives and sealants, McGraw-Hill Professional, 2007.

[75] H. C. Corporation, Huntsman International LLC, `http://www.huntsman.com` (2017).

[76] J. Earl, J. Dulie-Barton, R. Shenol, Determination of hygrothermal ageing effects in sandwich construction joints using thermoelastic stress analysis, Compos. Sci. Technol. 63 (2003) 211–223.

[77] V. Rao, K. K. Veni, P. Sinha, Behaviour of composite wing t-joints in hygrothermal environments, Aircraft Eng. Aerospace Technol. 76 (2004) 404–413.

[78] A. Zinno, A. Prota, E. D. Maio, C. Bakis, Experimental characterization of phenolic-impregnated honeycomb sandwich structures for transportation vehicles., Compos. Struct. 93 (2011) 2910–2924.

[79] Y. Jen, H. Lin, Temperature-dependent monotonic and fatigue bending strength of adhesively bonded aluminum honeycomb sandwich beams., Mater. Des. 45 (2013) 393–406.

[80] J. Nicholas, M. Mohamed, G. Dhaliwal, S. Anandan, K. Chandrashekhara, Effects of accelerated environmental aging on glass fiber reinforced thermoset polyurethane composites, Composites Part B. 94 (2016) 370–378.

[81] ISO 9142, Guide to the selection of standard laboratory ageing conditions for testing bonded joints, International Organization for Standardization, Technical Committee (2003) 1–24.

[82] A. Mukherjee, R. Mukherjee, Longman Geography for ICSE, Pearson Education India, 2009.

[83] J. Anderson, Introduction to Flight, McGraw-Hill Education, USA, 2011.

[84] A. Noor, W. Burton, C. Bert, Computational models for sandwich panels and shell, ASME Appl. Mech. Rev. 49 (1996) 155–199.

[85] M. Touratier, An efficient standard plate theory, Int. J. Eng. Sci. 29 (1991) 901–916.

[86] D. Backstrom, A. Nilsson, Modelling the vibration of sandwich beams using frequency-dependent parameters, J. Sound Vib. 300 (2007) 589–611.

[87] R. Shimpi, A. Ainapure, A beam finite element based on layerwise trigonometric shear deformation theory, Compos. Struct. 53 (2001) 153–162.

[88] R. Moreira, J. D. Rodrigues, A. Ferreira, A generalized layerwise finite element for multi-layer damping treatments., Comput. Mech. 37 (2006) 426–444.

[89] H. Arora, P. Hooper, J. Dear, Dynamic response of full-scale sandwich composite structures subject to air-blast loading, Composites Part A 42 (2011) 1651–1662.

152

[90] Y. Kwon, Analysis of laminated and sandwich composite structures using solid-like shell elements, Appl. Compos. Mater. 20 (2013) 355–373.

[91] S. Malek, L. Gibson, Effective elastic properties of periodic hexagonal honeycombs, Mech. Mater. 91 (2015) 226–240.

[92] X. Chen, L. Ge, J. Zhou, S. Wu, Dynamic Brazilian test of concrete using split Hopkinson pressure bar, Mater. Struct. 50 (2017) 1–15.

[93] A. Karakoc, J. Freund, Experimental studies on mechanical properties of cellular structures using nomex honeycomb cores, Compos. Struct. 94 (2012) 2017–2024.

[94] C. Schwingshackl, P. Cunningham, G. Aglietti, Honeycomb elastic material properties: A review of existing theories and a new dynamic approach, in: Proceedings of the international conference on noise and vibration engineering, Leuven, Belgium, 2004, pp. 1353–1366.

[95] L. Gibson, M. Ashby, Cellular Solids Structure and Properties, Cambridge University Press, UK, 1997.

[96] J.-M. Berthelot, Materiaux composites, lavoisier, Paris, 1992.

[97] J. Zhang, M. Ashby, The out of plane properties of honeycombs, Int. J. Mech. Sci. 34 (1992) 475–489.

[98] P. Bischoff, S. Perry, Compressive behavior of concrete at high strain rates, Mater. Struct. 24 (1991) 425–450.

[99] DIN EN 12390-3, Prüfung von festbeton -Teil 3: Druckfestigkeit von probekörpern, Deutsches Institut für Normung (DIN) Beuth Verlag Berlin.

[100] DIN EN 12390-5, Prüfung von festbeton -Teil 5: Biegezugfestigkeit von probekörpern, Deutsches Institut für Normung (DIN) Beuth Verlag Berlin.

[101] DIN 1045-2, Tragwerke aus beton, stahlbeton und spannbeton - Teil 2: Beton - festlegung, eigenschaften, herstellung und konformität, Deutsches Institut für Normung (DIN) Beuth Verlag Berlin.

[102] ASTM C496, Standard test method for splitting tensile strength of cylindrical concrete specimens, Annual Book of ASTM, Standards Philadelphia: ASTM, 11.02. (2004) 336–341.

[103] T. Powers, T. Brownyard, Physical properties of hardened cement paste, Am. Concr. Inst 18 (1994) 250–336.

[104] G. Luzio, G. Cusatis, Hygro-thermo-chemical modeling of high performance concrete. i:theory, Cem. Concr. Res. 31 (2009) 301–308.

[105] M. Hunger, An integral design concept for ecological self-compacting concrete, Ph.D. thesis, Eindhoven University of Technology (2010).

[106] R. Yu, Development of sustainable protective ultra-high performance fibre reinforced concrete (UHPFRC): design, assessment and modeling, Ph.D. thesis, Eindhoven University of Technology (2010).

[107] I. Markovic, High-performance hybrid-fiber concrete, Ph.D. thesis, Delft University of Technology (2006).

[108] A. A. Griffith, The theory of rupture, in: Proceedings of the international congress on applied physics, Delft, Netherland, 1924, pp. 55–63.

[109] E. Wang, N. Shrive, Brittle fracture in compression: Mechanisms, models and criteria, Eng. Fract. Mech. 52 (1995) 1107–1126.

[110] J. Buck, I. McDowel, M. Zhou, Effect of microstructure on load-carrying and energy-dissipation capacities of UHPC, Cem. Concr. Compos. 43 (2013) 34–50.

[111] C. Huifa, Elasticity and Plasticity, Architecture and Building Press, 2005.

[112] S. Nasiri, M. R. Khosravani, K. Weinberg, Fracture mechanics and mechanical fault detection by artificial intelligence methods: A review, Eng. Fail. Anal. 81 (2017) 270–293.

[113] M. R. Khosravani, S. Nasiri, D. Anders, Artificial intelligence approach for prediction of UHPFRC mechanical properties, To be submitted.

[114] M. R. Khosravani, S. Nasiri, K. Weinberg, Prediction of performance and fracture of honeycomb sandwich joints using case-based reasoning approach, in: Proceedings of the 22nd European conference on fracture, Belgrade, Serbia, Accepted, 2018.

[115] R. Kurzweil, The Age of Intelligent Machines, MIT Press. USA, 1990.

[116] S. Russell, P. Norvig, Solid Mechanics for Materials Engineers, Prentice Hall, USA, 1995.

[117] E. Faigenbaum, Expert Systems in the 1980's, Stanford University, USA, 1980.

[118] J. Gasching, R. Reboh, J. Reiter, Development of knowledge-based systems for water resource problems, Technical report SRI Project (1981) SRI International.

[119] R. Michaelson, D. Michie, A. Boulanger, The technology of expert systems, BYTE 10 (1985) 303–312.

[120] A. Badiru, Expert systems applications in engineering and manufacturing, Prentice Hall, USA, 1992.

[121] F. Menandro, E. Moyer, J. Liebowitz, H. Liebowitz, An expert system approach to fracture mechanics., Eng. Fract. Mech. 50 (1995) 631–637.

[122] H. Liebowitz, An expert system in fracture mechanics, Eng. Fract. Mech. 50 (1995) 609–629.

[123] T. Liao, Z. Zhan, C. Mount, An integrated database and expert system for failure mechanism identification: Part II - the system and performance testing, Eng. Fail. Anal. 6 (1999) 407–421.

[124] A. Kazaz, Application of an expert system on the fracture mechanics of concrete, Art. Int. Rev. 19 (2003) 177–190.

[125] X. Liu, F. Xuan, J. Si, S. Tu, Expert system for remnant life prediction of defected components under fatigue and creep-fatigue loading, Expert Syst. Appl. 34 (2008) 222–230.

[126] S. Kendal, M. Creen, An Introduction to Knowledge Engineering, Springer Science & Business Media, Boston, USA, 2007.

[127] P. Lucas, L. Gaag, Principles of Expert Systems, Addison-Wesley Longman Publishing Co. USA, 1991.

[128] F. Jensen, An introduction to Bayesian network, Springer, USA, 1996.

[129] A. Bobbio, L. Portinale, M. Minichino, E. Cianamerla, Improving the analysis of dependable systems by mapping fault trees into Bayesian networks, Reliab. Eng. Syst. Saf. 71 (2001) 249–260.

[130] L. Weiss, C. Amon, S. Finger, E. Miller, D. Romero, I. Verdinelli, L. Walker, Bayesian computer-aided experimental design of heterogeneous scaffolds for tissue engineering, Comput.-Aided Des. 37 (2005) 1127–1139.

[131] C. Rivirere, P. Lauret, J. M. Ramsamy, Y. Page, A Bayesian neural network approach estimating the energy equivalent, Accid. Anal. Prev. 38 (2006) 248–259.

[132] K.-V. Yuen, Recent developments of Bayesian model class selection and applications in civil engineering, Struct. Saf. 32 (2010) 338–346.

[133] B. Yet, A. Constantinou, N. Fenton, M. Neil, E. Leudeling, K. Shepherd, A Bayesian network framework for project cost, benefit and risk analysis with an agricultural development case study, Expert Syst. Appl. 60 (2016) 141–155.

[134] D. Li, T. Miwa, T. Morikawa, Modeling time-of-day car use behavior: A Bayesian network approach, Transp. Res. Part D. 47 (2016) 54–66.

[135] Y. Kang, C.-C. Wang, Y.-P. Chang, Gear fault diagnosis in time domains by using Bayesian networks, Theor. Adv. Appl. Fuzzy Logic Soft Comput. Adv. Soft. Comput. 42 (2007) 741–751.

[136] K. Gurney, An introduction to neural networks, UCL Press, London, 1997.

[137] S. Yildirim, I. Eski, Y. Polat, Design of adaptive neural prediction for failure analysis on hip and knee joints of humans, Neural Comput. Appl. 23 (2013) 73–78.

[138] V. Kodogiannis, A. Lolis, Forecasting financial time series using neural network and fuzzy system-based techniques, Neural Comput. Appl. 11 (2002) 90–102.

[139] B. Curry, L. Moutinho, Neural networks in marketing: Modelling consumer responses to advertising, Eur. J. Mark. 27 (1993) 5–20.

[140] Q. Wu, S. Ye, J. Yu, The prediction of size-limited structures in a coal mine using artificial neural networks, Int. J. Rock Mech. Min. Sci. 45 (2008) 999–1006.

[141] M. Cao, L. Pan, Y. Gao, D. Novak, Z. Ding, D. Lehky, X. Li, Neural network ensemble-based parameter sensitivity analysis in civil engineering systems, Neural Comput. Appl. 26 (2015) 1–8.

[142] S. Saberi, R. Yusuff, Neural network application in predicting advanced manufacturing technology implementation performance, Neural Comput. Appl. 21 (2012) 1191–1204.

[143] K. Genel, Application of artificial neural network for predicting strain-life fatigue properties of steel on the basis of tensile tests, Int. J. Fatigue 26 (2004) 1027–1035.

[144] H. Tanarslan, M. Secer, A. Kumanliouglu, An approach for estimating the capacity of RC beams strengthened in shear with FRP reinforcements using artificial neural networks, Constr. Build. Mater. 30 (2012) 556–568.

[145] M. Melanie, An Introduction to Genetic Algorithms, MIT Press, USA, 1996.

[146] J. Xiang, Y. Zhong, X. Chen, Z. He, Crack detection in a shaft by combination of wavelet-based elements and genetic algorithm, Int. J. Solids Struct. 45 (2008) 4782–4795.

[147] B. Samanta, K. Al-Balushi, S. Al-Amiri, Artificial neural networks and genetic algorithm for bearing fault detection, Soft Comput. 10 (2006) 264–271.

[148] L. Zadeh, Fuzzy sets, Information and Control 8 (1965) 338–353.

[149] D. Parhi, S. Choudhury, Intelligent fault detection of a cracked cantilever beam using fuzzy logic technology with hybrid membership functions, Artif. Intell. Comput. Res. 3 (2011) 9–16.

[150] J. Mendel, Fuzzy logic systems for engineering: A tutorial, in: Proceedings of the IEEE, 1995, pp. 345–377.

[151] K. Lee, C. Luo, Application of case-based reasoning in die-casting die design, Int. J. Adv. Manuf. Technol. 20 (2002) 284–295.

[152] Y. Seo, D. Sheen, T. Kim, Block assembly planning in shipbuilding using case-based reasoning, Expert Syst. Appl. 32 (2007) 245–253.

[153] Y.-J. Park, S.-H. Chun, B.-C. Kim, Cost-sensitive case-based reasoning using genetic algorithm: Application to medical diagnosis, Artif. Intell. Med. 51 (2011) 133–145.

[154] H. Ahn, K.-J. Kim, I. Han, A case-based reasoning system with two-dimensional reduction technique for customer classification, Expert Syst. Appl. 32 (2007) 1011–1019.

[155] E. Rissland, K. Ashley, L. Branting, Case-based reasoning and law, Knowl. Eng. Rev. 20 (2006) 293–298.

[156] R. Palton, V. R. Dehkordi, J. Martel, Hourly prediction of a building's electricity consumption using case-based reasoning, artificial neural networks and principal component analysis, Energy Build. 92 (2015) 10–18.

[157] G. Peng, G. Chen, C. Wu, H. Xin, Y. Jiang, Applying RBR and CBR to develop a vr based integrated system for machining fixture design, Expert Syst. Appl. 38 (2011) 26–38.

[158] P. Grant, P. Harris, L. Moseley, Fault diagnosis for industrial printers using case-based reasoning, Eng. Appl. Artif. Intell. 9 (1996) 163–173.

[159] F. Grupe, R. Urwiler, N. Ramarapu, M. Owrang, The application of case-based reasoning to the software development process, Inform. Software Tech. 40 (1998) 493–499.

[160] B. Villanueva, M. Mare, Case-based reasoning applied to textile industry processes, in: Proceedings of international conference on case-based reasoning, Lyon, 2012, pp. 428–442.

[161] M. Frize, R. Walker, Clinical decision-support systems for intensive care units using case-based reasoning, Med. Eng. Phys. 22 (2000) 671–677.

[162] P. Wriggers, M. Siplivaya, I. Joukova, R. Slivin, Intelligent support of the preprocessing stage of engineering analysis using case-based reasoning, Eng. Comput. 24 (2008) 383–404.

[163] A. Aamodt, E. Plaza, Case-based reasoning: Foundational issuses, methodological variations, and system approaches, AI commun. 7 (1994) 39–59.

[164] E. Rissland, J. Kolodner, D. Waltz, Case based reasoning from DARPA, in: Proceedings of the DARPA workshop on CBR, Florida, 1989, pp. 1–13.

[165] J. Kolodner, Case Based Reasoning, Morgan Kaufmann, USA, 1993.

[166] K. Ashley, E. Rissland, Compare and contrast, a test of expertiser, in: Proceedings of the 6th annual national conference on artificial intelligence, Seattle, USA, 1987, pp. 273–284.

[167] M. Devaney, B. Cheetham, Case-based reasoning for gas turbine diagnostics, in: Proceedings of 18th international florida artificial intelligence research scoiety conference, Florida, USA, 2005, pp. 105–110.

[168] M. Kurz, Handbook of Materials Selection, Wiley, New York, 2002.

[169] Y. Prawoto, Solid Mechanics for Materials Engineers, Lulu Enterprises Inc. USA, 2013.

[170] V. Astakhov, Metal Cutting Mechanics, CRC Press. USA, 1999.

[171] H. Kirsch, K. Kroschel, Applying bayesian networks to fault diagnosis, in: Proceedings of the 3rd IEEE conference on control applications, Glasgow, 1994, pp. 895–900.

[172] M. L. Schwall, J. C. Gerdes, A probabilistic approach to residual processing for vehicle fault detection, in: Proceedings of the American control conference, Anchorage, USA, 2002, pp. 2552–2557.

[173] R. Bickford, D. Malloy, Development of a real-time turbine engine diagnostic system, in: Proceedings of the 38th AIAA/ASME/SAE/ASEE joint propulsion conference and exhibition, Indiana, USA, 2002, pp. 1–10.

[174] B. Xu, Intelligent fault inference for rotating flexible rotors using bayesian belief network, Expert Syst. Appl. 39 (2012) 816–822.

[175] S. Jin, Y. Liu, Z. Lin, A Bayesian network approach for fixture fault diagnosis in launch of the assembly process, Int. J. Prod. Res. 50 (2012) 6655–6666.

158

[176] T. Mast, A. Reed, S. Yurkovich, M. Ashby, S. Adibhatla, Bayesian belief networks for fault identification in aircraft gas turbine engines, in: Proceedings of the IEEE international conference on control applications, Hawaii, USA, 1999, pp. 39–44.

[177] Z. Mao, M. Todd, A bayesian damage prognosis approach applied to bearing failure, Mod. Val. Uncertainty Quantif. 3 (2014) 237–242.

[178] T. Bruland, A. Aamodt, H. Langseth, Architectures integrating case-based reasoning and Bayesian networks for clinical decision support, Intell. Inf. Process. 340 (2010) 82–91.

[179] R. Lorenzo, G. Ingarao, F. Micari, On the use of artificial intelligence tools for fracture forecast in cold forming operations, J. Mater. Process. Technol. 177 (2006) 315–318.

[180] H. Balcioglu, A. Seckin, M. Aktas, Failure load prediction of adhesively bonded pultruded composites using artificial neural network, J. Compos. Mater. (2015) 1–15.

[181] R. Ganguli, I. Chopra, Helicopter rotor system fault detection using physics-based model and neural networks, AIAA Journal 36 (1998) 1078–1086.

[182] B. Zhong, J. MacIntyre, Y. He, J. Tait, High order neural networks for simultaneous diagnosis of multiple faults in rotating machines, Neural Comput. Appl. 8 (1999) 189–195.

[183] M. Sahin, R. Shenoi, Quantification and localisation of damage in beam-like structures by using artificial neural networks with experimental validation, Eng. Strcut. 25 (2003) 1785–1802.

[184] H. Li, C. He, J. Ji, H. Wang, C. Hao, Crack damage detection in beam-like structures using RBF neural networks with experimental validation, Int. J. Innovative Comput. Inf. Control 1 (2005) 625–634.

[185] H. Das, D. Parhi, Application of neural network for fault diagnosis of cracked cantilever beam, in: Proceedings of the world congress on nature and biologically inspired computing, Coimbatore, India, 2009, pp. 1303–1308.

[186] K. Aydin, O. Kisi, Damage diagnosis in beam-like structures by artificial neural networks, J. Civ. Eng. Manage. 21 (2015) 591–604.

[187] D. Gope, P. Gope, A. Thakur, A. Yadav, Application of artificial neural network for predicting crack growth direction in multiple cracks geometry, Appl. Soft Comput. 26 (2015) 1027–1035.

[188] S. Hakim, H. A. Razak, S. Ravanfar, Fault diagnosis on beam-like structures from modal parameters using artificial neural networks, Measurement 76 (2015) 45–61.

[189] P. Theocaris, P. Panagiotopoulos, Neural networks for computing in fracture mechanics. methods and prospects of applications, Comput. Methods Appl. Mech. Eng. 106 (1993) 213–228.

[190] A. Seibi, S. Al-Alawi, Prediction of fracture toughness using artificial neural networks (ANNs), Eng. Fract. Mech. 3 (1997) 311–319.

[191] Baghat, A fracture toughness estimation of plates containing surface cracks under certain conditions of temperature and loading, Ph.D. thesis, Pennsylvania State University (1975).

[192] R. Ince, Prediction of fracture parameters of concrete by artificial neural networks, Eng. Fract. Mech. 71 (2004) 2143–2159.

[193] D. E. Goldberg, Genetic Algorithms in Search, Optimization and Machine Learning, Addison-Wesley Publishing Co., 1989.

[194] C. Mares, C. Sarace, An application of enetic algorithms to identify damage in elastic structures, J. Sound Vib. 195 (1996) 195–215.

[195] J. Chou, J. Ghaboussi, Genetic algorithm in structural damage detection, Comput. Struct. 79 (2001) 1335–1353.

[196] R. Perera, R. Torres, Structural damage detection via modal data with genetic algorithms, J. Struct. Eng. 132 (2006) 1491–1501.

[197] F. Buezas, M. Rosales, C. Filipich, Damage detection with genetic algorithms taking into account a crack contact model, Eng. Fract. Mech. 78 (2011) 695–712.

[198] A. Senouci, M. El-Abbasy, T. Zayed, Fuzzy-based model for predicting failure of oil pipelines, J. Infrastruct. Syst. ASCE 20 (2014) 04014018.

[199] Q. Zhou, W. Wei, D. Liu, K. Li, Q. Qiao, Estimation of corrosion failure likelihood of oil and gas pipeline based on fuzzy logic approach, Eng. Fail. Anal. 70 (2016) 48–55.

[200] L. Zeng, H. Wang, Machine-fault classification: A fuzzy-set approach, Int. J. Adv. Manuf. Tech. 6 (1991) 83–94.

[201] C. Mechefske, Automatic Machinery Fault Detection and Diagnosis Using Fuzzy Logic, University of West Ontario, Canada, 1998.

[202] G. Goddu, B. Li, M. Chow, J. Hung, Motor bearing fault diagnosis by a fundamental frequency amplitude based fuzzy decision system, in: Proceedings of the 24th annual conference of the IEEE, Aachen, Germany, 1998, pp. 1961–1965.

[203] D. Skarlatos, K. Karakasis, A. Trochidis, Railway wheel fault diagnosis using a fuzzy-logic method, Appl. Acoust. 65 (2004) 951–966.

[204] J. Wang, H. Hu, Vibration-based fault diagnosis of pump using fuzzy technique, Measurement 39 (2006) 176–185.

[205] S. Cheng, Q. Wei, Z. Ye, Fuzzy-inference based fault diagnosis system for pneumatic press, Adv. Intell. Soft Comput. 62 (2009) 583–590.

[206] M. Chandrashekhar, R. Ganguli, Structural damage detection using modal curvature and fuzzy logic, Struct. Health Monit. 8 (2009) 267–282.

[207] H. Das, D. Parhi, Online fuzzylogic crack detection of a cantilever beam, Int. J. Knowledge-Based Intell. Eng. Syst. 12 (2008) 157–171.

[208] C. Cobb, A. Agogino, Case-based reasoning for the design of micro-electromechanical systems, in: Proceedings of the international design engineering technical conference, Philadelphia, USA, 2006, pp. 1–10.

[209] J. Hu, J. Qi, Y. Peng, New CBR adaptation method combining with problem - solution relational analysis for mechanical design, Comput. Ind. 66 (2015) 41–51.

[210] H. Hashemi, A. Shaharoum, I. Sudin, A cased-based reasoning approach for design of machining fixture, Int. J. Adv. Manuf. Technol. 74 (2014) 113–124.

[211] A. Yan, W. Wang, C. Zhang, H. Zhao, A fault prediction method that uses improved case-based reasoning to continuously predict the status of a shaft furnace, Inf. Sci. 259 (2014) 269–281.

[212] M. Han, Z. Cao, An improved cased-based reasoning method and its application in endpoint prediction of basic oxygen furnace, Neurocomputing 149 (2015) 1245–1252.

[213] E. Reyes, S. Negny, G. Robles, J. L. Lann, Improvement of online adaptation knowledge acquisition and reuse in cased-based reasoning: Application to process engineering design, Eng. Appl. Artif. Intell. 41 (2015) 1–16.

[214] T. Liao, Z. Zhang, C. Mount, A case-based reasoning system for identifying failure mechanisms, Eng. Appl. Artif. Intell. 13 (2000) 199–213.

[215] E. Olsson, P. Funk, M. Bengtsson, Fault diagnosis of industrial robots using acoustic signals and case-based reasoning, in: Proceedings of the 7th European conference on case-cased reasoning, Madrid, Spain, 2004, pp. 686–701.

[216] Y.-T. Tsai, Applying a case-based reasoning method for fault diagnosis during maintenance, IMechE Part C: J. Mech. Eng. Sci. 223 (2009) 2431–2441.

[217] F. Anguel, M. Sellami, Knowledge management for fault diagnosis of gas turbines using case based reasoning, Commun. of the IBIMA 10 (2009) 186–190.

[218] N. Dendani, M. Khadir, S. Guessoum, Use a domain ontology to develop knowledge intensive CBR systems for fault diagnosis, in: Proceedings of IEEE international conference on information technology and e-services, Sousse, Tunisia, 2012, pp. 1–6.

[219] M. Seera, C. Lim, A hybrid intelligent system for medical data classification, Expert Syst. Appl. 41 (2014) 2239–2249.

[220] M. Seera, C. Lim, C. Loo, Motor fault detection and diagnosis using a hybrid fmm-cart model with online learning, J. Intell. Manuf. (2014) 1273–1285.

[221] J. Calvo-Rolle, J. Casteleiro-Roca, H. Quintian, M. Meizoso-Lopez, Hybrid intelligent system for PID controller using in a steel rolling process, Expert Syst. Appl. 40 (2013) 5188–5196.

[222] P. Meesad, G. Yen, Pattern classification by a neurofuzzy network: application to vibration monitoring, ISA Trans. 39 (2000) 293–308.

[223] M. Shim, M. Suh, Crack identification using neuro-fuzzy-evolutionary technique, KSME Int. J. 16 (2002) 454–467.

[224] T. Liao, An investigation of a hybrid CBR method for failure mechanisms identification, Eng. Appl. Artif. Intell. 17 (2004) 123–134.

[225] B. Yang, S. Jeong, Y. Oh, A. Tan, Case based reasoning system with petri nets for induction motor fault diagnosis, Eng. Sys. Appl. 27 (2004) 301–311.

[226] G. Carpenter, S. Grossberg, The art of adaptive pattern recognition by a self-organizing neural network, IEEE Trans. Comput. 21 (1988) 77–85.

[227] T. Kohonen, Self-organizing maps, Springer, USA, 1995.

[228] C. Chiu, N.-H. Chiu, C.-I. Hsu, Intelligent aircraft maintenance support system using genetic algorithms and case-based reasoning, Int. J. Adv. Manuf. Technol. 24 (2004) 440–446.

[229] B. Samanta, Gear fault detection using artificial neural networks and support vector machines with genetic algorithms, Mech. Syst. Sig. Process. 18 (2004) 625–644.

[230] L. Jack, A. Nandi, Fault detection using support vector machines and artificial neural networks, augemented by genetic algorithms, Mech. Syst. Sig. Process. 16 (2002) 373–390.

[231] P. Pawar, R. Ganguli, Matrix crack detection in thin-walled composite beam using genetic fuzzy system, J. Intell. Mater. Syst. Struct. 16 (2005) 395–409.

[232] Y. Xu, Y. Zhang, C. Lina, Research of genetic training algorithm for identifying mechanical failure modes within the framework of case-based reasoning, Chin. J. Aeronaut. 18 (2005) 122–129.

[233] Z. Wu, C. Shi, W. He, D. Wang, Static and dynamic compressive properties of ultra-high performance concrete (UHPC) with hybrid steel fiber reinforcements, Cem. Concr. Compos. 79 (2017) 148–157.

[234] E. Cadoni, A. Caverzan, M. di Priscoi, Dynamic behaviour of HPFRCC in tension, in: Proceedings of the 10th international conference on the mechanical and physical behavior of materials under dynamic loading. Freiburg, Germany, 2012, pp. 1–6.

[235] A. Bragov, A. Konstantinov, A. Lomunov, D. Froni, G. Riganti, E. Cadoni, High strain rate response of UHP(FR)C in compression, in: Proceedings of the 11th international conference on the mechanical and physical behavior of materials under dynamic loading, Lugano, Switzerland, 2015, p. 010201010206.

[236] O. Millon, W. Riedel, K. Thoma, E. Fehling, M. Nöldgen, Fiber reinforced ultra-high performance concrete under tensile loads, in: Proceedings of the 9th international conference on mechanical and physical behavior of materials under dynamic loading. Brusse, Belgium, 2009, pp. 671–677.

[237] A. Resnyansky, S. Weckert, Damage of two concrete materials due to enhanced shape charges, in: Proceedings of the annual conference on experimental and applied mechanics, Greenville, USA, 2014, pp. 267–278.

[238] Y. Hao, H. Hao, Y. Wang, Experimental study of dynamic compressive behavior of concrete material reinforced with spiral steel fibers, in: Proceedings of the 10th international conference on shock and impact loads on structures, Singapore, 2013, pp. 343–352.

[239] R. Chen, Y. Liu, X. Guo, K. Xia, F. Lu, Dynamic tensile properties of steel fiber reinforced concrete, in: Proceedings of the annual conference on experimental and applied mechanics, Connecticut, USA, 2011, pp. 37–42.

[240] Y. Wang, Z. Wang, X. Liang, M. An, Experimental and numerical studies on dynamic compressive behavior of reactive powder concretes, Acta Mech. Solida Sinica 21 (2008) 420–430.

[241] Z. Rong, W. Sun, Experimental and numerical investigation on the dynamic tensile behavior of ultra-high performance cement based composites, Const. Build. Mater. 31 (2012) 168–173.

[242] Y. Su, J. Li, C. Wu, P. Wu, M. Tao, X. Li., Mesoscale study of steel fiber-reinforced ultra-high performance concrete under static and dynamic loads, Mater. Des. 116 (2017) 340–351.

[243] M. R. Khosravani, K. Weinberg, Experimental investigations of the environmental effects on stability and integrity of composite sandwich T-joints, Mat.-wiss. u. Werkstofftech. 48 (2017) 753–759.

[244] K. Weinberg, M. R. Khosravani, On the tensiel resistance of UHPC at impact, Eur. Phys. J. Spec. Top. Accepted.

[245] M. R. Khosravani, M. Silani, K. Weinberg, Fracture studies of ultra-high performance concrete using dynamic Brazilian tests, Theor. Appl. Fract. Mech. 93 (2018) 302–310.

[246] C. V. Katsiropoulos, A. Chamos, K. Tserpes, S. Pantelakis, Fracture toughness and shear behavior of composite bonded joints based on a novel aerospace adhesive, Composites Part B. 43 (2012) 240–248.

[247] I. Ashcroft, S. Shaw, Mode I fracture of epoxybonded composite joints, 2.Fatigue loading, Int. J. Adhes. Adhes. 22 (2002) 151–167.

[248] L. Kachanov, Introduction to continuum damage mechanics, Springer, USA, 1986.

[249] ARAMIS, Measuring system based on digital image correlation (DIC), http://www.gom.com/metrology-systems/aramis.html/ (2017).

[250] R. Adams, N. Peppiatt, Stress analysis of adhesive-bonded lap joints, J. Strain Anal. 9 (1974) 185–196.

[251] A. Crocombe, Global yielding as a failure criteria for bonded joints, Int. J. Adhes. Adhes. 9 (1989) 145–153.

[252] D. Gleich, M. V. Tooren, A. Beukers, Analysis and evaluation of bond line thickness effects on failure load in adhesively bonded structures, Int. J. Adhes. Adhes. 15 (2001) 1091–1101.

[253] L. da Silva, T. Rodrigues, M. Figueiredo, M. de Moura, J. Chousal, Effect of adhesive type and thickness on the lap shear strength, J. Adhes. 82 (2006) 1091–1115.

[254] D. Zhou, L. Louca, M. Saunders, Numerical simulation of sandwich T-joints under dynamic loading, Composites Part B. 39 (2008) 973–985.

[255] J. S. Yang, L. Ma, M. Chaves-Vagres, T. Huang, K. U. Schröder, R. Schmidt, L.-Z. Wu, Influence of manufacturing defects on modal properties of composite pyramidal truss-like core sandwich cylindrical panels, Compos. Sci. Technol. 147 (2017) 89–99.

[256] B. Beaumont, J. Schultz, Failure analysis of composite materials: Fractography, Technomic publication, USA, 1990.

[257] A. Vassilopoulos, Fatigue and fracture of adhesively-bonded composite joints, Elsevier, UK, 2015.

[258] S. J. Bass, GARTEUR AG14: Fractography of Composites, GARTEUR TP 083 (1994) 1–169.

[259] M. Stone, Evaluation of oven-cure, solid carbon-epoxy composites with various porosity levels, in: Proceedings of the 35th annual review of progress in quantitative nondestructive evaluation, Chicago, USA, 2008, pp. 1025–1032.

[260] E. Fehling, M. Schmidt, J. Walraven, T. Leutbecher, S. Fröhlich, Ultra-High Performance Concrete UHPC, Ernst & Sohn, 2014.

[261] Y. Tai, S. El-Tawil, T. Chung, Performance of deformed steel fibers embedded in ultra-high performance concrete subjected to various pullout rates, Cem. Concr. Res. 89 (2016) 1–13.

[262] C. Wu, D. Oehlers, M. Rebentrost, J. Leach, A. Whittaker, Blast testing of ultra-high performance fiber and FRP-retrofitted concrete slabs, Eng. Strcut. 31 (2009) 2060–2069.

[263] J. Li, C. Wu, H. Hao, An experimental and numerical study of reinforced ultra-high performance concrete slabs under blast loads, Mater. Des. 82 (2015) 64–76.

[264] P. Maca, R. Sovjak, P. Konvalinka, Mix design of UHPFRC and its response to projectile impact, Int. J. Impact Eng. 63 (2014) 158–163.

[265] J. Liu, C. Wu, J. Li, Y. Su, R. Shao, Z. Liu, G. Chen, Experimental and numerical study of reactive powder concrete reinforced with steel wire mesh against projectile penetration, Int. J. Impact Eng. 109 (2017) 131–149.

[266] N. Wang, S. Mindess, K. Ko, Fiber reinforces concrete beams under impact loading, Cem. Concr. Res. 26 (1996) 363–376.

Bibliography

[267] S. Park, D. Kim, S. Kim, Investigating the impact resistance of ultra-high-performance fiber-reinforced concrete using an improved strain energy impact test machine, Const. Build. Mater. 125 (2016) 145–159.

[268] Y. Xie, Q. Fu, K. Zheng, Q. Yuan, H. Song, Dynamic mechanical properties of cement and asphalt mortar based on SHPB, Const. Build. Mater. 70 (2015) 217–225.

[269] W. Zhang, Y. Zhang, Research on the static and dynamic compressive properties of high performance cementitious composite (HPCC) containing coarse aggregate, Arch. Civ. Mech. Eng. 15 (2015) 711–720.

[270] S. Woo, T. Kim, High strain-rate failure in carbon-kevlar hybrid woven composites via a novel SHPB-AE coupled test, Composites Part B 97 (2016) 317–328.

[271] J. Hopkinson, On the rupture of iron wire by a blow. Original papers-by the late John Hopkinson., Scientific Papaers. B. Hopkinosn (ed), Cambridge Univ. Press (1901) 316–320.

[272] B. Hopkinson, The effect of momentary stresses in metals, Proc. R. Soc. A. Lond. 74 (1904) 498–506.

[273] B. Hopkinson, A method of measuring the pressure produced in the detonation of high explosive or by the impact of bullets, Philos. Trans. R. Soc. A. 213 (1914) 437–456.

[274] R. Davies, A critical study of the Hopkinson pressure bar, Philos. Trans. R. Soc. A. 240 (1948) 375–457.

[275] H. Kolsky, An investigation of the mechanical properties of materials at very high rates of loading, Proc. Phys. Soc. B. 62 (1949) 676–700.

[276] U. Lindholm, Some experiments with split Hopkinson pressure bar, J. Mech. Phys. Solids. 12 (1964) 317–335.

[277] B. Gama, S. Lopatnikov, J. Gillespie, Hopkinson bar experimental technique: A critical review, Appl. Mech. Rev. 57 (2004) 223–250.

[278] J. Field, S. Walley, W. Proud, H. Goldrein, C. Siviour., Review of experimental techniques for high rate deformation and shock studies, Int. J. Impact Eng. 30 (2004) 725–775.

[279] J. Harding, E.Wood, J. Campbell, Tensile testing of materials at impact rates of strain, J. Mech. Eng. Sci. 2 (1960) 88–96.

[280] J. Duffy, J. Campbell, R. Hawley, On the use of a torsional split Hopkinson bar to study rate effects in 1100-0 aluminum, Trans ASME: J. Appl. Mech. 38 (1971) 83–91.

[281] X. Nie, B. Song, C. Loefflee, A novell splitting-beam laser extensometer technique for kolsky tension bar experiment, J. Dyn. Behav. Mater. 1 (2015) 70–74.

[282] J. Chen, B. Guo, H. Liu, H. Liu, P. Chen, Dynamic Brazilian test of brittle materials using the split Hopkinson pressure bar and digital image correlation, Strain 50 (2014) 563–570.

[283] S. Swantek, A. Wicks, L. Wilson, An optical method of strain measurement in the split hopkinson pressure bar, in: proceedings of IMAC-XIX: a conference on structural dynamics. Florida, USA, 2001, pp. 1471–1477.

[284] H. Kolsky., Stress waves in solids, Dover Book on Physic, New York, 1963.

[285] D. Parry, P. Dixon, S. Hodson, N. Al-Maliky, Stress equilibrium effects within Hopkinson bar specimens, J. Phys. IV. C8 (1994) 107–112.

[286] J. H. M. Aleyasin, Wave dispersion and attenuation in viscoelastic polymeric bars: Analysing the effect of lateral inertia, Int. J. Mech. Sci. 52 (2010) 754–757.

[287] W. Chen, B. Song, Split Hopkinson (Kolsky) bar, Springer, 2011.

[288] G. Gray, Classic split Hopkinson pressure bar testing, ASM handbook: Mechanical testing and evaluation. Am. Soc. Met. 8 (2000) 462–476.

[289] X. Wu, D. Gorham, Stress equilibrium in the split Hopkinson pressure bar test, J. Phys. IV. 7 (1997) 91–96.

[290] G. Ravichandran, G. Subhash, Critical appraisal of limiting strain rates for compression resting of ceramics in a split Hopkinson pressure bar, J. Am. Ceram. Sco. 77 (1994) 263–267.

[291] Q. Li, H. Meng, About the dynamic strength enhancement of concrete-like materials in a split Hopkinson pressure bar test, Int. J. Solids Struct. 40 (2003) 343–360.

[292] X. Zhou, H. Hao., Modelling of compressive behavior of concrete-like materials at high strain rate, Int. J. Solids Struct. 45 (2008) 4648–4661.

[293] F. Dai, S. Huang, K. Xia, Some fundamental issues in dynamic compression and tension tests of rock using split Hopkinson pressure bar, Rock. Mech. Rock. Eng. (2010) 657–666.

[294] V. Garas, K. Kurits, L. Kahn, Creep of UHPC in tension and compression: Effect of thermal treatment, Cem. Concr. Compos. 34 (2012) 493–502.

[295] I. Yang, G. Peng, Y. Gao, H. Zhang, Torsional behavior of ultra-high performance concrete squared beams, Eng. Struct. 56 (2012) 523–532.

[296] P. Forquin, B. Erzar, Dynamic fragmentation process in concrete under impact and spalling tests, Int. J. Frac. 163 (2010) 193–215.

[297] J. Klepaczko, A. Brara, An experimental method for dynamic tensile testing of concrete by spalling, Int. J. Impact Eng. 25 (2001) 387 – 409.

[298] F. Diaz-Rubio, J. R. Perez, V. S. Galvez, The spalling of long bars as a reliable method of measuring the dynamic tensile strength of ceramics, Int. J. Impact Eng. 27 (2) (2002) 161–177.

[299] H. F. Denoual C., A damage model for the dynamic fragmentation of brittle solids, Comp. Methods Appl. Mech. Eng. 183 (2000) 247258.

[300] F. Hild, C. Denoual, P. Forquin, X. Brajer, On the probabilistic-deterministic transition involved in a fragmentation process of brittle materials, Comput. Struct. 81 (2003) 1241–1254.

[301] B. Erzar, P. Forquin, Experiments and mesoscopic modelling of dynamic testing of concrete, Mech. Mater. 43V (2011) 505–527.

[302] H. Schuler, C. Mayrhofer, K. Thoma, Spall experiments for the measurement of the tensile strength and fracture energy of concrete at high strain rates, Int. J. Impact Eng. 32 (10) (2006) 1635–1650.

[303] S. Novikov, I. Divnov, A. Ivanov, The study of fracture of steel, aluminum and copper under explosive loading, Fiz. Met. Metalloved. 21 (1966) 608–615.

[304] S. Novikov, A. Chernov, Determination of the spall strength from measured values of the specimen free-surface velocity, J. Appl. Mech. Tech. Phys. 23 (1982) 703–705.

[305] M. Nöldgen, O. Millon, K. Thomas, E. Fehling, Hochdynamische Materialeigenschaften von Ultrahochleistungsbeton UHPC, Beton- und Stahlbetonbau 104 (2009) 717–727.

[306] B. Erzar, P. Forquin, An experimental method to determine the tensile strength of concrete at high rates of strain, Exp. Mech. 50 (2010) 941–955.

[307] Photron FASTCAM Analysis (PFA): Photron launches motion analysis software, http://photron.com/photron-launches-motion-analysis-software-pfa/ (2017).

[308] M. Nöldgen, Modellierung von ultrahochfestem Beton (UHPC) unter Impaktbelastung, Ph.D. thesis, Universität Kassel (2010).

[309] O. Millon, W. Riedel, C. Mayrhofer, K. Thoma, Failure mechanisms of UHPC components under explosive loadingr, in: Proceedings of HiPerMat 2012. 3rd international symposium on UHPC, Kassel, Germany, 2012, pp. 583–592.

[310] M. Orgass, Y. Klug, Fibre reinforced ultra-high strength concretes, in: Proceedings of the international symposium on ultra-high performance concrete. Kassel, Germany, 2004, pp. 637–647.

[311] J. Scheydt, O. Millon, H. Muller, K. Thoma, Entwicklung eines brandbeständigen ultrahochfesten Betons für hochdynamische Beanspruchungen, Beton-und Stahlbetonbau 107 (2012) 289–301.

[312] L. Hollaway, M. Leeming, Strengthening of Reinforced Concrete Structures, Woodhead Publishing, 1999.

[313] H. Schuler, Experimentelle und numerische Untersuchungen zur Schdigung von stobeanspruchtem Beton, Dissertation, Universität der Bundeswehr München (2004).

[314] M. Nöldgen, Modellierung von ultrahochfestem Beton (UHPC) unter Impaktbelastung, Dissertation, Universität Kassel (2010).

[315] C. Rossello, M. Elices, G. Guinea, Fracture of model concrete: 2. Fracture energy and charecteristic length, Cement and Concrete research. 36 (2006) 1345–1353.

[316] H. Relinc, SURE-Pulse software under the GNU General Public License, V. 3.0, `http://www.relinc.net/software/` (2017).

[317] DIN EN 12390-6, Testing hardened concrete - Part 6: Tensile splitting strength of test specimens, Deutsches Institut für Normung (DIN) Beuth Verlag Berlin.

[318] J. Rodriguez, C. Navaro, V. Sanchez-Gavalez., Splitting tests: an alternative to determine the dynamic tensile strength of ceramic materials, J. Phys. IV. 04 (1994) 101–106.

[319] D. Frew, M. Forrestal, W. Chen, Pulse shaping techniques for using brittle materials with a split Hopkinson pressure bar, Exp. Mech. 42 (2002) 93–106.

[320] Y. Lu, Q. Li, Appraisal of pulse-shaping technique in split Hopkinson pressure bar test for brittle materials, Int. J. Protec. Struct. 1 (2010) 363–390.

[321] W. Heard, B. Martin, X. Nie, T. Slawson, P. Basu, Annular pulse shaping technique for large-diameter kolsky bar experiments on concrete, Exp. Mech. 54 (2014) 1343–1354.

[322] Y. G. Huang, L. G. Wang, Y. L. Lu, J. R. Chen, J. H. Zhang, Semi-analytical and numerical studies on the flattened Brazilian splitting test used for measuring the indirect tensile strength of rocks, Rock Mech. Rock Eng. 48 (2015) 18491866.

[323] Q. Wang, F. Feng, M. Ni, X. Gou, Measurement of mode I and mode II rock dynamic fracture toughness with cracked straight through flattened Brazilian disc impacted by split Hopkinson pressure bar, Eng. Fract. Mech. 78 (2011) 2455–2469.

[324] E. Dave, A. Braham, W. Buttlar, G. Paulino, Development of a flattened indirect tension test for asphalt concrete, J. Test. Eval. 39 (2011) 1–8.

[325] A. Elghazel, R. Taktak, J. Bouaziz., Determination of elastic modulus, tensile strength and fracture toughness of bioceramics using the flattened Brazilian disc specimen: analytical and numerical results, Ceram. Int. 41 (2015) 12340–12348.

[326] Q. Wang, X. Jia, S. Kou, Z. Zhang, P. Lindqvist, The flattened Brazilian disc specimen used for testing elastic modulus, tensile strength and fracture toughness of brittle rocks: analytical and numerical results, Int. J. Rock Mech. Min. Sci. 41 (2004) 245–253.

[327] V. Malarics, Ermittlung der Betonzugfestigkeit aus dem Spaltzugversuch an zylindrischen Betonproben, Ph.D. thesis, Karlsruher Institut für Technologie (2011).

[328] M. M. Frocht, Photoelasticity, John Wiley & Sons Inc., USA, 1948.

[329] H. Awaji, S. Sato, Diametral compressive stress considering the hertzian contact, J. Soc. Mater. Sci. 27 (1978) 336–341.

[330] J. Ju, J. Summers, J. Ziegert, G. Fadel, Design of honeycomb for modulus and yield strain in shear, J. Eng. Mater. Technol. 134 (2012) 1–15.

[331] S. Keshavanarayana, H. Shahverdi, A. Kothare, C. Yang, J. Bingenheimer, The effect of node bond adhesive fillet on uniaxial in-plane responses of hexagonal honeycomb core, Compos. Struct. 175 (2017) 111–122.

[332] Q. Yang, M. Thouless, S. Ward, Numerical simulation of adhesively-bonded beams failing with extensive plastic deformation, J. Mech. Phys. Solids 47 (1999) 1337–1353.

[333] T. Ferracin, C. Landis, F. Delannay, T. Pardoen, On the determination of the cohesive zone properties of an adhesive layer from the analysis of the wedge-peel test, Int. J. Solids Struct. 40 (2003) 2889–2904.

[334] A. Karac, B. Blackman, V. Cooper, A. Kinloch, S. R. Sanchez, W. Teo, A. Ivankovic, Modelling the fracture behaviour of adhesively-bonded joints as a function of test rate, Eng. Fract. Mech. 78 (2011) 973–989.

[335] T. Pardoena, T. Ferracina, C. Landisb, F. Delannay, Constraint effects in adhesive joint fracture, J. Mech. Phys. Solids 53 (2005) 1951–1983.

[336] V. Cooper, A. Ivankovic, A. Karac, N. Murphy, The dynamic fracture energy of concrete, in: Proceedings of the 32nd annual meeting of the adhesion society, Savannah, USA, 2009, pp. 33–35.

[337] J. Ferrante, J. R. Smith, J. H. Rose, Universal binding energy relations in metallic adhesion, Mater. Sci. Eng. 7 (1981) 19–30.

[338] K. Weinberg, T. Dally, C. Bilgen, Numerical simulation of a SHB spallation of UHPC, subm. to Eng. Fract. Mech.

[339] J. Hutchinson, A. Evanes, Mechanics of materials: Top-down approaches to fracture, Acta Mater. 48 (2000) 125–135.

[340] A. Pandolfi, K. Weinberg, A numerical approach to the analysis of failure modes in anisotropic plates, Eng. Fract. Mech. 78 (2011) 2052–2069.

[341] M. Alfano, F. Furgiuele, A. Leonardi, C. Maletta, G. H. Paulino, Mode I fracture of adhesive joints using tailored cohesive zone models, Int. J. Fract. 157 (2009) 193–204.

[342] R. Campilho, M. Banea, J. Neto, L. daSilva, Modelling adhesive joints with cohesive zone models: effect of the cohesive law shape of the adhesive layer, Int. J. Adhes. Adhes. 44 (2013) 48–56.

[343] M. Alger, Polymer Science Dictionary, Springer, London, UK, 2017.

[344] A. Pandolfi, K. Weinberg, Analysis of failure modes in silicon dies, Eng. Fract. Mech. 78 (2011) 2052–2069.

[345] A. Needleman, An analysis of decohesion along an imperfect interface, Int. J. Fract. 42 (1990) 21–40.

[346] A. Documentation, Abaqus standard user manual, Dessault Systems, 2014.

[347] N. Möes, T. Belytschko, Extended finite element method for cohesive crack growth, Eng. Fract. Mech. 69 (2002) 813–833.

[348] M. R. Khosravani, P. Wagner, D. Fröhlich, R. Trettin, K. Weinberg, Dynamic fracture investigations of Ultra-High Performance Concrete, subm. to Int. J. Solids Strcut.

[349] H. Wu, Q. Zhang, F. Huang, Q. Jin, Experimental and numerical investigation on the dynamic tensile strength of concrete, Int. J. Impact. Eng. 32 (2005) 605–617.

[350] A. Brara, J. Klepaczko, Experimental characterization of concrete in dynamic tension, Mech. Mater. 38 (2006) 253–267.

[351] F. Pierron, P. Forquin, Ultra-high speed full-field deformation measurement on concrete spalling specimens and stiffness identification with the virtual field method, Strain 48 (2012) 388–405.

[352] A. Brara, R. Janusz, J. R. Klepaczko, Fracture energy of concrete at high loading rates in tension, Int. J. Impact Eng. 34 (2007) 424–435.

[353] D. Asprone, E. Cadoni, A. Prota, Experimental analysis on tensile dynamic behavior of existing concrete under high strain rates., ACI Struct. J. 106 (2009) 106–113.

[354] J. Weerheijm, I. Vegt, The dynamic fracture energy of concrete, in: Proceedings of the fracture mechanics for concrete and concrete structure, Jeju, Korea, 2010, pp. 419–427.

[355] J. V. Doormaal, J. Weerheijm, L. Sluys, Experimental and numerical determination of the dynamic fracture energy of concrete., J. Phys. IV. 1 (1994) 501–506.

[356] R. Pedersen, L. Sluys, J. Weerheijm, A. Simone, A computational study of the fracture behavior of concrete in a modified split Hopkinson bar test., in: Proceedings of the 11th international conference on fracture, Turin, Italy, 2005, pp. 1241–1246.

[357] F. Gatuingt, L. Snozzi, J. F. Molinari, Numerical determination of the tensile response and the dissipated fracture energy of concrete: role of the mesostructure and influence of the loading rate, Int. J. Numer. Anal. Meth. Geomech. 37 (2013) 3112–3130.

[358] C. Ross, J. Tedesco, S. Kuennen, Effects of strain rate on concrete strength, ACI. Mater J. 92 (1995) 37–45.

[359] A. Brara, F. Camborde, J. Klepaczko, C. Mariotti, Experimental and numerical study of concrete at high strain rates in tension, Mech. Mater. 33 (2001) 33–45.

[360] B. Erzar, P. Forquin, Analysis and modelling of the cohesion strength of concrete at high strain-rates, Int. J. Solids Struct. 51 (2014) 2559–2574.

[361] J. Ozbolt, A. Sharma, B. Irhan, E. Sola, Tensile behavior of concrete under high loading rates, Int. J. Impact. Eng. 69 (2014) 55–68.

[362] S. Das, A strain rate dependent tensile damage model for brittle materials under impact loading., PhD thesis, University of Sydney (2016).

[363] X. Gu, Q. Zhang, D. Huang, Y. Yv, Wave dispersion analysis and simulation method for concrete SHPB test in peridynamics, Eng. Fract. Mech. 160 (2016) 124–137.

[364] S. Knell, M. Sauer, O. Millon, W. Riedel, Mesoscale simulation of concrete spall failure, Eur. Phys. J. Spec. Top. 206 (2012) 139–148.

[365] G. Ruiz, M. Ortiz, A. Pandolfi, Three-dimensional finite-element simulation of the dynamic Brazilian tests on concrete cylinders, Int. J. Numer. Methods Eng. 48 (2000) 963–994.

A. Appendix

Table A.1.: Reported some mechanical properties of concrete by spalling tests at different strain rate.

Reference	strain rate (s^{-1})	E_{dyn}(GPa)	R_m (MPa)	$\mathcal{G}_c$ (N/m)
[39]	$\dot{\varepsilon} = 80$	43.6	10.8	—
[296]	$\dot{\varepsilon} = 123$	38	14.4	—
[297]	$\dot{\varepsilon} = 120$	41.5	28	—
[302]	$\dot{\varepsilon} = 37$	38.6	13.2	175.3
[306]	$\dot{\varepsilon} = 150$	37.9	20	—
[349]	$\dot{\varepsilon} = 100$	42.8	20	—
[350]	$\dot{\varepsilon} = 112$	31	57	—
[351]	$\dot{\varepsilon} = 110$	32	15.2	—
[352]	$\dot{\varepsilon} = 25$	—	—	300
[353]	$\dot{\varepsilon} = 1$	—	—	137
[354]	1300 GPa/s	—	—	289
[355]	24 MPa/s	40	—	125
[356]	1000 GPa/s	46.2	15.9	230
[357]	39 GPa/s	—	5.5	120

Table A.2.: Numerical simulations of concrete and UHPC under spalling and Brazilian tests by SHB.

Reference	Experiment	material	Studied parameter	Result
[92]	Brazilian	concrete	tensile strength	$\sigma_{\mathrm{dyn}}^{\mathrm{f}}$=14.5 MPa
[301]	spalling	concrete	tensile strength	$\sigma_{\mathrm{dyn}}^{\mathrm{f}}$=15.1 MPa
[306]	spalling	concrete	tensile strength	$\sigma_{\mathrm{dyn}}^{\mathrm{f}}$=13.6 MPa
[358]	Brazilian	concrete	tensile strength	$\sigma_{\mathrm{dyn}}^{\mathrm{f}} = 6.31$MPa
[359]	spalling	concrete	tensile strength	$\sigma_{\mathrm{dyn}}^{\mathrm{f}}$=20 MPa
[349]	spalling	concrete	tensile strength	$\sigma_{\mathrm{dyn}}^{\mathrm{f}}$=20 MPa
[241]	spalling	UHPFRC	tensile strength	$\sigma_{\mathrm{dyn}}^{\mathrm{f}}$=37 MPa
[360]	spalling	concrete	tensile strength	$\sigma_{\mathrm{dyn}}^{\mathrm{f}}$=12.1 MPa
[361]	spalling	concrete	fracture energy	$G_{\mathrm{dyn}}^{\mathrm{c}}$=154.9 J/m^2
[362]	Brazilian	concrete	tensile strength	$\sigma_{\mathrm{dyn}}^{\mathrm{f}}$=10.5 MPa
[362]	spalling	concrete	tensile strength	$\sigma_{\mathrm{dyn}}^{\mathrm{f}}$=13.3 MPa
[242]	Brazilian	UHPFRC	tensile strength	$\sigma_{\mathrm{dyn}}^{\mathrm{f}}$=18 MPa
[363]	Brazilian	concrete	tensile strength	$\sigma_{\mathrm{dyn}}^{\mathrm{f}}$=10 MPa
[364]	spalling	concrete	tensile strength	$\sigma_{\mathrm{dyn}}^{\mathrm{f}}$=15.5 MPa
[364]	spalling	concrete	fracture energy	$G_{\mathrm{dyn}}^{\mathrm{c}}$=100 J/m^2
[356]	spalling	concrete	tensile strength	$\sigma_{\mathrm{dyn}}^{\mathrm{f}}$=15.9 MPa
[365]	Brazilian	concrete	tensile strength	$\sigma_{\mathrm{dyn}}^{\mathrm{f}}$=9.6 MPa